

**COUPLED FLOW OF WATER IN SATURATED KAOLINITE CLAY  
UNDER MULTIPLE POTENTIALS**

by

**Mustafa Tuncan**

**A Dissertation**

**Presented to the Graduate and Research Committee  
of Lehigh University  
in Candidacy for the Degree of  
Doctor of Philosophy**

in

**Civil Engineering**

**Lehigh University**

**October, 1991**

## Certificate of Approval

Approved and recommended for acceptance as a dissertation in partial fulfillment of the requirements for the degree of Doctor of Philosophy.

9 / 24 / 1991

(date)

Sibel Pamukcu  
Professor in Charge

Accepted 9 / 24 / 1991

(date)

Special committee directing  
The doctoral work of  
Mustafa Tuncan

H. Y. Fang, Chairman

R. Chaney

C. Moses

K. Tuzla

## **ACKNOWLEDGEMENTS**

The author expresses his appreciation to his research advisor, professor Sibel Pamukcu for her support, helpful guidance and being a constant source of constructive criticism during the course of this investigation. Gratitude is expressed to Professors Hsai Y. Fang, Ronald C. Chaney, Carl O. Moses, and Kemal Tuzla for reviewing this dissertation and providing many hours of helpful discussions on the course of the study.

Thanks are extended to the Anadolu University, Eskisehir, Turkey, which provided my scholarship during July, 1987 and January, 1991.

Several individuals contributed significantly towards the completion of this research. I would like to thank my father, Ismail Tuncan, and my mother, Guner Tuncan, for their support and patience during my study in the U.S.A. I am grateful for the moral support and help provided to me by my brother Ahmet Tuncan.

I would also like to express my gratitude to my wife Gonul and sons Ibrahim and Kasim for their understanding and encouragement while conducting this research.

This research was partially funded by National Science Foundation, Grant No. MSS-8909963.

**TO MY**  
**FATHER, ISMAIL TUNCAN**  
**MOTHER, GUNER TUNCAN**

# TABLE OF CONTENTS

Acknowledgements .....	iii
List of Figures .....	viii
List of Tables .....	xv
Abstract .....	1
<b>CHAPTER ONE INTRODUCTION</b>	
A. PROBLEM STATEMENT .....	3
B. SCOPE OF DISSERTATION .....	5
<b>CHAPTER TWO BACKGROUND</b>	
A. INTRODUCTION .....	6
B. CONDUCTION THEORIES	
1- DARCY'S LAW FOR FLOW THROUGH POROUS MEDIA .	7
2- FICK'S LAW OF CHEMICAL DIFFUSION .....	8
3- FOURIER'S LAW OF HEAT CONDUCTION .....	9
C. COUPLED EQUATION .....	10
D. THERMAL POTENTIAL .....	13
E. CHEMICAL POTENTIAL .....	16
F. ELECTRICAL POTENTIAL .....	18
G. COUPLED FLOW UNDER HYDRAULIC, CHEMICAL, AND THERMAL GRADIENTS .....	20
<b>CHAPTER THREE EQUIPMENT DEVELOPMENT AND EXPERIMENTS</b>	
A. INTRODUCTION .....	22
B. CONSIDERATION IN EQUIPMENT DEVELOPMENT .....	23
1. TRIAXIAL CELL .....	27
2. CONTROL PANELS .....	33

2.1 MAIN CONTROL PANEL .....	33
2.2 SUB CONTROL PANEL .....	37
2.3 TEMPERATURE CONTROL PANEL .....	37
2.4 COOLING UNIT .....	42
2.5 COMPUTER AIDED DATA ACQUISITION .....	42
C. TESTING .....	45
1. SAMPLE PREPARATION .....	47
2. SAMPLE SETUP .....	48
3. EXPERIMENTS UNDER ISOLATED GRADIENT .....	49
3.1 HYDRAULIC GRADIENT .....	50
3.2 CHEMICAL GRADIENT .....	51
3.3 THERMAL GRADIENT .....	55
4. EXPERIMENTS UNDER MULTIPLE GRADIENTS.....	60
5. UNDRAINED TRIAXIAL SHEAR STRENGTH .....	62
D. COMPRESSIBILITY	
1. TERZAGHI' S ONE DIMENSIONAL CONSOLIDATION THEORY .....	63
2. DETERMINATION OF THE COEFFICIENT OF CONSOLIDATION, $C_v$ FROM ONE-DIMENSIONAL CONSOLIDATION TEST .....	65
3. DETERMINATION OF THE COEFFICIENT OF CONSOLIDATION, $C_v$ FROM PORE PRESSURE DATA OBTAINED USING THE NEW TESTING SYSTEM .....	65
3.1 CALCULATION OF $C_v$ .....	66

## CHAPTER FOUR EXPERIMENTAL RESULTS

A. INTRODUCTION .....	67
B. FLOW UNDER ISOLATED GRADIENT .....	68
C. MEASUREMENT OF COUPLED COEFFICIENT OF HYDRAULIC PERMEABILITY UNDER DRAINED AND UNDRAINED BOUNDARY CONDITIONS.....	89
D. FLOW UNDER MULTIPLE GRADIENTS .....	90

	E. ISOTROPICALLY CONSOLIDATED UNDRAINED ICU TRIAXIAL TESTS	
	1. STRESS-STRAIN RELATION .....	100
	2. PORE WATER PRESSURE .....	115
	F. COMPRESSIBILITY .....	121
CHAPTER FIVE	DISCUSSION OF RESULTS	
	A. COUPLED FLUX AND STRESS-STRAIN .....	123
	B. COUPLED FLOW UNDER MULTIPLE GRADIENTS .....	127
	C. COMPRESSIBILITY .....	128
	D. USE OF EQUIPMENT .....	129
CHAPTER SIX	CONCLUSIONS AND RECOMMENDATIONS	
	A. CONCLUSIONS .....	135
	B. RECOMMENDATIONS .....	139
REFERENCES	.....	141
APPENDIX A	USER'S MANUAL FOR EXPERIMENTAL SYSTEM	
	A. TRIAXIAL CONSOLIDATION .....	147
	B. APPLICATION OF HYDRAULIC GRADIENT .....	149
	C. APPLICATION OF TEMPERATURE GRADIENT .....	151
	D. ( CIU ) TRIAXIAL SHEAR TEST .....	152
APPENDIX B	DATA ACQUISITION PROGRAMS .....	158
APPENDIX C	DOCUMENTATION .....	173
	( SOME OF THE CALCULATIONS AND PROCEDURES USED IN THIS DISSERTATION )	
VITA	.....	176

## LIST OF FIGURES

Figure 2.1: Schematic representation of Darcy's experiment .....	7
Figure 2.2: Schematic diagram of water flow situation in soils .....	13
Figure 3.1: Schematic representation of the experimental set-up .....	24
Figure 3.2.a: Schematic representation of the experimental system .....	25
Figure 3.2.b: Photograph of the entire assembly .....	26
Figure 3.3.a: Schematic representation of the triaxial assembly .....	29
Figure 3.3.b: Photograph of the platens and other triaxial cell accessories....	30
Figure 3.4.a: Schematic diagram of the end platens .....	31
Figure 3.4.b: Schematic representation of a mounted between the platens .....	32
Figure 3.5: Detailed representation of the insulator .....	33
Figure 3.6: Schematic representation of the main control panel .....	35
Figure 3.7: Photograph of the main control panel .....	36
Figure 3.8: Schematic representation of the sub-control panel.....	38
Figure 3.9: Photograph of the sub control panel.....	39
Figure 3.10: Schematic representation of heat control panel.....	40



Figure 3.11: Photograph of the heat control panel .....	41
Figure 3.12: Schematic representation of cooling unit.....	43
Figure 3.13: Photograph of the data acquisition system .....	44
Figure 3.14 : Schematic representation of the flow chart of the testing program .....	46
Figure 3.15.a : Photograph of the one dimensional consolidation cell .....	48
Figure 3.15.b : Photograph of the consolidation set-up .....	48
Figure 3.16 : Schematic diagram of water flow situation in the specimen under hydraulic gradient .....	50
Figure 3.17 : Schematic diagram of water flow situation in the specimen under chemical gradient .....	52
Figure 3.18 : Variation of predicted Na concentration in soil in 30 days .....	54
Figure 3.19 : Schematic diagram of water flow situation in the specimen under temperature gradient .....	56
Figure 3.20 : Predicted temperature variation profiles in the radial and longitudinal cross-section .....	57
Figure 3.21 : Predicted isotherms in soil cross-section .....	58
Figure 3.22 : Predicted temperature variation in soil at steady state .....	59

Figure 4.1: Time variation of cumulative volume of flow under isolated gradients, $\sigma'_c$ : 100 kPa .....	71
Figure 4.2: Time variation of cumulative volume of flow under isolated gradients, $\sigma'_c$ : 200 kPa .....	72
Figure 4.3: Time variation of cumulative volume of hydraulic flow (average of replicate tests with error band approximately the size of a data point) (distilled water) .....	73
Figure 4.4: Time variation of cumulative volume of hydraulic flow (average of replicate tests with error band approximately the size of a data point) (salt solution) .....	74
Figure 4.5: Time variation of cumulative volume of thermo-osmotic flow...	75
Figure 4.6: Time variation of cumulative volume of thermo-osmotic flow.....	76
Figure 4.7 : Time variation of cumulative volume of hydraulic flow ( $\sigma'_c$ = 100 kPa) .....	78
Figure 4.8: Time variation of cumulative volume of hydraulic flow ( $\sigma'_c$ = 200 kPa) .....	79
Figure 4.9: Time variation of thermo-osmotic permability ( $\sigma'_c$ = 100 kPa) .....	80
Figure 4.10: Time variation of thermo-osmotic permability ( $\sigma'_c$ = 200 kPa) .....	81

Figure 4.11: Time variation of osmotic permeability under chemical gradient [R=refilling the bottom platen reservoir with NaCl solution of original concentration = 3.0 M ( 175 g/lit ) ( $\sigma'_c = 100$ kPa) .....	82
Figure 4.12: Time variation of osmotic permeability under chemical gradient [R=refilling the bottom platen reservoir with NaCl solution of original concentration = 3.0 M ( 175 g/lit ) ( $\sigma'_c = 200$ kPa) .....	83
Figure 4.13: Variation of predicted and measured Na concentration in soil in 30 days ( $D^*$ : effective diffusion coefficient) .....	86
Figure 4.14: Variation of normalized Na concentration profiles with time using calculated effective diffusion coefficient ( $\sigma'_c = 100$ kPa) .....	87
Figure 4.15: Variation of normalized Na concentration profiles with time using calculated effective diffusion coefficient ( $\sigma'_c = 200$ kPa) .....	88
Figure 4.16: Time variation of measured cumulative volume hydraulic flow under the combined effect of multiple gradients with drained boundaries .....	92
Figure 4.17: Time variation of measured and predicted cumulative volume hydraulic flow under the combined effect of multiple gradients with drained boundaries ( $\sigma'_c = 100$ kPa) .....	93

Figure 4.18: Time variation of measured and predicted cumulative volume hydraulic flow under the combined effect of multiple gradients with drained boundaries ( $\sigma'_c = 100$ kPa) .....	94
Figure4.19: Predicted cumulative flow vs. measured cumulative flow under the combined effect of multiple gradients (drained boundaries)...	95
Figure 4.20: Comparison of predicted volume of hydraulic flow under the combined effect of multiple gradients with drained and undrained boundaries .....	97
Figure 4.21: Comparison of time variation of predicted volume of hydraulic flow under the combined effect of multiple gradients with drained and undrained boundaries .....	98
Figure 4.22: Predicted cumulative flow vs. measured cumulative flow under the combined effect of multiple gradients. (undrained boundaries) .....	99
Figure 4.23: Bilinear representation of stress-strain relation .....	103
Figure 4.24: Axial strain vs. deviatoric stress variation of base specimens following hydraulic permeation with distilled water under hydraulic gradient .....	108
Figure4.25: Axial strain vs. deviatoric stress variation of salt solution mixed specimen following permeation with high concentration of salt solution under chemical gradient .....	109
Figure4.26: Axial strain vs. deviatoric stress variation of salt solution mixed specimen following the pore pressure built up due to chemical gradient .....	110

Figure 4.27: Axial strain vs. deviatoric stress variation of salt solution mixed specimens following permeation with salt solution under temperature gradient .....	111
Figure 4.28: Axial strain vs. deviatoric stress variation of salt solution mixed specimens following permeation with salt solution under multiple gradients .....	112
Figure 4.29: Combined graphs of axial strain vs. deviatoric stress variation of the salt solution mixed specimens following permeation with salt solution under isolated and multiple gradients ( $\sigma'_c = 100$ kPa) .....	113
Figure 4.30: Combined graphs of axial strain vs. deviatoric stress variation of the salt solution mixed specimens following permeation with salt solution under isolated and multiple gradients ( $\sigma'_c = 200$ kPa) .....	114
Figure 4.31: Axial strain vs. pore water pressure response of the base specimens in triaxial shear following hydraulic permeation with distilled water.....	116
Figure 4.32: Axial strain vs. pore water pressure response of salt solution mixed specimens in triaxial shear following permeation with high concentration of salt solution under chemical gradient .....	117
Figure 4.33: Axial strain vs. pore water pressure response of salt solution mixed specimens in triaxial shear following pore pressure built up due to chemical gradient (initial at bottom = 5.0 kPa) .....	118

Figure 4.34: Axial strain vs. pore water pressure response of salt solution mixed specimens in triaxial shear following permeation with salt solution under temperature gradient.....	119
Figure 4.35: Axial strain vs. pore water pressure response of salt solution mixed specimens in triaxial shear following permeation with salt solution under multiple gradient .....	120
Figure 5.1 : Sodium diffusion into saturated kaolinite under chemical potential .....	126
Figure 5.2.a : SEM micrograph of pure kaolinite specimen consolidated at 2 kg/cm <sup>2</sup> , [horizontal cross-section] .....	131
Figure 5.2.b : SEM micrograph of pure kaolinite specimen consolidated at 2 kg/cm <sup>2</sup> , [vertical cross-section] .....	132
Figure 5.3.a : SEM micrograph of kaolinite specimen consolidated at 2 kg/cm <sup>2</sup> and subjected to the salt gradient , [horizontal cross-section] .....	133
Figure 5.3.b : SEM micrograph of kaolinite specimen consolidated at 2 kg/cm <sup>2</sup> and subjected to the salt gradient , [vertical cross-section] .....	134
Figure C.1 : Determination of K coefficient for normally consolidated kaolinite specimens with distilled water .....	174
Figure C.2 : Variation of K coefficient with the induced gradients .....	175

## LIST OF TABLES

Table 3.1: Physical properties of some of the material used in the triaxial cell. ....	28
Table 4.1: Summary of flow measuring tests results at consolidation pressure 100 kPa. ....	69
Table 4.2: Summary of flow measuring tests results at consolidation pressure 200 kPa. ....	70
Table 4.3: Summary of the coupled coefficient of hydraulic permeability ...	84
Table 4.4: Summary of flow measuring test results .....	90
Table 4.5: Summary of parameters from CIU triaxial tests of specimens at consolidated at 100 kPa .....	101
Table 4.6 : Summary of parameters from CIU triaxial tests of specimens at consolidated at 200 kPa .....	102
Table 4.7 : Summary of the plastic and elastic parameters determined from bilinear representation of stress-strain diagrams .....	106
Table 4.8 : Summary of strength parameters .....	107
Table 4.9 : Experimental determined $C_v$ using the proposed method .....	122

## **ABSTRACT**

The purpose of this research was to test in the laboratory the validity of a phenomenological equation which combines linearly the forces causing flow of water in continuous clay systems. The equation is based on postulates of irreversible thermodynamics, the validity of which has not been established for clays subjected to combination of hydraulic, thermal and chemical potentials simultaneously. This provided the basis for the development of a new equipment with the objective of obtaining reliable data of water conduction through soil under these multiple potentials.

A triaxial test system was developed to simultaneously apply constant hydraulic, thermal, and chemical potentials to a cylindrical soil specimen under confining pressure. The test system had five functional units, loading, heating, cooling, flexible wall permeability, and diffusion of chemicals. The various parts of the equipment can withstand large temperature differences (80 °C) and chemical environments with pH values ranging from as low as 1 to as high as 12. In addition to its conduction measurement capability, the system is also a conventional triaxial compression testing machine with computer aided data acquisition and real time display of load, displacement and pore pressures. The initial calibration tests showed good repeatability of data and thus stable functioning of the equipment.

The potentials were initially applied separately, and then they were combined simultaneously with either flow allowed or not allowed through the end



boundaries of replicate kaolinite clay specimens. The experimental findings of cumulative flow of water under simultaneous application of the three gradients agreed well with the predictions made for cumulative flow using the superpositioning of the linear relations between the water flux and the forces. The agreement was observed despite the measured changes in the consistency and composition of the soil specimens under the particular magnitude and duration of the potentials applied. This validated the applicability of superpositioning to predict coupled flow with the applied hydraulic, osmotic, and thermal potentials. The superpositioning of the forces was not validated when the coupled coefficients were determined from pore pressure measurements at the potential application sites. In this case, superpositioning overestimated the flow since potential induced consolidation was not accounted for in the calculated coefficients.

# CHAPTER I

## INTRODUCTION

### A. PROBLEM STATEMENT

The phenomenon of flow of water in soils under environmental stresses, i.e., hydraulic, chemical, temperature, and electrical potentials, is important for geotechnical engineering analysis related to consolidation, seepage, and stability. Rapid technological developments have created considerable waste problems which impact the ground. Hazardous and toxic waste sites may contaminate the ground water in their vicinity and may change the subsurface environment (Fang, 86, 89). Chemical and nuclear dumps are not only sources of contamination but heat and electrical potentials as well. The mechanics and behavior of the surrounding soil may also change because of the changing environmental conditions. Hence, geotechnical engineers need to consider the so called " environmental stresses " as well as the " mechanical stresses " in such cases.

Flow of water in soil is usually determined under hydraulic potentials. Numerous research has been conducted to determine the contribution of other potentials, such as osmotic, electro-osmotic and thermal, to the net movement of water through soils ( Biggar and Nelson, 1960, Cassel et al. 1968, Campanella et al., 68, Gray and Mitchell, 67, and Schackelford, 88 ). The net effect of combined or

multiple gradients on the water flow has not been investigated thoroughly in the laboratory. A good example of multiple gradients in soil may be a hydraulic, chemical, and thermal gradients acting simultaneously and causing water flow from one point to another in the ground. This may be a complicated problem in actuality such as in the case of waste plume migration from a point source. In addition to influencing water flow, gradients of different types may cause a number of changes in soil including changes in volume, shear strength, physico-chemistry and microstructure (Barbour et al., 89, Tuncan, 91, Pamukcu and Tuncan, 90). For example, temperature changes in soils may cause pore water pressures and may decrease or increase their strengths (Baldi et al., 86). Yet another example is the change in pore fluid chemistry which may result in changes in particle microstructure (Fisher, 91).

Theories that have been suggested to predict flow of water through saturated porous medium under multiple gradients, otherwise known as coupled flow, are not sufficient for the absence of rigorous experimental information to verify them. There is much experimental information generated about coupled flow of water under single potentials, which do satisfy the theories behind them (Beziat, 88, Goodall and Quicgly, 77, Olsen, 72). This has not been done as rigorous for a combination of more than 2 gradients at a time. If a saturated clay is subjected to more than one gradient simultaneously, i.e. hydraulic, chemical, and thermal, the water flow will probably be governed by the dominant gradient. It is not yet clear if and how this flow will be affected with long term application of these potentials. For example, if a temperature gradient is maintained over a period of time, effects such as volume changes and pore water pressure generation will be observed. Similarly, intrusion of certain chemical species into the pore space would cause physico-chemical changes in soil structure over a period of time. Therefore, there seems to be a need to obtain reliable data in the laboratory in order to understand better the behavior of soils under such complex environmental effects.

Obviously, it should be quite difficult to simulate a complex environmental condition in the laboratory. But, if a combination of possible gradients that may occur in a field situation can be applied simultaneously to a finite soil specimen with well known characteristics and configuration and under a set of known

boundary conditions, the corresponding water flow can be measured for each case and compared with the theory. In order to do this properly, one needs suitable equipment in which the boundary conditions can be controlled properly.

In this study, such equipment was developed to make the appropriate measurements to determine the accuracy of a coupled hydraulic flow equation under multiple gradients which combines linearly the flow of water in porous medium under hydraulic, thermal, and chemical gradients.

## B. SCOPE OF DISSERTATION

The scope of this dissertation includes: 1) the development of new laboratory equipment to measure the flow of water through saturated clay soil under single and multiple gradients, and 2) determination of the accuracy of a phenomenological equation of water flux which combines linearly the forces causing flow.

In Chapter Two the appropriate background and literature review pertaining to the flow of water in soils under different potentials are presented. A complete description of the new equipment with its accessories and capabilities and also the various testing techniques used in this research are presented in Chapter Three. In Chapter Four, results of these tests are presented in detail.

Chapter Five contains the discussion of the results and the discussion of the application of the new equipment to simulate three cases of field situations. A summary and conclusions with recommendations for future work is presented in Chapter six. Finally, a complete user's manual for the equipment; computer program used for data acquisition are provided in the Appendices.

## **CHAPTER II**

### **THEORITICAL BACKGROUND AND LITERATURE REVIEW**

#### **A. INTRODUCTION**

Prediction of flow of water in soils is important in analysis and design in geotechnical engineering. Water flow through porous soil is caused by either natural or man-made potentials. These potentials can be in the form of hydraulic, chemical, temperature, or electrical. All of these potentials often exist simultaneously in the ground contributing to the net flow of water. The extent of each contribution under different boundary and initial conditions is not well understood. This becomes even more important when working with soil at or within same vicinity of contaminated ground for which potentials other than hydraulic may play an important role.

In this chapter, pertinent theory for the development of the coupled flow equation and the related literature review is presented. The information was examined and presented in four groups which are the followings : (1) review of conduction theories, (2) theories of coupled flow, (3) flow under isolated potentials, and (4) coupled flow under multiple potentials.

## B. CONDUCTION THEORIES

### 1. DARCY'S LAW FOR FLOW THROUGH POROUS MEDIA

In 1856, Darcy first examined the flow through porous medium. He established a relationship between the discharge velocity, and head loss, over a length of soil. Figure 2.1 shows a schematic diagram of an experimental set-up, by which Darcy's law can be verified easily using uniform sand as the porous material.

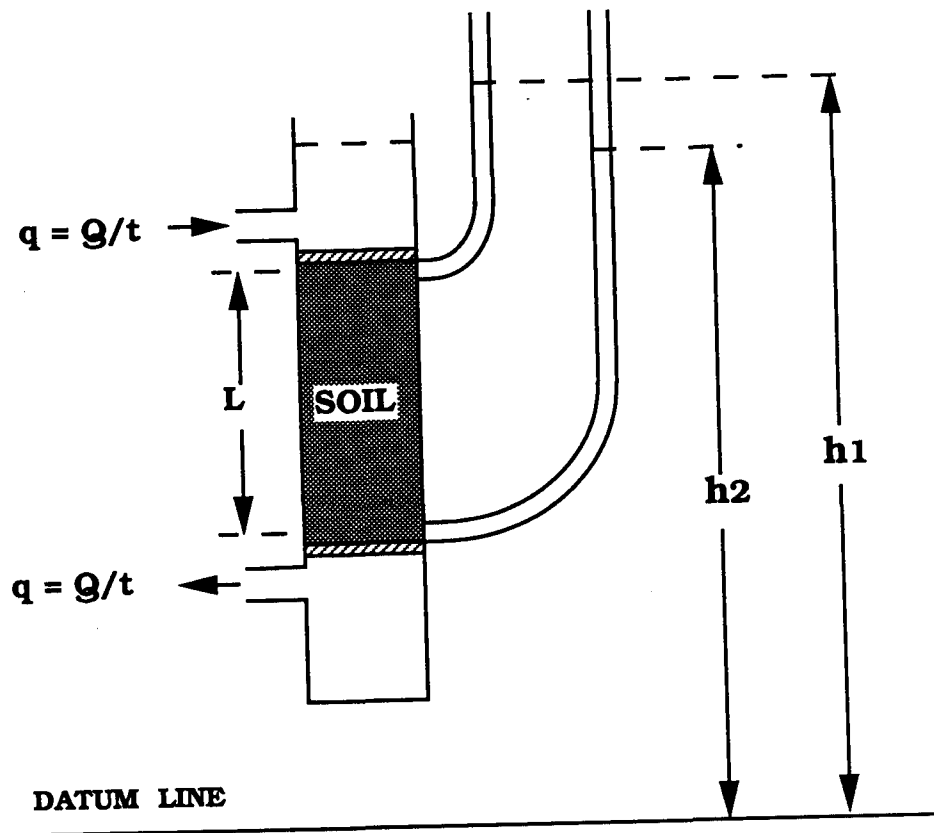


Figure 2.1 Schematic representation of Darcy's experiment

Darcy's law can be written in the following forms :

$$q = \frac{Q}{t} = v A = k i A = k \frac{\Delta H}{L} A \dots\dots\dots ( 2.1 )$$

where,

$Q$  = volume of flow through the cross-sectional area, A in time t.

t = duration of time for the volume of flow.

A = cross-sectional area of the soil.

L = length of the soil.

H =  $h_1 - h_2$  : difference in head.

i = hydraulic gradient.

k = coefficient of permeability.

## 2. FICK'S LAW OF CHEMICAL DIFFUSION

Chemical diffusion is a transport process in which a chemical in solution flows in response to a gradient in its concentration. Fick's first law describes the resulting mass flux of the solute to be directly proportional to the concentration gradient and it can be written in the following form:

$$J = D i_c$$

or

$$q = D^* \cdot \frac{\partial c}{\partial x} \dots\dots\dots ( 2.2 )$$

where q : the rate of flow,

$D^*$ : the effective diffusion coefficient,

[  $D^* = D \cdot n \cdot S_r$  ( D : diffusion coefficient, n : porosity, and  $S_r$  : saturation degree ) ]

c : concentration of chemical solution,

x : distance.

Fick's first law describes steady state flux of solutes. Fick's second law is for the time-dependent transport of chemical solution in soil :

$$\frac{\partial c}{\partial t} = D^* \cdot \frac{\partial^2 c}{\partial x^2} \dots\dots\dots ( 2.3 )$$

where t is the time.

### 3. FOURIER'S LAW OF HEAT CONDUCTION

When a temperature gradient exists, there is an energy transfer from the high temperature region to the low temperature region. Fourier's law states that the energy is transferred by conduction and that the rate of heat flow per unit area is proportional to the normal temperature gradient. It can be written in the following form:

$$q = k_T \cdot A \cdot \frac{\partial T}{\partial x} \dots\dots\dots ( 2.4 )$$

where q : the heat transfer rate,

$k_T$ : the coefficient of thermal conductivity,

A: cross-sectional area,

$dT/dx$ : the temperature gradient in the direction of flow.

Two-dimensional steady-state heat conduction can be written in cylindrical coordinates as follows :

$$\frac{\partial^2 T}{\partial r^2} + \frac{1}{r} \cdot \frac{\partial T}{\partial r} + \frac{\partial^2 T}{\partial z^2} = 0 \dots\dots\dots ( 2.5 )$$

where r : radial distance,

z : longitudinal distance.



### C. COUPLED FLOW EQUATION

" The general phenomenon of a gradient of one type causing a flow of another type is expressed by

$$J_i = L_{ij} X_j \quad \text{----- (2.6)}$$

where  $J_i$  : flux of component  $i$

$X_j$  : gradient of component  $j$

$L_{ij}$  : " coupling coefficients ".

For the case of fluid flow through a soil under the coupled influence of hydraulic, thermal, chemical, and electrical gradients,  $X_H$ ,  $X_T$ ,  $X_C$ , and  $X_E$ , respectively, equation 2.6 becomes

$$J_H = L_{HH} X_H + L_{HT} X_T + L_{HC} X_C + L_{HE} X_E \quad \text{----- (2.7)}$$

where  $L_{HH}$  is the coefficient for hydraulic flow under a hydraulic gradient,  $L_{HT}$  is the coefficient for hydraulic flow under a thermal gradient,  $L_{HC}$  is the coefficient for hydraulic flow under a chemical gradient, and  $L_{HE}$  is the coefficient for hydraulic flow under an electrical gradient" (Mitchell, 1976).

Using the the first and the second postulates of irreversible thermodynamics and Onsager reciprocal relations ( Miller, 1960 ), the phenomenological equation of water flow in a continuous soil system under multiple potentials can be written as follows ( Taylor and Cary, 1964 ):

$$J_H = \sum_{k=1}^n L_{Hk} \cdot \left[ F_k - T \cdot \frac{d(\mu_k / T)}{dz} \right] - L_{Hu} \cdot \frac{d \ln T}{dz} \quad \text{..... ( 2.8 )}$$

where  $J_H$  : water flux

$F_k$  : any external force acting on the component  $k$

$\mu_k$  : chemical potential of substance  $k$

$z$  : distance

$T$  : absolute temperature

$L_{hk}, L_{hu}$  : phenomenological coefficients, where

$$L_{Hk} = L_{kH}$$

$$L_{Hu} = L_{uH}$$

Equation 2.8 can be rewritten for water flux of hydraulic and osmotic coupling as follows (Mitchell et al., 1973)

$$J_H = -L_{H1} \cdot V_w \cdot \frac{dP}{dz} - L_{Hz} \cdot \frac{RT}{C} \cdot \frac{dC}{dz} \dots\dots\dots ( 2.9 )$$

where  $R$  : gas constant

$C$  : number of moles of solute per unit volume of solution

$V_w$  : volume of water per mole of solution

$dP/dz$  : pressure gradient.

Equation 2.9 is valid with the following assumptions :

- 1) isothermal conditions,
- 2) dilute solution,
- 3) complete saturation,
- 4) isotropy and homogeneity,
- 5) no ion exchange during diffusion,
- 6) no electric-magnetic gradients,
- 7) no dissociation,
- 8) external forces do not influence flow.

Equation 2.8 can also be written as the following for flow of water in soil under hydraulic and thermo-osmotic coupling ( Taylor and Cary, 1964 ):

$$J_H = -L_{H1} \cdot V_w \cdot \frac{dP}{dz} - L_{Hq} \cdot \frac{d \ln T}{dz} \dots\dots\dots ( 2.10 )$$

where  $L_{Hq}$  : coefficient in terms of calorimetric heat flow.

Equation 2.10 is valid under the following assumptions:

- 1) The temperature, moisture content and potential distributions vary only in z direction.
- 2) The soil column is subjected to a constant temperature difference across its ends.

Superpositioning equations 2.9 and 2.10 result in :

$$J_H = -L_{HI} \cdot V_w \cdot \frac{dP}{dz} - L_{Hz} \cdot \frac{RT}{C} \cdot \frac{dC}{dz} - L_{Hq} \cdot \frac{d \ln T}{dz} \dots\dots\dots (2.11)$$

in which, let :  $k_{HH} = -L_{HI} V_w \gamma_w$  (  $\gamma_w$  : unit weight of water ).

$$k_{HC} = L_{Hz} RT / 2.303$$

$$k_{HT} = -L_{Hq} / 2.303$$

then :

$$J_H = k_{HH} \cdot \frac{dH}{dz} - k_{HC} \cdot \frac{d(\log C)}{dz} + k_{HT} \cdot \frac{d(\log T)}{dz} \dots\dots\dots (2.12)$$

where,  $k_{HH}$  : coefficient of hydraulic permeability,

$k_{HC}$  : coefficient of osmotic permeability,

$k_{HT}$  : coefficient of thermo-osmotic permeability.

Consider the situation given in the diagram in Figure 2.2, where a soil element of length L and area A is subjected to hydraulic, chemical, and temperature potentials simultaneously, such that :

$H_a, H_b$  = hydraulic heads at the ends **a** and **b**.

$C_a, C_b$  = chemical concentrations at the ends **a** and **b**.

$T_a, T_b$  = temperatures at the ends **a** and **b**.

Then Equation 2.12 can be rewritten to express the net volume of flow per unit time from **a** to **b** as follows :

$$Q_h = k_{hh} \cdot \frac{\Delta H}{L} \cdot A - k_{hc} \cdot \frac{\log(Ca / Cb)}{L} \cdot A + k_{ht} \cdot \frac{\log(Ta / Tb)}{L} \cdot A \dots\dots\dots ( 2.13 )$$

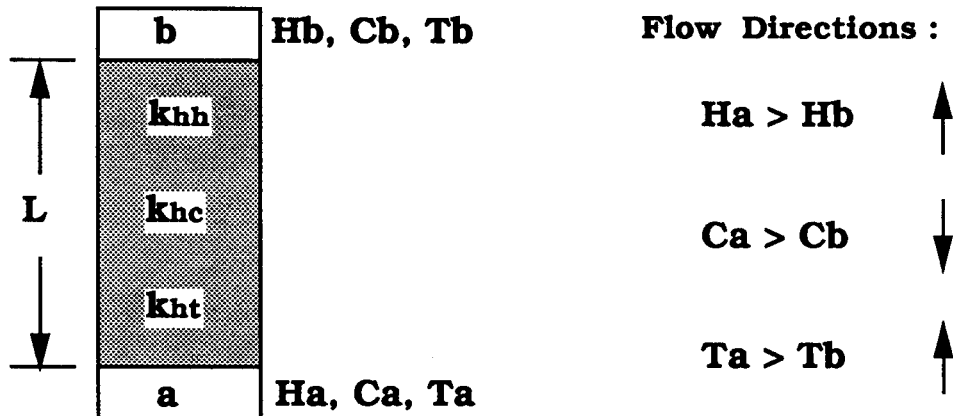


Figure 2.2 Schematic diagram of water flow situation in soils.

#### D. POTENTIAL IN SOILS

##### 1) THERMAL POTENTIAL

The effect of temperature variations through the soils have been investigated in the design of engineering structures such as buried transmission lines, pipelines, heat generating structures; and also development of technical processes such as geothermal energy utilization, thermal enhancement of oil recovery, and hazardous waste disposal. In all these situations, the flow of the water in soils is significantly influenced by temperature variations.

The effect of temperature gradient on the movement and distribution of water in the soil was studied by Gurr, et al. ( 1952 ) in closed columns of soil for a wide range of initial water contents. They found that the maximum net transfer of water was from the hot to the cold end.

Analyses have been presented by Campanella and Mitchell (1968) for the interpretation of volume changes due to thermal expansion of the soil, compressibility of the soil, and the physico-chemical effects. They used a specially designed temperature controlled triaxial equipment. The sample temperature was changed by circulating preconditioned water through the triaxial cell until the sample reached the desired temperature. From their experiments they found that water drains out of the sample during temperature increase and it is absorbed back during temperature decrease. They also observed that when the temperature of a normally consolidated specimen was increased, two effects took place: 1- if the increase in temperature was rapid, a significant positive pore pressure might develop, even though the sample was maintained under fully drained condition, 2- an increase in temperature caused a decrease in the shearing strength of individual interparticle contacts.

Cassel, et al. (1968) found that the temperature variation with depth gives rise to thermal gradients which tend to move water in both vapor and liquid phases. They used fine sandy loam in their soil column experiments. Temperature gradients were established lengthwise along the column by circulating preheated or precooled water through the endplate reservoirs. They had two considerations in their investigation: first consideration was the difficulty in measuring the net water flux and the second consideration was the manner in which boundary temperatures are established including the provision to have no heat flux in the radial direction. Their experience showed that experiments to measure soil water transfer in the presence of temperature gradients are difficult to conduct. They suggested that future laboratory investigations be conducted using soil columns in which water is allowed to transfer across both end boundaries.

Thermal performance of fine-grained soils was studied by Salomone, et al. (1984). They performed laboratory thermal probe tests to determine the thermal resistivity of the soil samples. The instruments they used in their investigation were laboratory thermal probes and a thermal property analyzer. From their experiments they concluded that resistivity varies strongly with moisture content when the moisture content of the soil is less than its critical moisture content, which is indirectly proportional to soil dry density.

Houston, et al. ( 1985 ) performed a laboratory investigation to determine thermo-mechanical behavior of seafloor sediments. Two types of soils were tested in their investigation : illitic and smectite-rich ocean sediments. They found that the change in pore fluid pressure with temperature depends strongly on the compressibility and stiffness characteristics of the soil. They summarized the effect of temperature on consolidation behavior as follows: 1) soils densify when the temperature is increased at a constant mechanical effective stress under drained conditions, 2) the densification increases with increasing temperature and is a result of thermal primary and secondary compressions, 3) the elevation of the temperature of a fully saturated clayey soil for undrained conditions and constant total stress confinement results in a decrease of the soil effective stress.

Results were reported by Baldi, et al. ( 1986 ) on the effect of temperature and pore fluid on shear characteristics of clay. They used a high temperature and pressure triaxial system in their experimental investigation. They presented preliminary experimental results concerning clay thermo-mechanical behavior evaluated in the context of a generalized thermo-plastic Cam-Clay model. They drew two major conclusions concerning thermoplasticity of clay : 1- clay may manifest substantial irreversible volumetric thermal strains due to pure thermal loading, 2- the plastic yielding is continuous during heating .

Naik ( 1986 ) investigated in the laboratory the influence of hazardous and toxic waste permeants and heat on the geotechnical properties of soils. He used sand and bentonite as the base materials to prepare laboratory samples. Following the consolidated undrained shear strength tests of these samples he concluded that: 1) for a saturated soil sample moisture content of soil increases with increasing temperature, 2) shear strength decreases with increasing temperature and increasing pH of the pore fluid, 3) for a consolidated sample the change in moisture content depends on the increase in the bound water, and loss of free water with increasing temperature, 4) for any particular moisture content, shear strength increases with the increase in the ratio of the bound water to free water.

Bezlat, et al. ( 1988 ) performed a series of experiments to investigate the effect of compaction pressure and water content on the thermal conductivity of highly compacted Ca-smectite, Na-semectite, illite, and palygorkite clays. He

looked at this property as a function of density (i.e., compaction pressure), water content and temperature of the clay samples. Use of, so called "dynamic" method was adopted to determine the thermal conductivity of materials because of the less time required to attain thermal equilibrium in each sample. They found that the thermal conductivity increased with density and water content. They concluded that the important parameters for heat transfer in clays are the water content and density, whereas temperature and minerology type appeared to be of less importance.

The heat and moisture transfer characteristics of a compacted silt was determined by Evgin and Svec ( 1988 ) in a laboratory investigation. They found that the relation between the transport coefficients and volumetric moisture content of a compacted Mackenzie Valley silt was similar to that of other soils in the literature. This relation was that the increase in temperature resulted in decrease in moisture content.

A mathematical model was developed by Geraminegad and Saxena ( 1987 ) to predict the transient coupled flow of heat, moisture and gas in porous media. Their results showed that the model predicted a temperature distribution which was in good agreement with the measured values. They solved a group of problems as examples, all of which agreed well with the measured values. Their model included soil deformations as a result of changes in the moisture and gas phases only.

## 2. CHEMICAL POTENTIAL

Chemical potentials give way to diffusion in soils. Diffusion is a transport process in which a chemical in solution flows in response to a gradient in its concentration. There are two processes of transport of solutes in soils; advection and dispersion. Advection is a solute transport process depending on the total hydraulic head. Dispersion is essentially a microscopic phenomenon caused by a combination of molecular diffusion and hydrodynamic mixing occurring with laminar flow through porous media. Diffusion is only significant at relatively low

seepage velocities and over long periods of time. Many studies have shown that molecular diffusion may be an important mechanism of solute transport.

Michaels and Lin ( 1955 ) investigated the effect of electrolyte concentration on hydrogen kaolinite permeability. The streaming potential and conductivity measurements of a compacted kaolinite bed indicated that counter electro-osmosis may be responsible for a small but detectable resistance to water permeation. If sodium ion exchange was prevented by keeping the activity ratio of sodium to hydrogen ion in solution constant, the change in the permeability of kaolinite was small and reversible. Finally, they observed that increasing the pH of a permeant containing a fixed sodium chloride concentration was accompanied by a marked and essentially irreversible reduction in the permeability of hydrogen kaolinite.

Biggar and Nelson ( 1960 ) studied miscible displacement in several porous materials, saturated and unsaturated, at different average flow velocities. They observed that the magnitude of the volume of water was not readily displaced at saturation and it increased when the soil was desaturated. They stated that because the total flux of water moving through natural soils is generally small, the role of hydrodynamic dispersion and diffusion in transporting dissolved solutes must be included in the theories of soil water transport processes.

Goodall and Quigly ( 1977 ) studied two young landfills. Their objective was to determine the actual pollutant migration which had occurred beneath the landfill sites and to compare these results with those obtained from the commonly applied seepage calculations. They established pollution profiles of the landfill sites by measuring the concentrations of the cations Na, K, Ca, and Mg in the porewater squeezed from clay samples obtained in shelby tubes. They showed that the diffused pollution fronts could be attributed to mostly chemical diffusion which, had overwhelmed the seepage flow, in the early stages of both landfills.

Schackelford ( 1988 ) showed that molecular diffusion is an important mechanism of solute transport, especially in relatively thin layers of fine grained materials. He found that the effect of diffusion is to cause breakthrough of contaminants much earlier than would be predicted assuming purely advective flow. Therefore, he suggested that the design of waste containment facilities utilizing fine grained materials should be based not only on consideration of



advective flow, but also on the diffusive flow of contaminants.

Barbour and Fredlund (1989) studied mechanism of volume change caused by osmotic flow in clay soils. They used a numerical analysis scheme to demonstrate the characteristic behavior of a clay soil undergoing volume change by osmotic flow. They found from their laboratory tests that the dominant mechanism of volume change associated with brine contamination of a soil sample was osmotic consolidation. They emphasized for future work to verify the use of "physico-chemical" stress state variables and material properties in prediction of volume changes in soils.

### 3. ELECTRICAL POTENTIAL

In geotechnical application, flow under electrical potential is generally in the form of electro-osmosis. In the past, consolidation by electro-osmosis has been performed successfully in the field. The basic idea in consolidation by electro-osmosis is drawing the soil water to a cathode along with excess cations at a faster rate than could be accomplished by hydraulic gradients. Such fast movement of water out of the soil matrix causes consolidation of the soil. Casagrande (1952), and Bjerrum, et al. (1967) accomplished successful field applications of electro-osmosis for consolidation and dewatering. As a result of electro-osmotic consolidation the undrained shear strength of a clay increased four times in the field. The gain in shear strength exceeded the anticipated values, clearly demonstrating that the effect of electro-osmosis was not only to reduce the water content of clay but also to change its fundamental physical-chemical properties.

Gray and Mitchell (1967) adopted a conceptual approach based on thermodynamics to reconcile existing kinetic models. They showed that electro-osmosis depends primarily on ion distribution and the exclusion of ions of one sign within a porous mass. These ionic parameters depend in turn on the exchange ion population, water content, and the external electrolyte concentration. They concluded that fine grained soils with low exchange capacities such as silts and kaolin clays exhibit very high electro-osmotic flow when saturated by dilute

electrolyte solutions. A specific relationship was also observed between electro-osmotic water transport and water content.

Esrig (1968) showed that introducing an electric field in a soil mass would cause consolidation of the soil. Soil consolidation was manifested by the development of pore-water pressures. They found that the magnitude of the pore-water pressures were dependent on the ratio of the coefficient of electro-kinetic permeability,  $k_e$ , and the hydraulic permeability,  $k_h$ , and also on the voltage at each point in the soil mass. Laboratory and field data were presented to substantiate each of these arguments. They concluded that the phenomenon of electrical consolidation is understood sufficiently well and that it may be used with some confidence and predictability for pertinent engineering problems.

Segall, et al. (1980) studied electro-osmotic water chemistry and quality from a dredged material. They found that this water was highly alkaline, contained organic material, high concentrations of heavy metals, pesticides, and other materials. Based on these findings, they indicated that electro-osmosis may be developed into a viable technology for waste site remediation.

Mitchell and Yeung (1991) investigated use of electro-kinetic barriers in compacted clay. They developed a laboratory testing program to establish the effectiveness of electro-osmosis in driving water through both partially saturated and fully saturated compacted clay. The apparatus they used consisted of fixed wall permeameters. One set of permeameters were equipped with electrodes, and the others served as controls. Through their results they concluded that the coupled flow theory reasonably predicted the migration of ions under the influences of the hydraulic, electrical, and chemical gradients. They also concluded that an electrical gradient may move some chemical species in soils much more effectively than a hydraulic gradient.

#### 4. COUPLED FLOW UNDER HYDRAULIC, THERMAL, CHEMICAL, AND ELECTRICAL GRADIENTS

Liquid movement in soils occurs not only in response to hydraulic gradients but also in response to chemical, temperature, and electrical gradients as well. Flow through soils under each of these potentials have been investigated extensively for the last 50 years, as reviewed in the previous sections. Coupled flow in soils with combined potentials have also been investigated, but not as rigorously. These investigations were made under different combinations of potentials using different types of equipments and experimental techniques. Some of the studies were experimental, whereas others were basically development of theoretical models.

Thermo-osmotic and thermo-electric coupling in saturated soils have been investigated by Gray (1968) in the laboratory. The flow cell was designed to apply known thermal, electrical, and hydraulic pressure gradients across a confined clay samples. He showed that thermally induced osmotic gradients are the dominant transfer mechanism in a saturated, charged membrane system.

Olsen (1972) measured the hydraulic, osmotic, and electro-osmotic conductivities of sodium kaolinite as a function of consolidation pressure ranging from 1 atm to approximately 600 atm. He concluded that the evidence presented indicated that Darcy's law may not provide the sufficient basis to predict either the directions or the magnitudes of liquid movement through deep confining beds. The linear coupled flow equation was validated by the data they generated. However, their measurement durations were short which helped to avoid consolidation and any pore fluid concentration changes during osmotic conductivity tests.

Radhakrishna, et al. (1984) developed a method to numerically model the coupled heat and moisture flow through soils. The numerical results were in good agreement with data from controlled laboratory and field experiments.

Abdel-Hadi and Mitchell (1981) used the Philip and De Vries theory to predict the thermally induced moisture movement in unsaturated soils. They concluded from this theoretical analysis that the important parameters affecting the rate and amount of moisture migration away from a buried electrical cable

are the source temperature and the soil type.

Mitchell et al., ( 1973 ) studied the chemico-osmotic effects in clays. They derived an equation for osmotic consolidation of clays based on postulates of irreversible thermodynamics, continuity and diffusion equations. They concluded that although small, chemico-osmotic coupling is able to move soil water and dissolved salts to cause consolidation.

Winterkorn ( 1943 ) showed theoretically that superposition of hydraulic, thermodynamic, and electrical forces that cause water flow in soils should be valid for most field situation.

## **CHAPTER III**

### **EQUIPMENT DEVELOPMENT AND EXPERIMENTS**

#### **A. INTRODUCTION**

The recent geotechnical engineering needs and inadequacies in existing theories have provided the basis for the development of a new equipment with the objective of obtaining reliable data of water conduction through soil under multiple gradients. The main purpose of the experimental system is to generate data to verify or to modify the existing theoretical concept of the coupled flow under multiple gradients. Using the equipment, it is possible to apply temperature differences up to 80° C across a soil specimen of 14 cm in height. The functional units of the equipment can withstand chemical environments with pH values ranging from as low as 1 to as high as 12. In addition to its conduction measurement capability, the system is also a conventional triaxial compression machine with computer aided data acquisition of load, displacement, and pore pressures.

This chapter describes the new experimental system and the pertinent experiments conducted. The first group of experiments were performed to calibrate the equipment. The second group of experiments were conducted to evaluate the coupled flow equation. The general procedure of testing used in this study consisted of the following steps: 1) placing clay slurry in a consolidation cell, 2) subjecting the clay

slurry to one dimensional consolidation, 3) trimming a sample to the required dimensions and placing this sample into a triaxial cell to isotropically consolidate with backpressure, 4) applying a selected gradient or gradients and measuring the rate of flow, and finally 5) conducting an undrained triaxial shear strength test, with pore water pressure measurements at the top and the bottom of the sample.

## B. CONSIDERATIONS IN EQUIPMENT DEVELOPMENT

Many geotechnical designs and subsequent constructions in the ground or with the ground necessitate proper prediction of flow through ground soil. In order to better understand the real phenomenon that may take place in soil, regarding the flow under the combined effect of different potentials, there was a need to develop appropriate equipment that would be used to simulate these potentials in the laboratory.

A triaxial test system, as shown schematically in Figure. 3.1, was developed for simultaneous application of multiple potentials or gradients to a cylindrical soil specimen under a confining pressure. These gradients, are hydraulic, chemical, thermal, and electrical gradients. They can be applied in an isolated manner or combined simultaneously with either flow allowed or not allowed through the end boundaries of a specimen.

The system has five functional units. These are loading, heating, cooling, chemical injection, and flexible - wall permeability ( Evans and Fang, 1984 ). From the operational point of view, the system is mainly a triaxial cell, with three control panels, and computer aided data acquisition as illustrated in Figure 3.2. a. Figure 3.2. b shows a photograph of the test system. Each of the system components are discussed in detail in this chapter including equipment design considerations. In addition, a detailed "Users' Manual" is provided in Appendix A, which can be used separately for this dissertation.

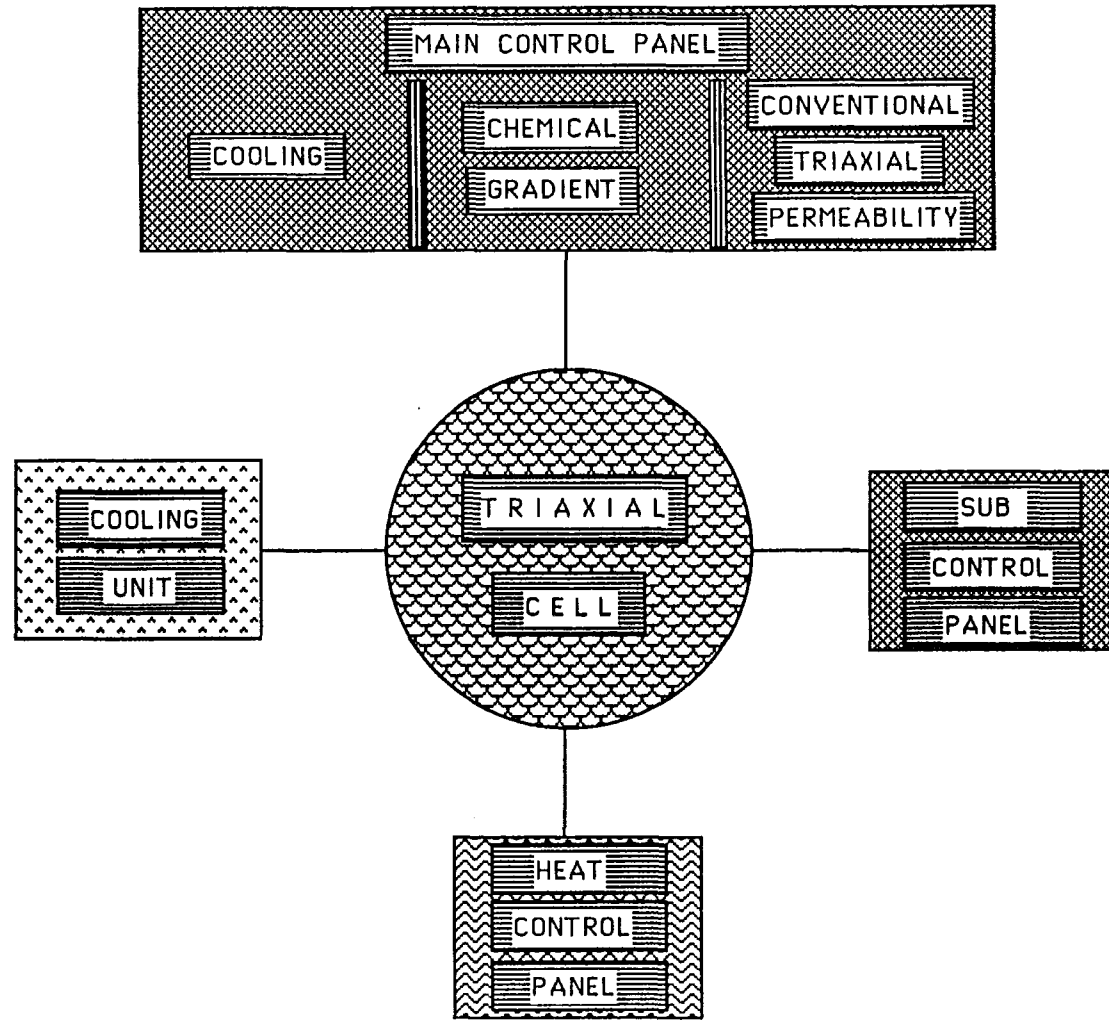


Figure 3.1 : Schematic representation of the experimental set-up.

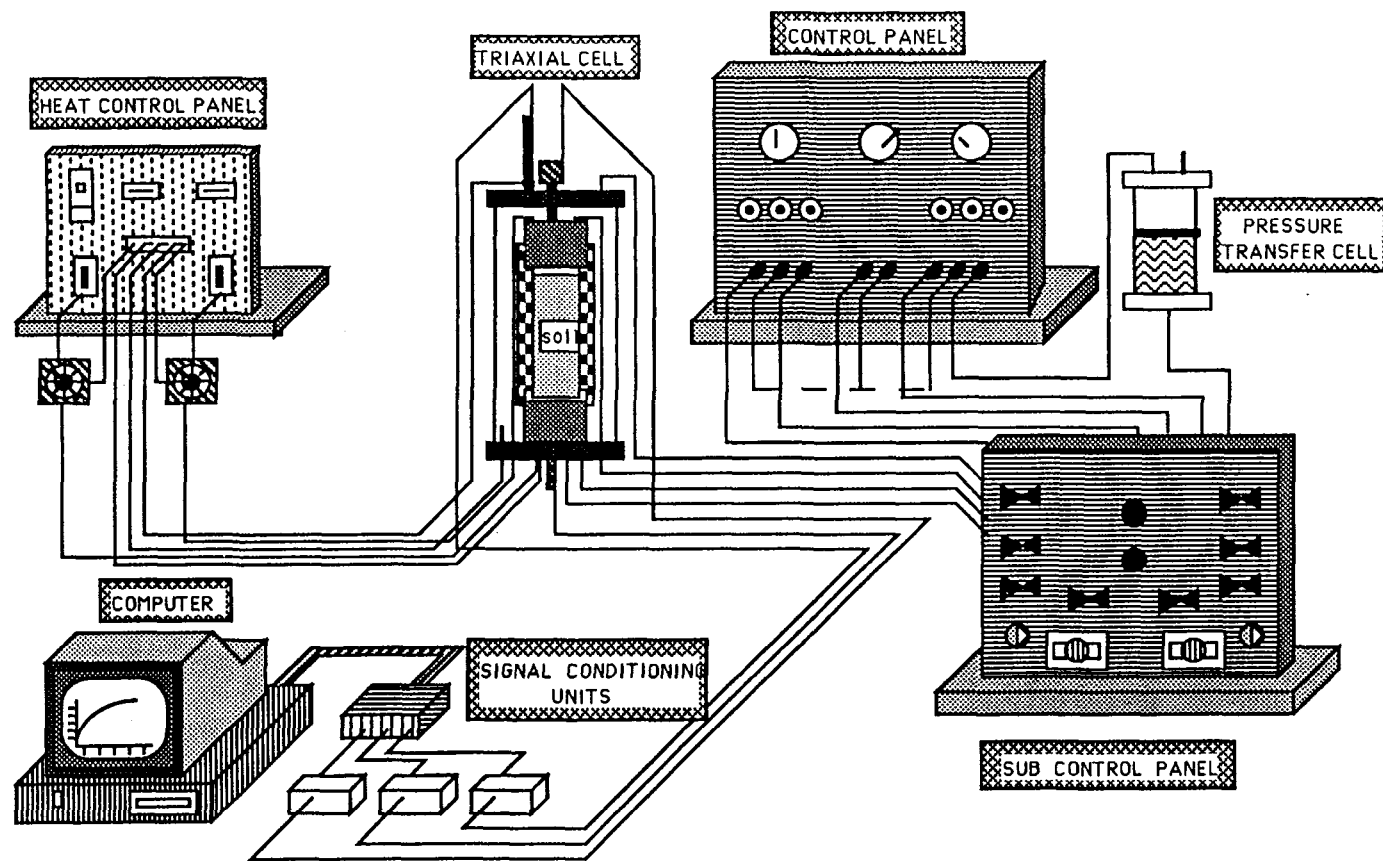


FIG. 3.2a Schematic Diagram of the experimental system.





FIG. 3.2. b: Photograph of the Entire Assembly

## 1. TRIAXIAL CELL

Soil in the field exists under three dimensional state of stress which may be referred to as the "mechanical stresses". However, in the natural subsurface environment there also exist hydraulic, thermal, chemical, and electrical potentials which may create other states of stresses. These may be referred to as "environmental stresses". The triaxial cell in this dissertation was designed to apply some of these states of stresses and their combinations. The details of this cell are shown in Figures 3.3. a and 3.3.b.

The cell essentially consists of five parts : clear acrylic tube, custom designed sample top and bottom platens and their associated attachments, and top and bottom plates to seal the cell. The maximum pressure that the cell was tested to withstand safely is 700 kPa.

**Clear acrylic tube** is sealed between the top and the bottom plates. It is 20 cm. OD, 18.75 cm. ID, and 30 cm. long. The soil specimen is placed inside this tube between the top and bottom platens. It is essentially a pressure chamber to confine the soil specimen.

**Top and bottom platens** are shown in Figures 3.4 a and 3.4 b. They are 7.6 cm in diameter and 4 cm high. These platens were designed to resist various environmental effects such as high and low pH and temperature. They were made out of a light material called Micarta<sup>R</sup> which possesses high strength, low coefficient of thermal expansion, and low thermal conductivity. The properties of this material are given in Table 3.1.a. The platens accomodate thermofoil heaters, thermocouples , and carbon electrodes. Heaters were selected to generate high temperature and resist high compressive strength, and also various pH environments. They are thin, flexible heating elements consisting of an etched-foil resistive element laminated between layers of flexible insulation. Two thermocouples, are mounted on each platen, and they are connected to a temperature control unit. These 0.10 cm diameter junction thermocouples assure precise temperature measurement. The properties of thermofoil heaters and thermocouples are given in Tables 3.1.b and 3.1.c, respectively. Provisions were made for carbon electrodes to be mounted on each platen to apply electrical gradient. However, this option was not used in this study.

**Table 3.1 Physical properties of some of the material used in the triaxial cell**

Micarta <sup>R</sup> Nema grade C, cloth base	Thermal Conductivity  °F/in	Thermal Expansion Coeff.  in / in °C	Tensile Stress  psi	Compres. Stress  psi	Flexural Stress  psi	Shear Stress  psi
	7 x 10 <sup>-4</sup>	3.95 x 10 <sup>-5</sup>	11,000	40,000	19,000	11,000

\*R- Westinghouse Electric Corporation, Micarta Division, Hampton, S.C. 29924.

**( a ) Platens**

THERMOFOIL HEATER	Width  in	Length  in	Insulation Material	Heating Element	Resistance  ohms	Supply Voltage Volts
	0.10	12	Kapton	Fine wire	27	45 (max)

**( b ) Thermofoil heater**

THERMOCOUPLES	Insulation	Wire Diameter in	AWG Gage	Calibration	Length in
	teflon	0.010	30	K	36

**( c ) Thermocouples**

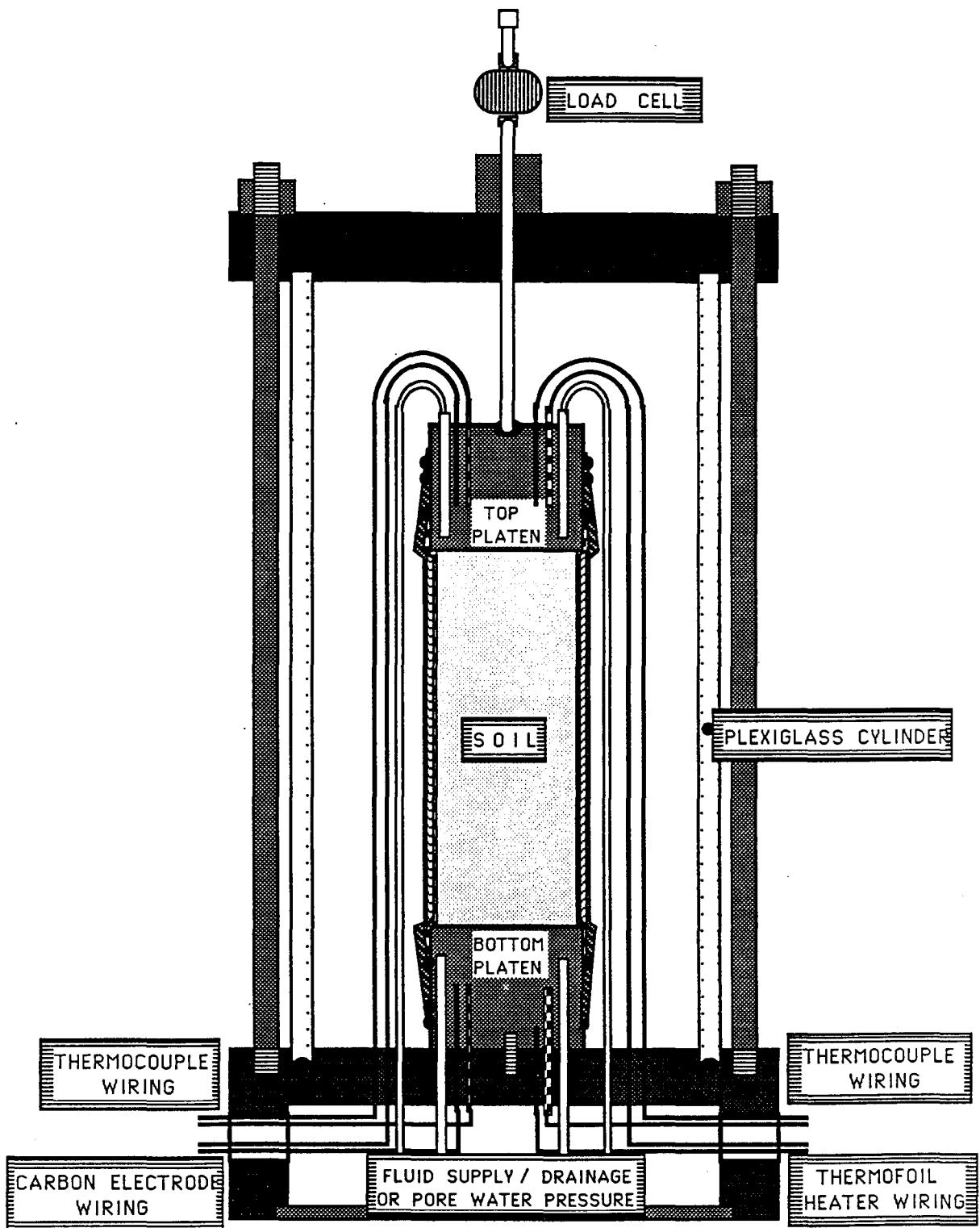


FIG. 3.3.a : Schematic Representation of Triaxial Assembly

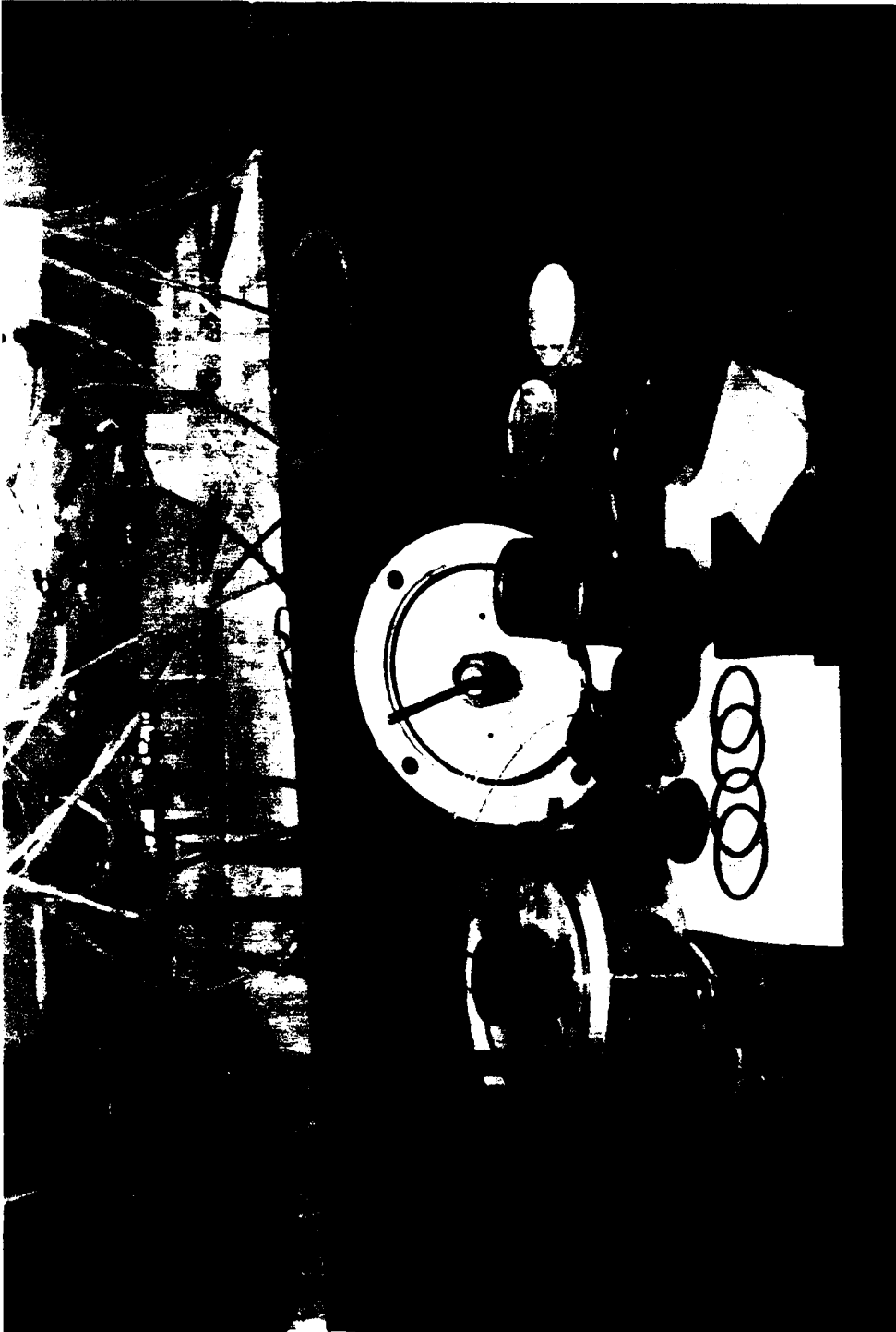


FIG. 3.3.b: Photograph of the Platens and other Triaxial Cell Accessories

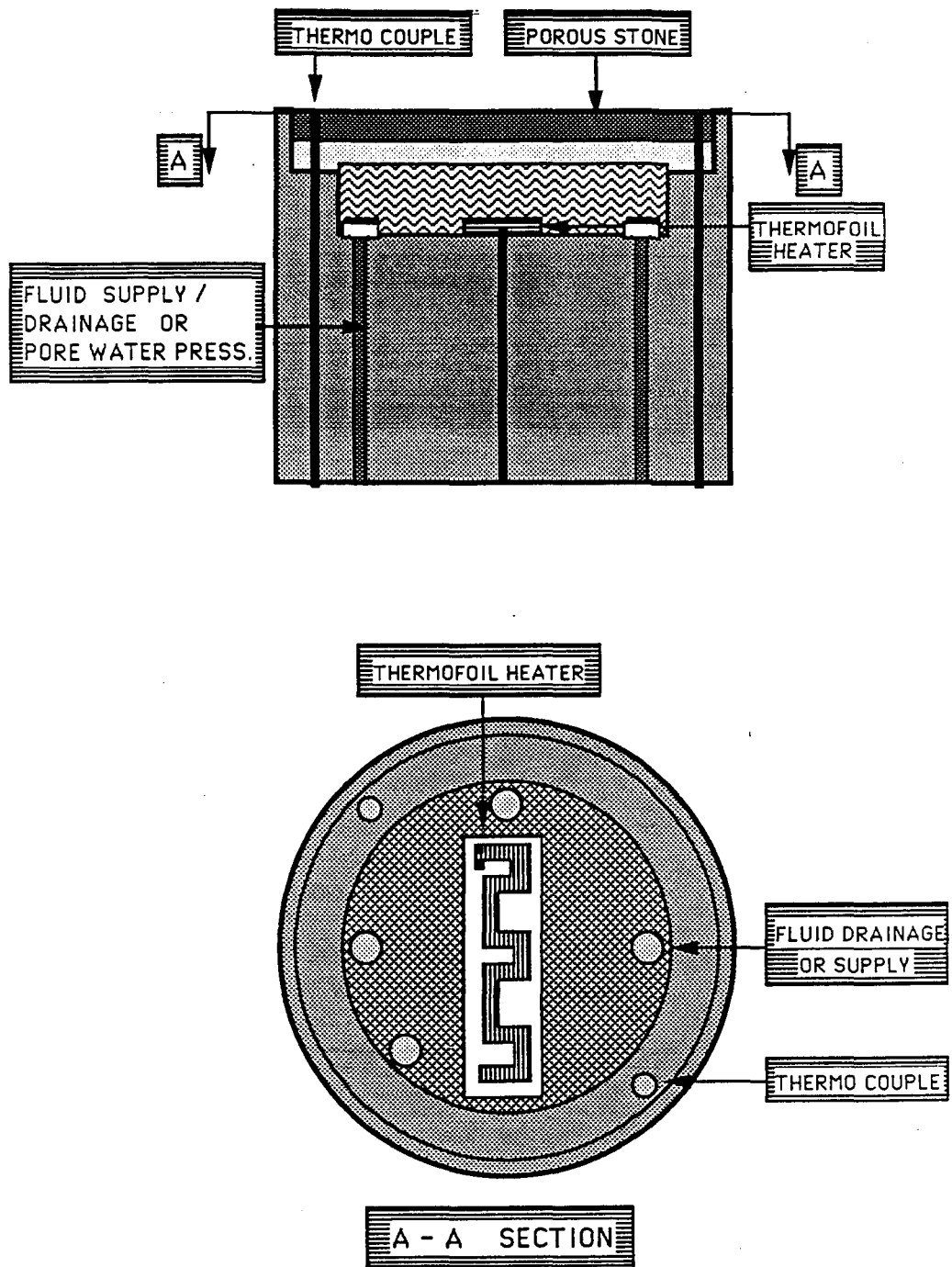


Figure. 3.4.a Schematic Diagram of the End Platens

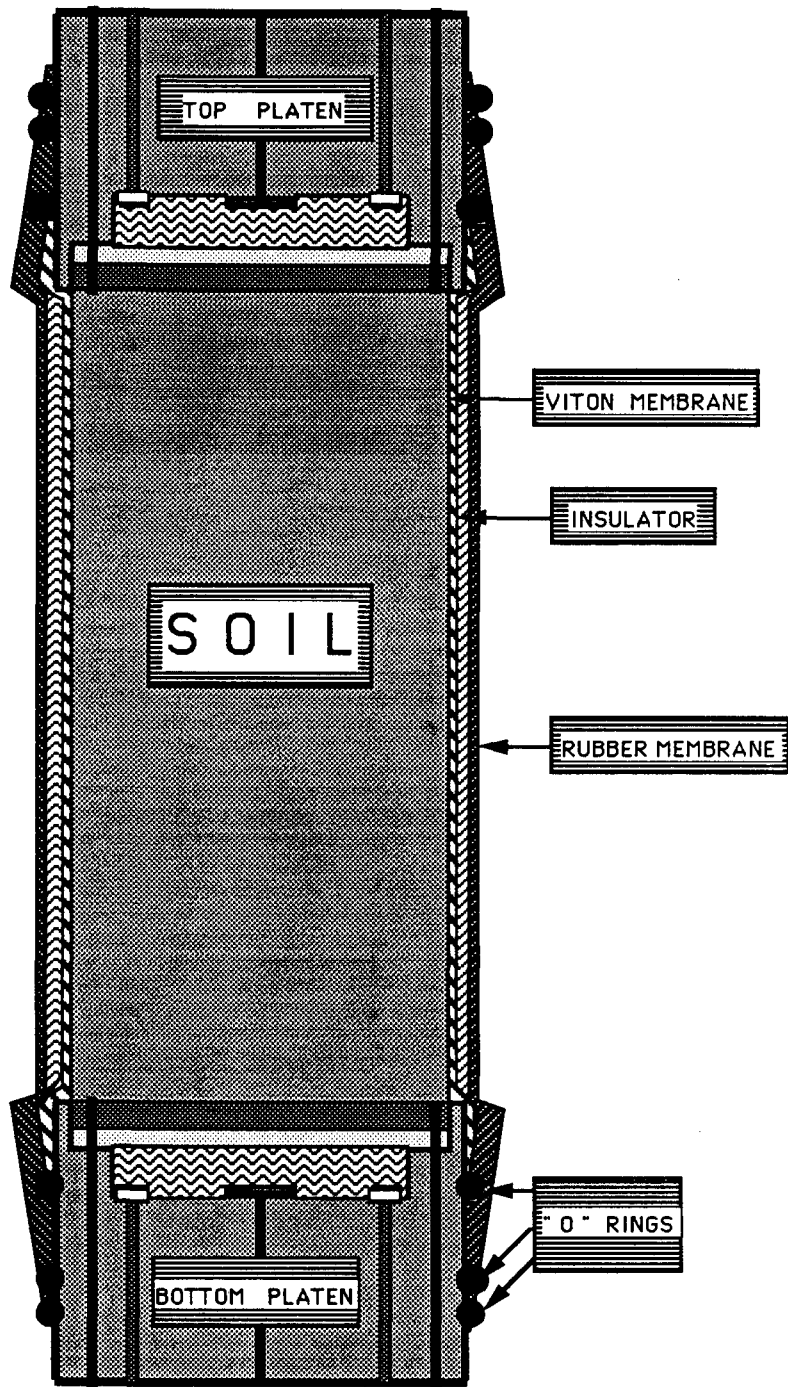
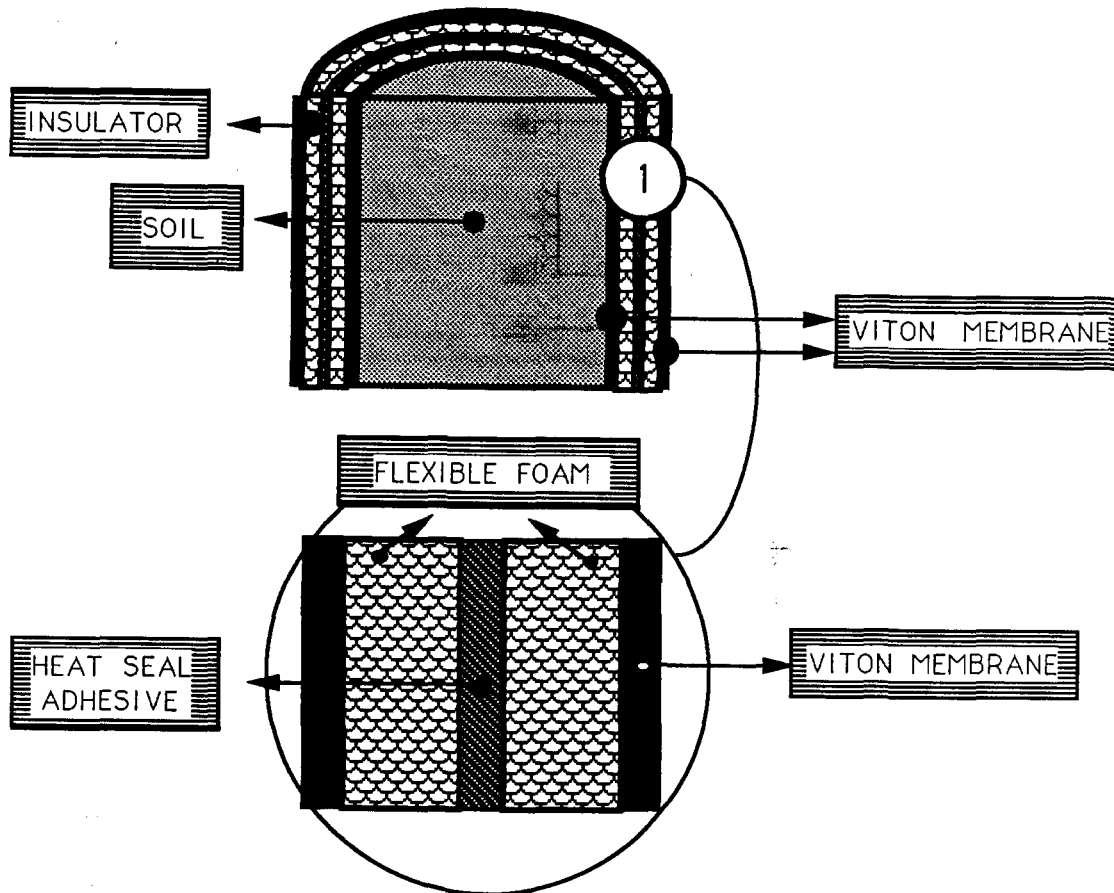


Figure 3.4.b Schematic Representation of a Soil Sample in Mounted Between the Platens

An insulator is used in between two plastic ( VITON ) membranes around the soil specimen to prevent heat transfer between the soil specimen and the cell water. The details of this configuration are given in Figure 3.5. The insulator consists of three layers: two flexible foam layers and in between a layer of heat seal adhesive. Heat seal adhesive is melted in between the two layers of flexible foam to prevent air and water permeation between the soil and the water in the pressure cell. Each flexible foam layer contains appreciable amount of air pockets for insulation.

**Top and bottom plates**, are made of aluminum. They are clamped together with four nuts screwed onto the four aluminum rods extending along the acrylic tube. The bottom plate was designed to accomodate all the connections outside the cell ( Figure 3.3.a ). All drainage and pressure lines, thermocouple wires, and thermofoil heater wires ( a total of 11 ) connections exit through the bottom plate. The top plate accomodates the loading piston inside a frictionless gear bed.



**Figure 3.5 Detailed Representation of the Insulator**



## 2. CONTROL PANELS






### 2.1 MAIN CONTROL PANEL

The panel was designed to supply pressure to the sample ( cell pressure and back pressure) and to monitor flow through the sample. As shown in Figure 3.6, the panel consists of two standpipes ( inflow and outflow ), two pressure regulators for back pressure ( top and bottom ) and confining or cell pressure, pressure gauges; vacuum gauge, and the fluid reservoirs. Manual readings are taken from the inflow and outflow standpipes with time steps to measure flow through soil. Frequent readings help to detect leaks in the cell at any time during the process or volume change in soil when saturated specimens are tested. Furthermore, the panel design allows easy change of the permeant and filling or emptying of the standpipes. Inflow and outflow standpipes are acrylic tubing of 100 cm length, 0.656 cm ID. The reading accuracy is 0.1 cm.

The panel is equipped with pressure regulators that can accommodate pressures up to a maximum of 700 kPa (100 psi). Valves, tubings, and fittings which are in contact with the permeating fluid are constructed of teflon. Brass valves and fittings are used for pressure supply connections.

The Main Control Panel has connections to an air pressure pump, a vacuum pump, a pressure transfer cell, and a sub control panel. A pressure transfer cell is used to supply confining pressure to the triaxial cell. In the transfer cell, air pressure is transferred to water through a 1 cm thick oil layer between air and water which acts as an incompressible layer. It is calibrated to supply up to 700 kPa ( 100 psi ) pressure safely. The pressure transfer cell is also connected to a sub control panel which is discussed in the next section. A photograph of the main panel is shown as Figure 3.7 .

**LEGEND**

-  TWO WAY VALVE
-  THREE WAY VALVE
-  PRESSURE REGULATOR
-  T CONNECTION
-  ELBOW CONNECTION

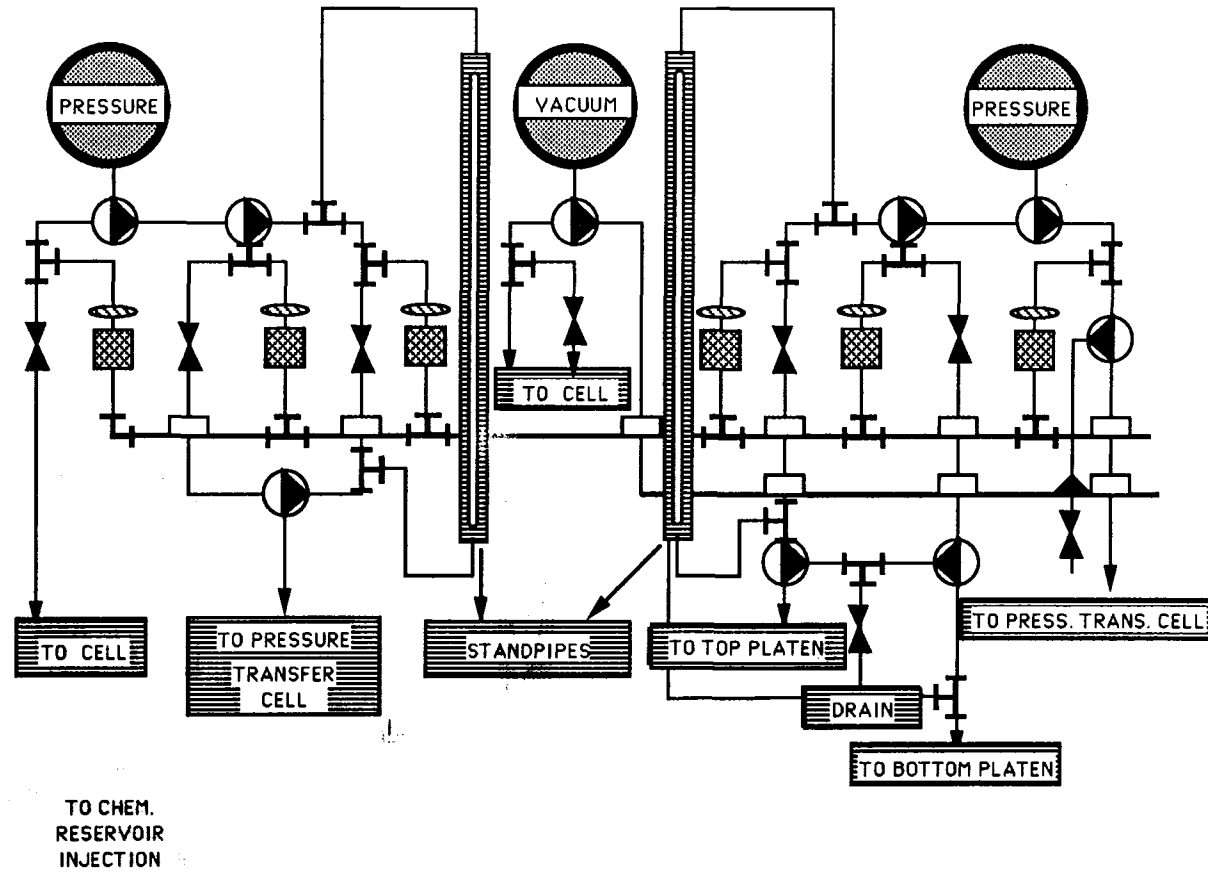


Figure 3.6 : Schematic Representation of the Main control Panel

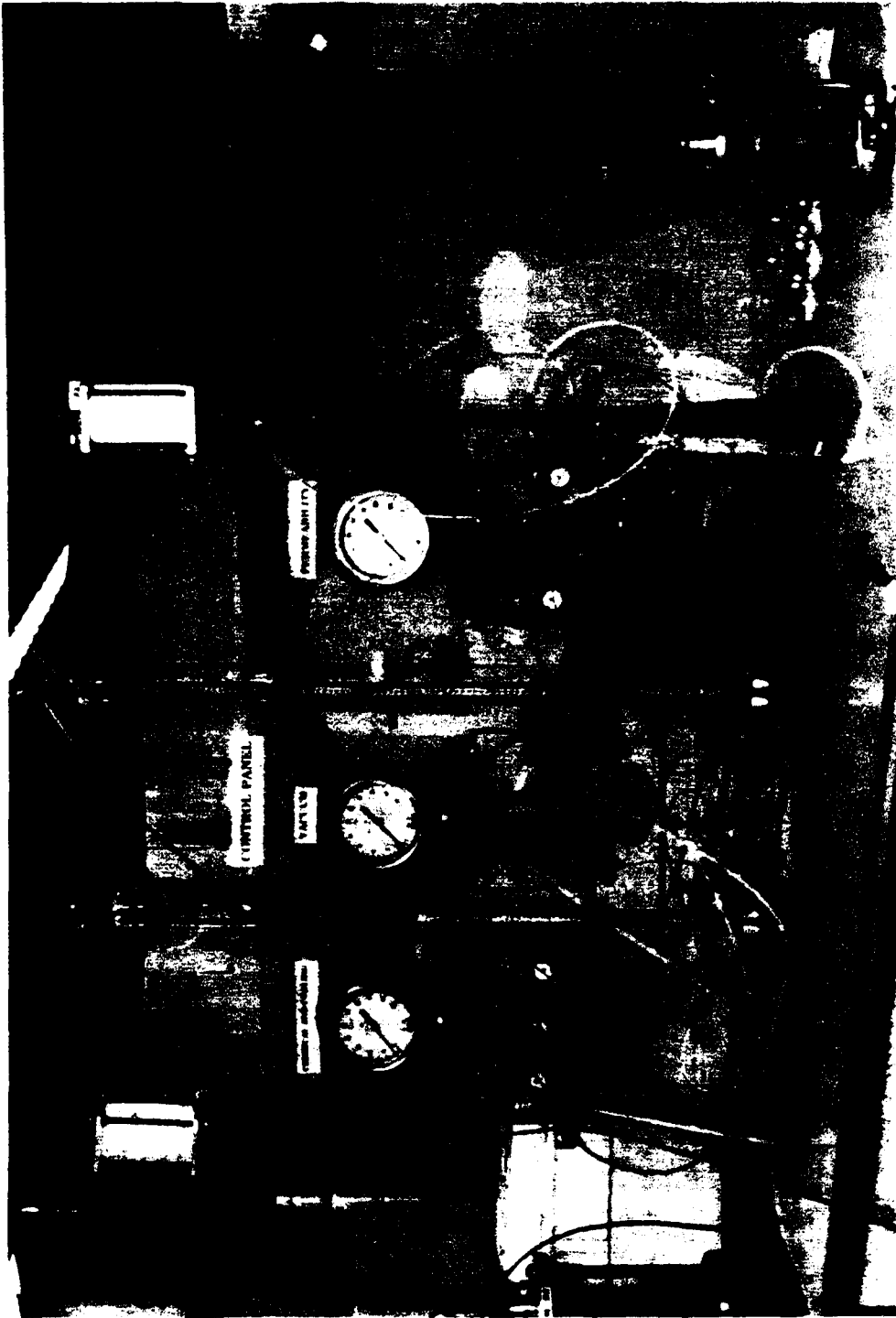


FIG. 3.7: Photograph of the Main Control Panel

## 2.2 SUB CONTROL PANEL

The sub control panel was designed to provide flexibility for filling and emptying or pressurizing the triaxial cells. It is used to supply back pressure to the specimen, connect pore water pressure transducers, or drain the inflow and the outflow tubes through the top and the bottom platens. On this panel, valves and fittings are brass and tubings are teflon. A schematic presentation and a photograph of the sub control panel are shown in Figures 3.8 and 3.9, respectively.

## 2.3 TEMPERATURE CONTROL PANEL

The temperature control panel was designed to supply voltage to the thermofoil heaters through temperature controllers. The panel consists of two temperature controllers, a thermometer, two voltage regulators, and a connection board as illustrated in Figure 3.10. A photograph of the panel is shown in Figure 3.11.

Temperature controllers are used for on / off or proportional control. The proportional band can be adjusted from 0 - 8 %, for precise control of temperature. Each unit has a manual reset adjustment to compensate offset (control bandwidth) without allowing fluctuation around a set point. Their ranges are from  $-50^{\circ}\text{C}$  to up to  $1200^{\circ}\text{C}$  with  $\pm 2.6^{\circ}\text{C}$  resolution.

A digital thermometer is used for measuring cell water and room temperatures during a test. It can display temperature differences, and store minimum and maximum values, and a reading for a later call. It has an autoranging feature, with  $0.1^{\circ}\text{C}$  resolution between  $\pm 199.9^{\circ}\text{C}$ .

Voltage regulators are used to reduce the city voltage to the required value for the thermofoil heaters. They are capable of reducing 110 V AC to as low as 5 V AC. They were also found to be very useful in adjusting constant source for a fixed temperature gradient application. This was done by increasing or decreasing the voltage until the desired temperatures were reached and stabilized.

The connection board is for the thermocouple wire connections with the

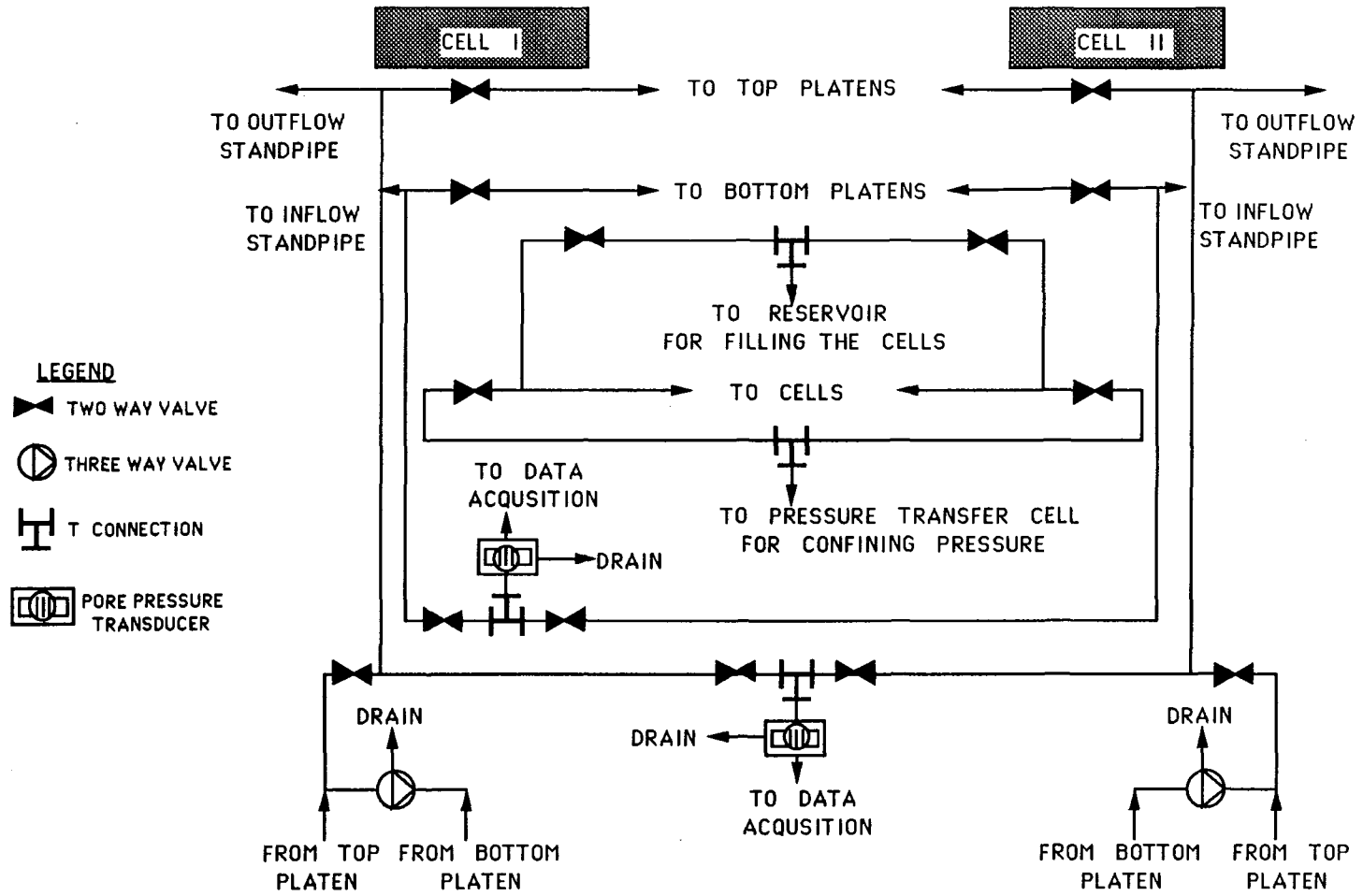


Figure 3.8 : Schematic Representation of the Sub-control Panel

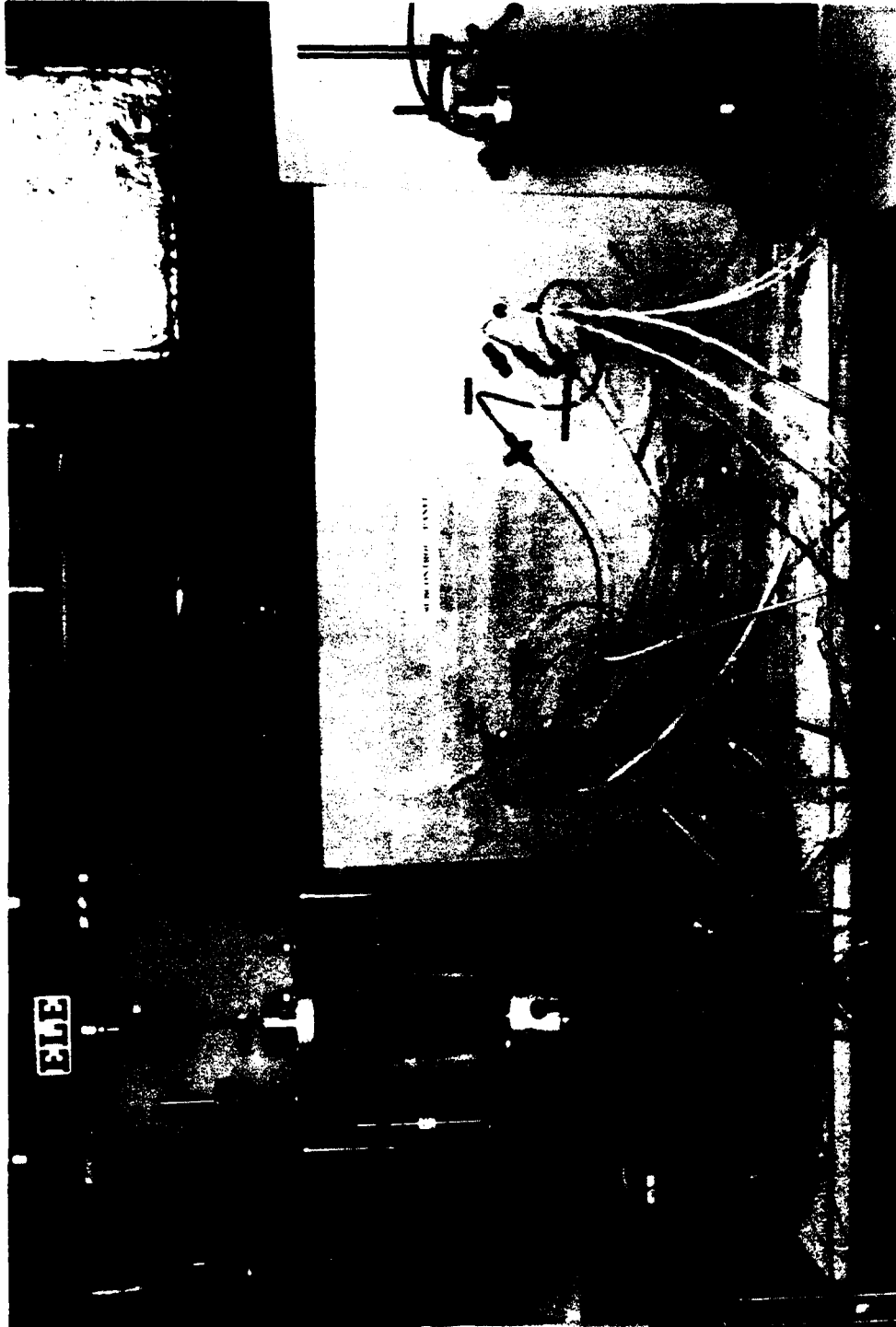


FIG. 3.9: Photograph of the Sub - control Panel

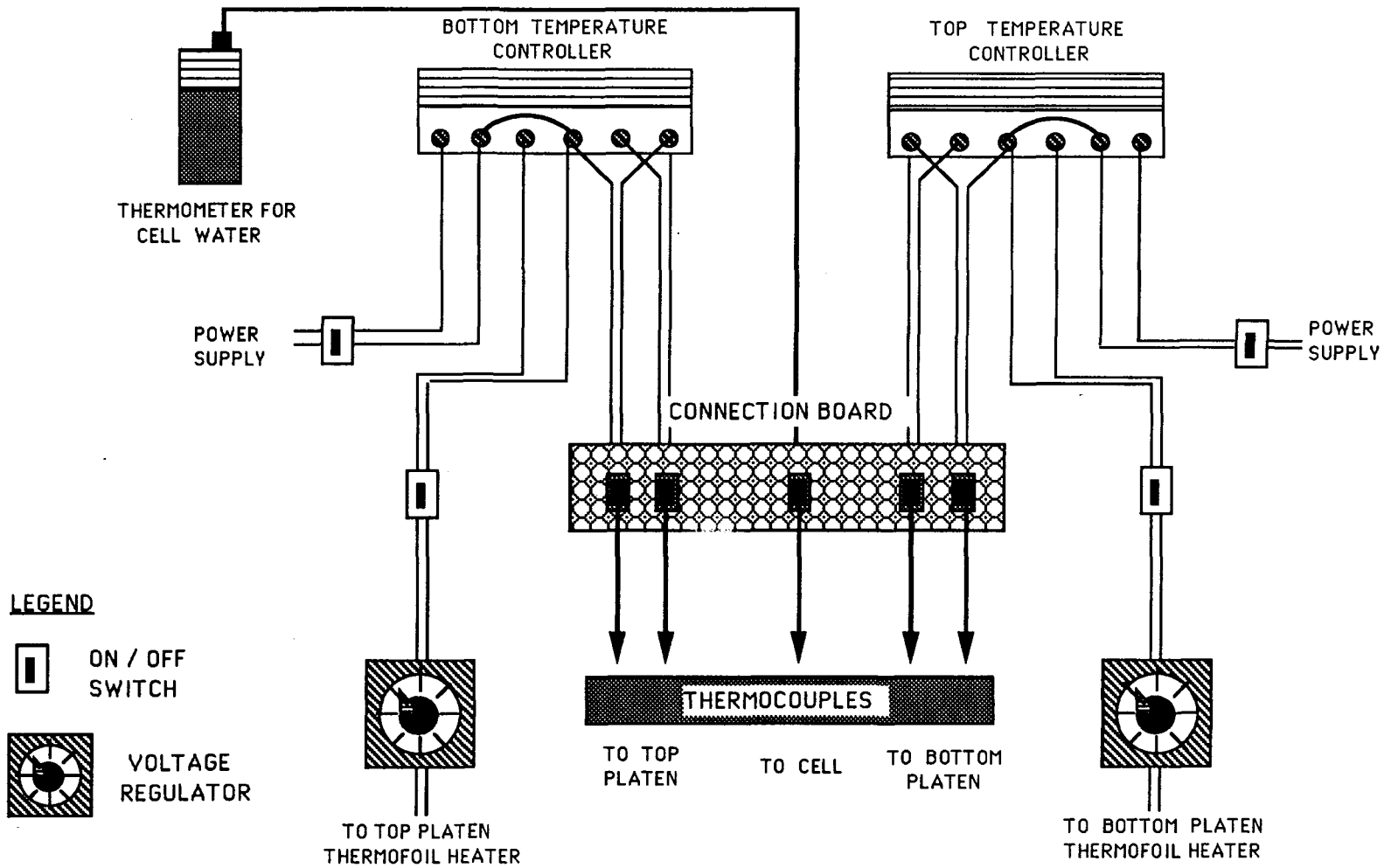


Figure 3.10 : Schematic Representation of Heat Control Panel



FIG. 3.11: Photograph of the Heat Control Panel



temperature controllers and the thermocouples inside the top and the bottom platens.

## 2.4 COOLING UNIT

The cooling unit was designed to apply low temperatures at either the ends or around a soil specimen. The unit can be used in two different ways: 1- to freeze uniformly the soil specimen. 2- to create large temperature gradients between the two ends of a soil specimen by keeping one end below room temperature. As shown in Figure 3.12, the unit has five parts. These are: an air pressure pump, a container, a pressure regulator, a rotameter, and a cooling cell. The air pressure pump is used to supply air to the unit. The container is filled with liquid nitrogen which is used to cool the air in a copper tubing. The tubing is connected to a pressure regulator. Pressurized cool air is injected into the rotameter. The rotameter is a device used to control flow rate of cool air. It is calibrated to apply the desired low temperature. When the cooling is used to freeze the entire specimen, the temperature of the confining water should be lowered also to control heat flux into the specimen.

## 2.5 COMPUTER AIDED DATA ACQUISITION

The equipment used in this research required automatic data acquisition partially. During the application of chemical and temperature gradients for which flow was not allowed through the specimen boundaries, and also during the undrained triaxial compression tests, it was necessary to measure the pore water pressures at the top and the bottom of the specimen simultaneously. The stresses and strains were also measured simultaneously in the latter case. The number of instrumentation channels was limited by the 8 input/output ports on the daughter board which was connected to the mother board inside the computer. The mother board was a TEKMAR unit with programable gain, A/D and D/A capabilities.

Pore pressures were measured with pressure transducers calibrated for the expected pore pressure range which was between 7 to 200 kPa. They were connected to signal conditioners which supplied 10 volts DC as input voltage and amplified

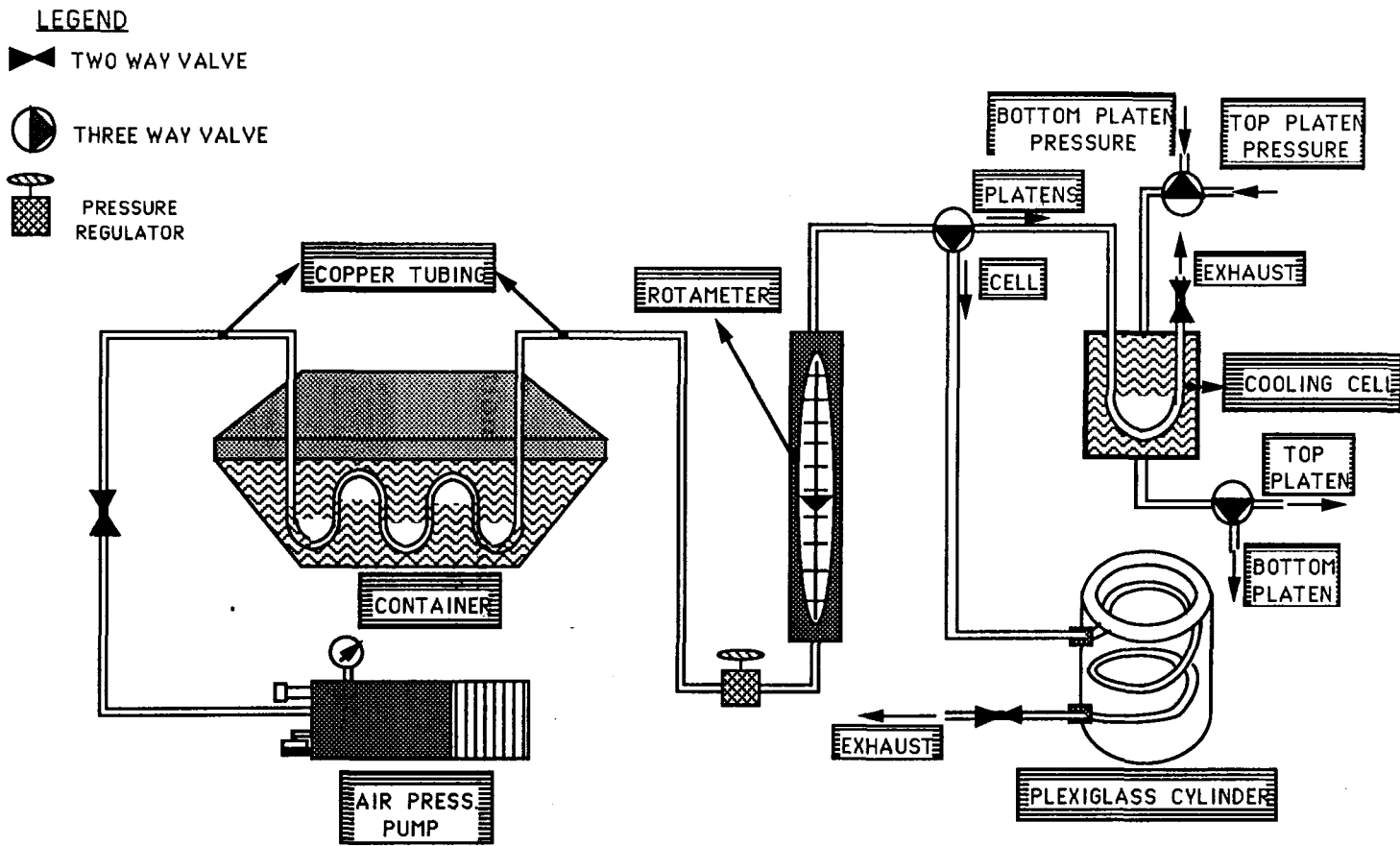


Figure 3.12 : Schematic Representation of Cooling System

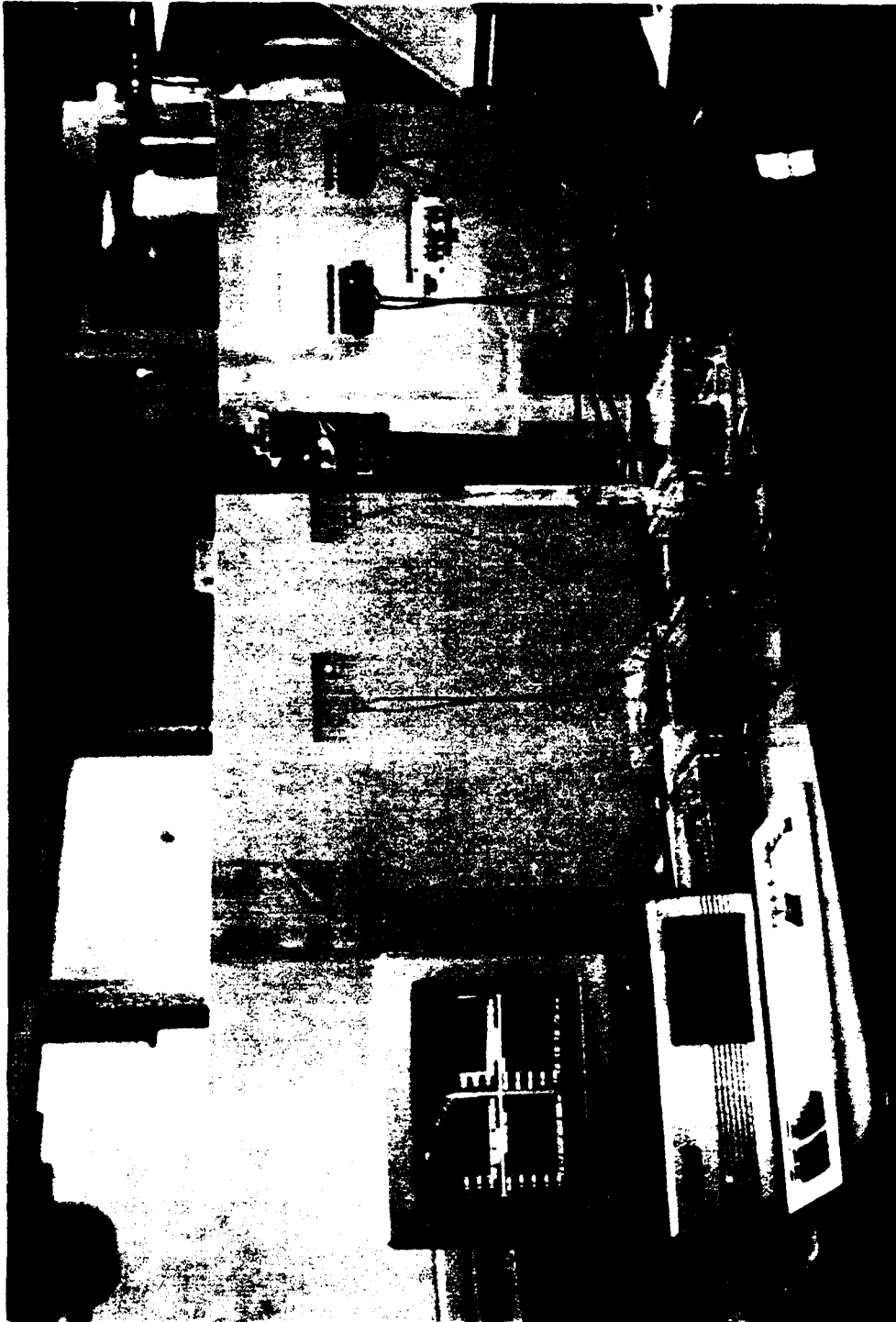


FIG. 3.13 : Photograph of the Data Acquisition System

the output voltage within 0 to 10 volts DC. The stress was monitored by a load cell mounted between the loading shaft and the loading frame. It was connected to its own signal conditioner unit which supplied 10 volts DC as input voltage and amplified the output voltage between 0 to 10 volts DC. The displacement was monitored by a linear variable differential transformer (LVDT). The LVDT was mounted on to the triaxial base. It was also connected to a signal conditioning unit which supplied 6 volts DC as input voltage and amplified the output voltage within 0 to 10 volts DC. A photograph of the data acquisition unit is shown in Figure 3.13.

A Zenith 286 computer was used for data acquisition. A computer program in C language was developed for the automatic data acquisition. This program was used to record pore pressures, load, and displacement simultaneously, and also display the data in real time in graphical format. The program is capable of displaying 8 windows of graphics, three of which are time versus corresponding voltage measurement of strain, stress, and pore pressure responses (slow, medium, and fast modes), one is strain versus stress, two are strain versus pore pressure (the top and the bottom), and also two stress versus pore pressure graphics. The source code of this program is provided in Appendix B. Commercial details about the data acquisition parts are provided in Appendix A.

### C- TESTING

In this section, a detailed explanation of the testing program is presented under the sub sections of soil sample preparation, sample set up, experiments with isolated gradients, and experiments with multiple gradients. A flowchart of the testing program is given in Figure 3.14.

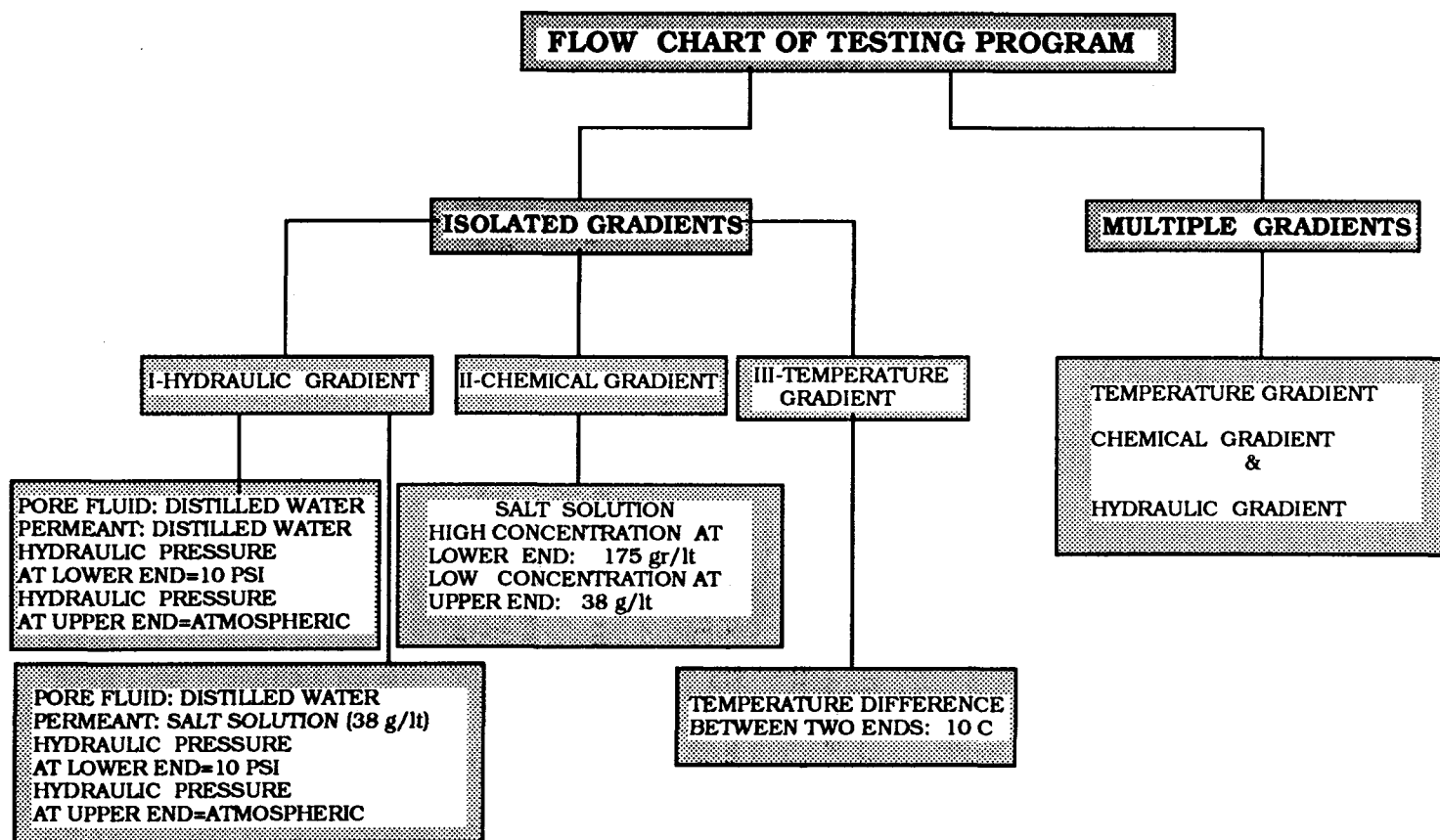
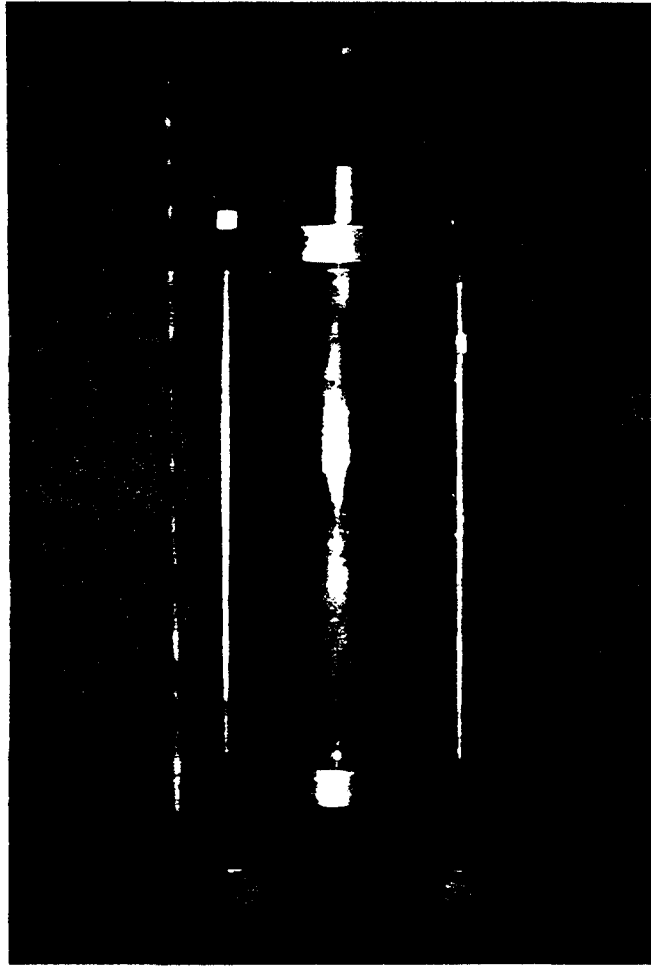
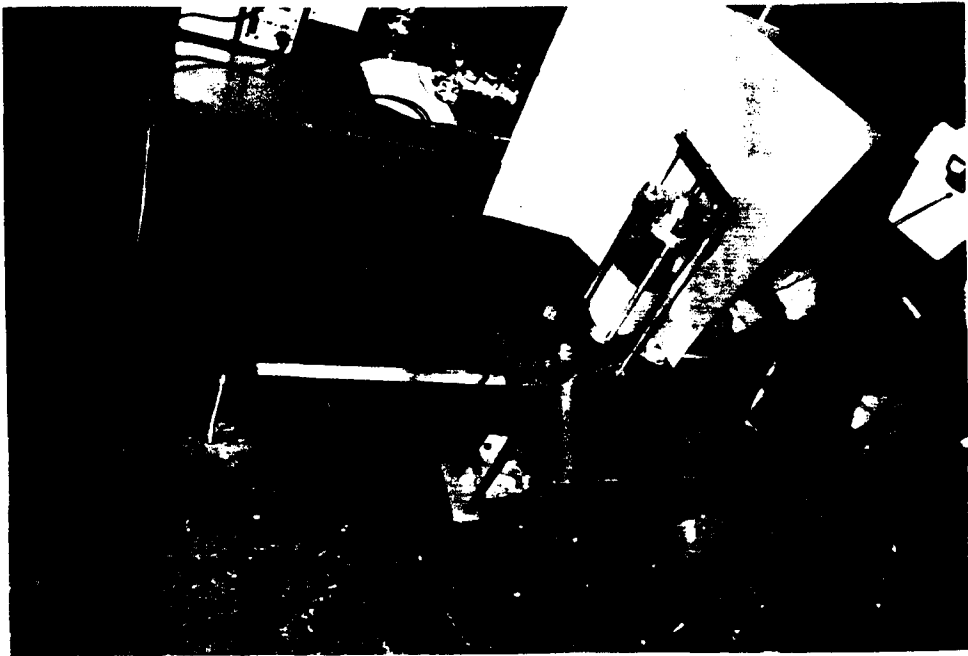


Figure 3.14: Schematic representation of the flow chart of the testing program.



**FIG. 3.15. a : Photograph of the Consolidation Cell**



**FIG. 3.15.b : Photograph of the Consolidation Equipment**

## 1- SOIL SAMPLE PREPARATION

Powdered Georgia Kaolinite was mixed thoroughly with water. The index properties of this clay were:

LL = 70 %

PI = 39 %

Gs = 2.60

Mixing was done by a tall hand held electric mixer until the mixture attained the consistency of a uniform slurry. The initial water content of the mixture ranged from 105 - 110 percent. This initial water content was adjusted so that the minimum amount of water needed was used to give the mixture a consistency which was thick enough to prevent water from leaking from inside the one dimensional consolidometers. Details of these consolidometers are shown in Figures 3.15. a and 3.15. b.

The slurry was poured into the consolidometer cell. A perforated platen was placed on top of the mixture when the slurry reached a predetermined level. This platen was attached to a one pivot cantilever load application system which amplified the magnitude of the actual hanging weight 7 times. Finally, top plate was secured on the cell, and a vertical load was applied to achieve a vertical pressure of  $0.25 \text{ kg/cm}^2$  initially. Drainage took place through the top and bottom porous stones which were in contact with the soil slurry. For each successive cycle of loading, the vertical load was increased to achieve a pressure increment in the amount of  $0.25 \text{ kg/cm}^2$ . The final consolidation pressure was  $1 \text{ kg/cm}^2$  for the first set of samples, and  $2 \text{ kg/cm}^2$  for the second set. Each loading increment duration was 48 hours. No precise volume change measurements were made during the consolidation. The 48 hours for each increment of loading was determined based on data from previous sample preparations which produced well saturated and reasonably consolidated specimens at the end of this duration.

## 2- SAMPLE SET UP

At the completion of the one-dimensional consolidation the resulting soil sample is considered a remoulded sample. It is necessary to obtain a more or less homogeneous specimen of this sample in the desired dimensions for testing in a triaxial machine. In this research, the specimens used had diameter (D) of 7.1 cm ( 2.8 in. ) and length (L) of 14 cm ( 5.5 in. ). The L/D ratio was kept at two. According to ASTM D , this is the minimum L/D ratio required for strength testing to prevent the sample end effects influencing the test.

After the mixture was consolidated under the desired vertical pressure ( 1 kg/cm<sup>2</sup> or 2 kg/cm<sup>2</sup> ) and a specimen trimmed to the desired dimensions, the soil was now ready to be placed into the triaxial cell. A selected confining pressure ( cell pressure: 100 or 200 kPa ) was applied around the specimen. Back pressures were applied from the top and the bottom platens to ensure full saturation of soil. If initially a confining pressure of 207 KPa ( 30 psi ) was applied and back pressures adjusted to 138 kPa ( 20 psi ) at the top and bottom platens, the confining pressure would then be increased by 138 KPa ( 20 psi ) to maintain the pressure equilibrium. Therefore, the overall confining pressure would now be 345 kPa ( 50 psi ). The specimen would then be left in this state for 72 hours to complete its isotropic consolidation under the effective consolidation pressure of 207 KPa ( 30 psi ). The completion of consolidation was checked by observing the rate of flow in the inflow and outflow tubes. When these rates were approximately equal, the consolidation was assumed to have completed under the applied effective pressure. The saturation was checked by B value determination which ranged from about 0.95 to 0.97 for all the specimens tested.

## 3- EXPERIMENTS UNDER ISOLATED GRADIENTS

In this study, the three gradients of interest were: hydraulic, chemical, and temperature gradients. Initially each gradient was applied separately to determine the coupled coefficient of water permeability of the clay soil under each applied gradient. Each group of tests were conducted using two different confining or cell



pressures, namely 100 kPa and 200 kPa.

3.1 **Hydraulic gradient :** First group of the experiments were the base experiments under hydraulic gradients to calibrate the equipment. The specimens were prepared using distilled water. After the 7 to 10 days of isotropic consolidation the soil specimen would reach the state of normal consolidation with zero excess pore water pressures. Hydraulic gradient was applied by increasing the bottom platen pressure by 69 kPa ( 10 psi). This created a hydraulic pressure difference of 69 kPa ( 10 psi) along the specimen. However, with the existing 135 kPa (20 psi) backpressures applied at both ends, the overall average pore water pressure would now be 172 kPa (25 psi) along the specimen. Since the average pore water pressure was increased by 34.5 kPa ( 5 psi) amount in the soil, the confining pressure was readjusted by that to 379 kPa (55 psi), to maintain equilibrium. This ensured the preservation of the applied hydraulic pressure gradient along the length of the soil. The water flow direction in these specimens is shown in Figure 3.16. The permeant was distilled water.

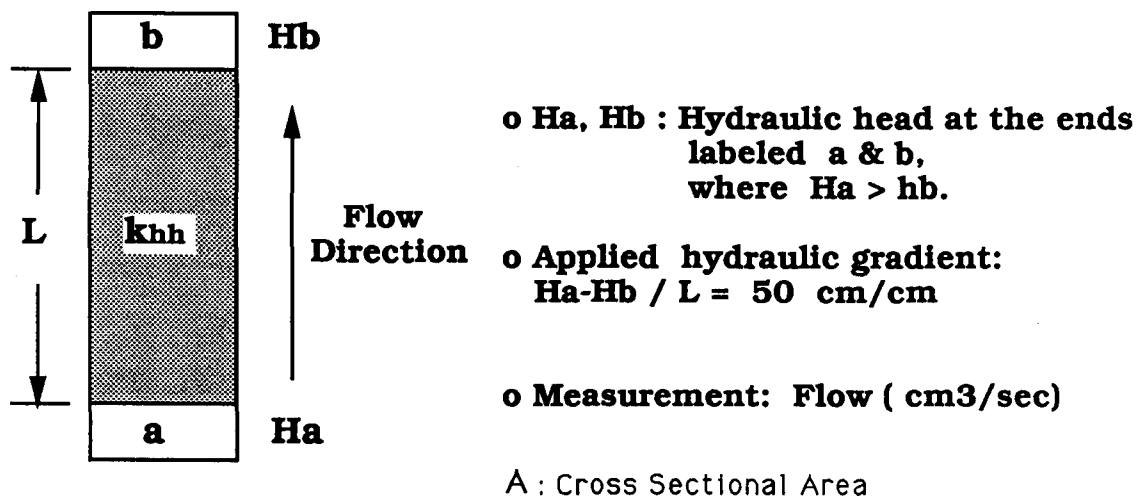


Figure 3.16: Schematic diagram of water flow situation in the specimen under hydraulic gradient.

Flow under the hydraulic gradient was allowed to continue until the water level

movement in the inflow and outflow standpipes reached a steady state with measured fluctuations less than 1% between the two standpipes.

The coefficient of permeability was calculated as below with the following boundary conditions.

Using equation 2.13, set  $T_a = T_b = C_a = C_b = 0$ , and  $H_a \neq H_b \neq 0$  measure  $Q_h$ , cumulative flow at steady-state and  $t$ , the corresponding time, then :

$$Q = k_{hh} \cdot \frac{\Delta H}{L} \cdot A \cdot t$$

where  $\Delta H = H_a - H_b$

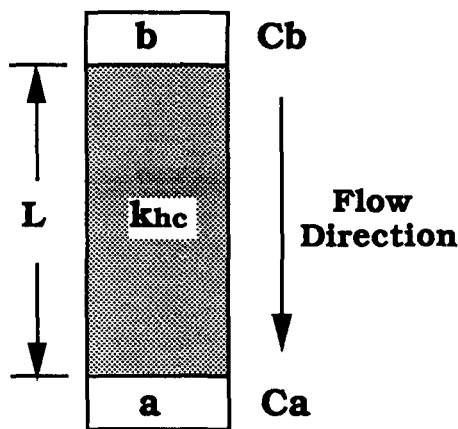
rearranging

$$k_{hh} = \frac{Q_h}{A \cdot t} \cdot \frac{L}{\Delta H}$$

The hydraulic permeability tests were also conducted using specimens slurried with salt solution (0.65 M) and permeated with salt solution of same concentration. The same steps were applied as above.

**3.2 Chemical gradient :** Second group of the tests were performed under a chemical gradient. The expected direction of water flow in the specimen is shown in Figure 3.17. Chemical gradient in one direction produces water flow in the opposite direction. This is also called "counterflow". For chemical gradient application the specimen would be prepared and conditioned using the same procedure given in the section of soil preparation. But this time, the slurry would be prepared with a selected concentration of a chemical mixed in the water. The same concentration of chemical solution would be used to fill the reservoir connected to the top platen. The bottom platen would be connected to a reservoir containing a higher concentration solution of the same chemical. The solution in this reservoir would be replenished periodically to maintain the same chemical gradient throughout a test.

Using NaCl as the solute, the Na concentration of the solution (3 M) in the bottom reservoir was checked every other day. A small sample would be retrieved from the diluted solution and first checked for significant decrease in conductivity with respect to the initial value. Depending on the magnitude of this reduction, a second check would be done by measuring the actual reduction in Na concentration. After several spot checking, it became apparent that the reservoir needed refilling with the original concentration solution as frequently as every seven days or sooner. Then the reservoir would be emptied completely and refilled with the high concentration solution. This process would be completed automatically using the external connections to the platen in approximately 10 to 15 minutes; therefore ensuring the smooth continuation of chemical diffusion as much as possible.



o  $C_a, C_b$  Chemical concentrations at the ends labeled a & b, where  $C_a > C_b$ .

o Chemical gradient:  
 $\log (C_a/C_b)/L = 0.047 \text{ cm.}$

o Measurements:  
 1) Flow ( $\text{cm}^3/\text{sec}$ )  
 or 2) Pore water pressures ( $U_a$  and  $U_b$ ) at a & b with undrained boundaries at a & b.

A : Cross Sectional Area

Figure 3.17: Schematic diagram of water flow situation in the sample under chemical gradient.

At the end of the testing, the soil specimen was immediately removed from the cell. It was then sectioned into 12 equal pieces, and a soil sample was taken from the center of each piece. Chemical analysis of Na concentration would be performed on these soil samples using Atomic Absorption Spectroscopy. The

theoretical distribution of sodium concentration along the soil was calculated using numerical solution of one - dimensional diffusion equation ( Equation 2.3 ) with effective diffusion coefficients of  $5 \times 10^{-6} \text{ cm}^2/\text{sec}$  and  $1 \times 10^{-6} \text{ cm}^2/\text{sec}$ . Figure 3.18 shows the predicted distribution of  $\text{Na}^+$  after ( 30 ) days of diffusion.

In this category of tests, two types of tests were conducted varying the boundary conditions. In the first type the valves to the standpipes were kept open so that flow of water took place under the applied gradient. This case is referred to as " DRAINED BOUNDARIES " case. In the second type of tests, the gradient was applied but the valves to the flow pipes were kept closed. Instead of flow, the pore pressures were measured in time at each end of the specimen. This case is referred to as " UNDRAINED BOUNDARIES " case.

The hydraulic permeability under chemical gradient was calculated for each set of boundary conditions as follows:

In the **drained boundaries** case , using equation 2 .13, set  $H_a = H_b = T_a = T_b = 0$  and  $C_a \neq C_b \neq 0$ , measure  $Q_h$  and  $t$ , then:

$$Q_h = -k_{hc} \cdot \frac{\log(C_a / C_b)}{L} \cdot A \cdot t$$

rearranging

$$k_{hc} = \frac{Q_h}{A \cdot t} \cdot \frac{L}{\log(C_a / C_b)}$$

In the **undrained boundaries** case , again using equation 2 .13, set  $Q_h = 0$  and  $H_a = H_b = 0$   $T_a = T_b = 0$ , and  $C_a = C_b = 0$ , measure  $U_a$  and  $U_b$ , the pore water pressures at ends **a** and **b**, respectively, then:

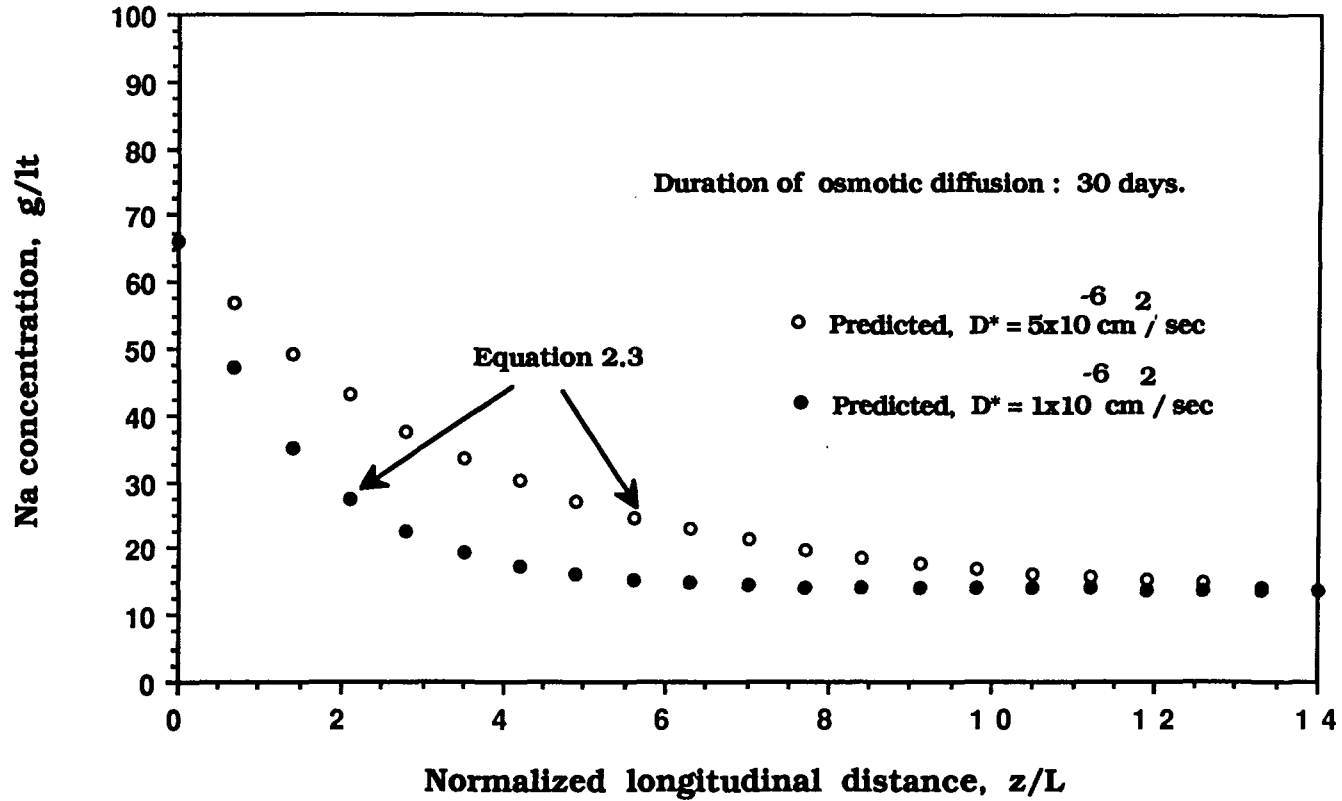


Figure 3.18 : Variation of predicted Na concentration in soil in 30 days.  
(  $D^*$  : effective diffusion coefficient )

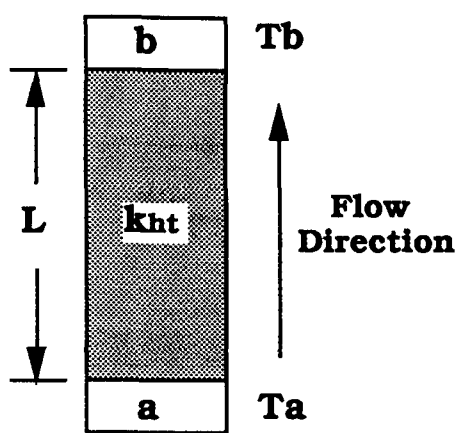
$$\Delta H = \frac{(U_a - U_b)}{\gamma_w} = -\frac{k_{hc}}{k_{hh}} \cdot \log(C_a / C_b)$$

or

$$k_{hc} = \frac{(U_a - U_b)}{\gamma_w} \cdot \frac{k_{hh}}{\log(C_a / C_b)}$$

**3.3 - Temperature gradient:** The third group of the tests were performed under temperature gradient. The expected direction of water flow is shown in Figure 3.19. Temperature gradient produces water flow from the higher temperature area toward the lower temperature area. The specimen was prepared and conditioned in the same manner as earlier. A selected level of temperature was applied at the bottom of the specimen via thermofoil heaters which was controlled by a voltage regulator. Voltage adjustments were made until the desired temperature was reached. The voltage was increased slowly while monitoring the increase in temperature at the bottom and also the temperature difference between the top and bottom platens. This was done due to the nonlinear variation of temperature with the applied voltage, and also the expected heat loss through sample wall inspite of the insulation. For example; at room temperature of 24 °C the voltage regulator was set to 10 V AC. Corresponding to this voltage the temperature at the bottom platen reached 29 °C within a few minutes while the top platen temperature remained the same as the room temperature. Consequently, the voltage regulator was adjusted to 20 V AC. Once again, within a few minutes temperature at the bottom platen reached to 34 °C. At this time, the temperature at the top platen increased to 26 °C. This process was continued with small increments of voltage until the temperature at the bottom platen reached a stable value of 39 °C and the temperature at the top platen reached to 29 °C, and stabilized. At this time the temperature in the cell water around the specimen also reached 29 °C and stabilized at that value for the duration of testing. Although

there was insulation around the specimen some heat loss did occur into the surrounding water.



o  $T_a, T_b$  temperatures at the ends a & b

o Temperature Gradient:  $\log (T_a/T_b)/ L$

o Measurements :

- 1) Flow ( $\text{cm}^3/\text{sec}$ ) with drained boundaries.
- 2) Pore water pressure ( $U_a$  and  $U_b$ ) at a and b with undrained boundaries at a and b.

A: Cross Sectional Area

Figure 3.19: Schematic diagram of water flow situation in the specimen under temperature gradient.

The insulator helped to prevent large heat losses and probably helped to achieve uniform temperature in the cell water around the specimen.

An analytical model was solved numerically with boundary conditions of fixed temperatures at the top and the bottom of the sample and heat flux allowed through its side walls. Figure 3.20 illustrate schematically these boundary conditions. Figure 3.21 shows the isotherms developed from the numerical solution of Equation 2.5 with the applied conditions. The radial gradients of temperature from the center to the sides of the specimen decreased toward the top end of the specimen. This called for a check on the validity of one dimensional uniform flow in the cross-section through the length of the sample. Numerical solution of the heat conduction equation (Equation 2.5) gave the predicted radial distribution of temperature along the length of a specimen. Figure 3.22 shows the temperature distribution along the sample length at the center, half radial distance from the center and at radial distance at steady-state. The closeness of

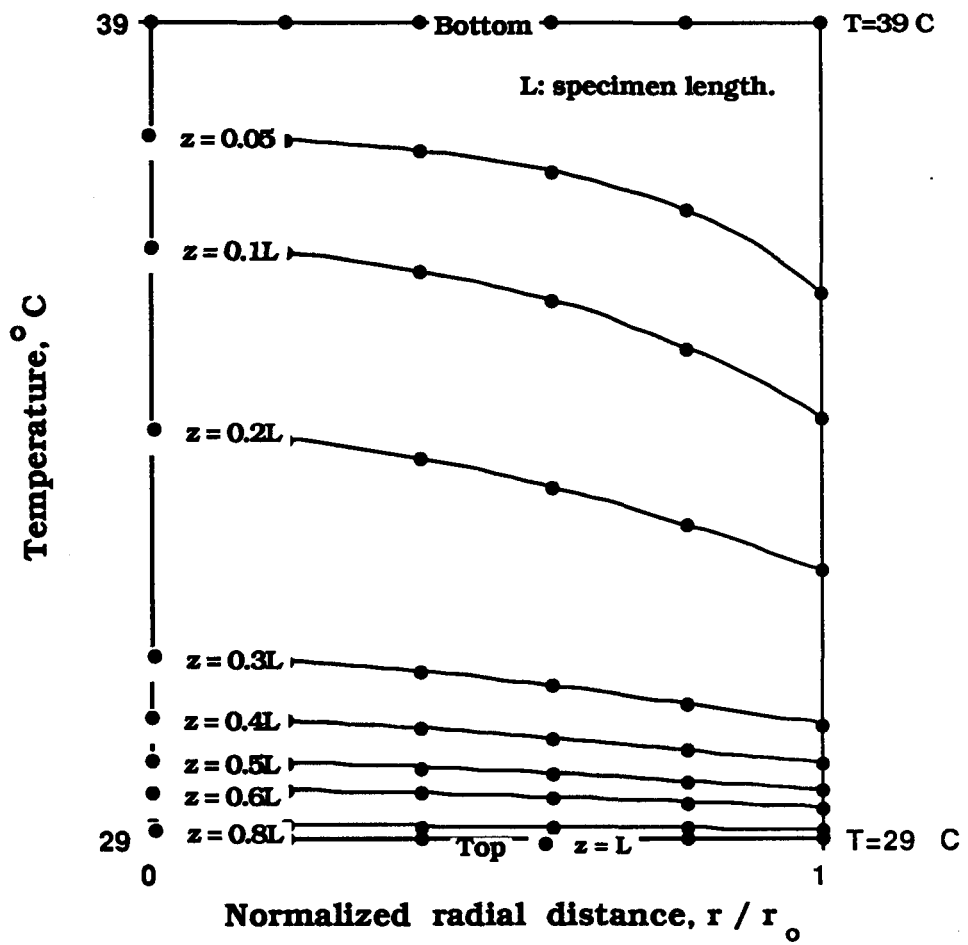


Figure 3.20 : Predicted temperature variation profiles in the radial and longitudinal cross-section.



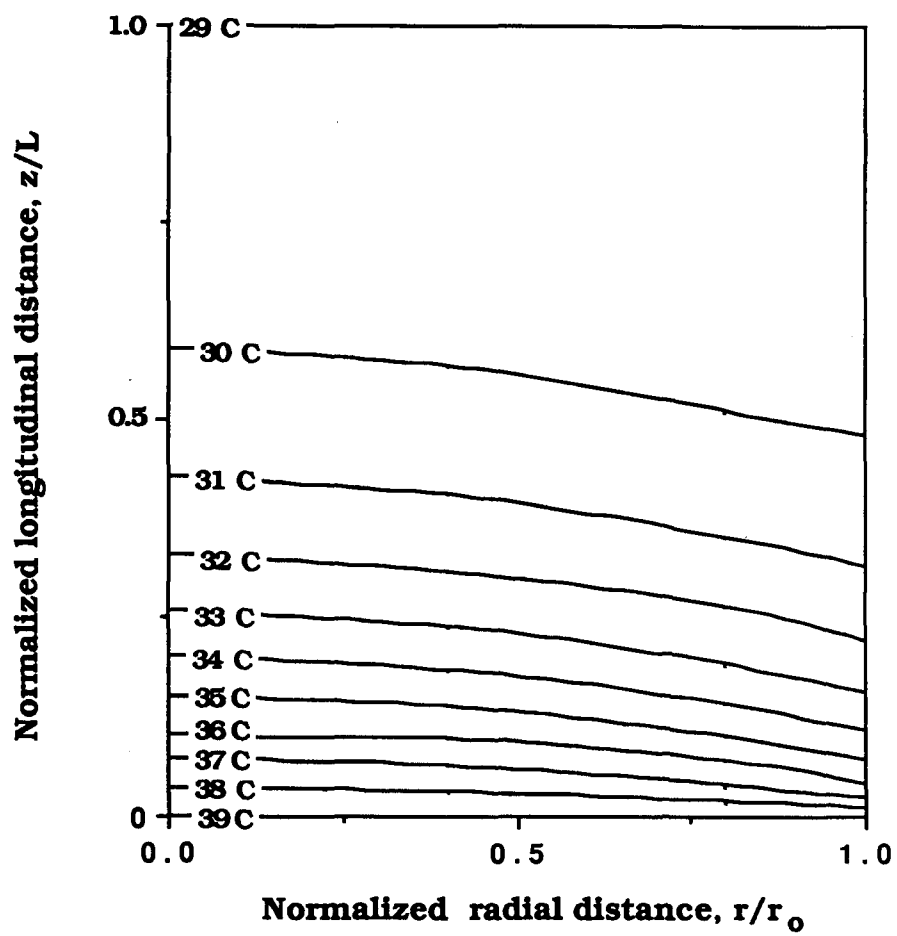


Figure 3.21 : Predicted isotherms in soil cross-section

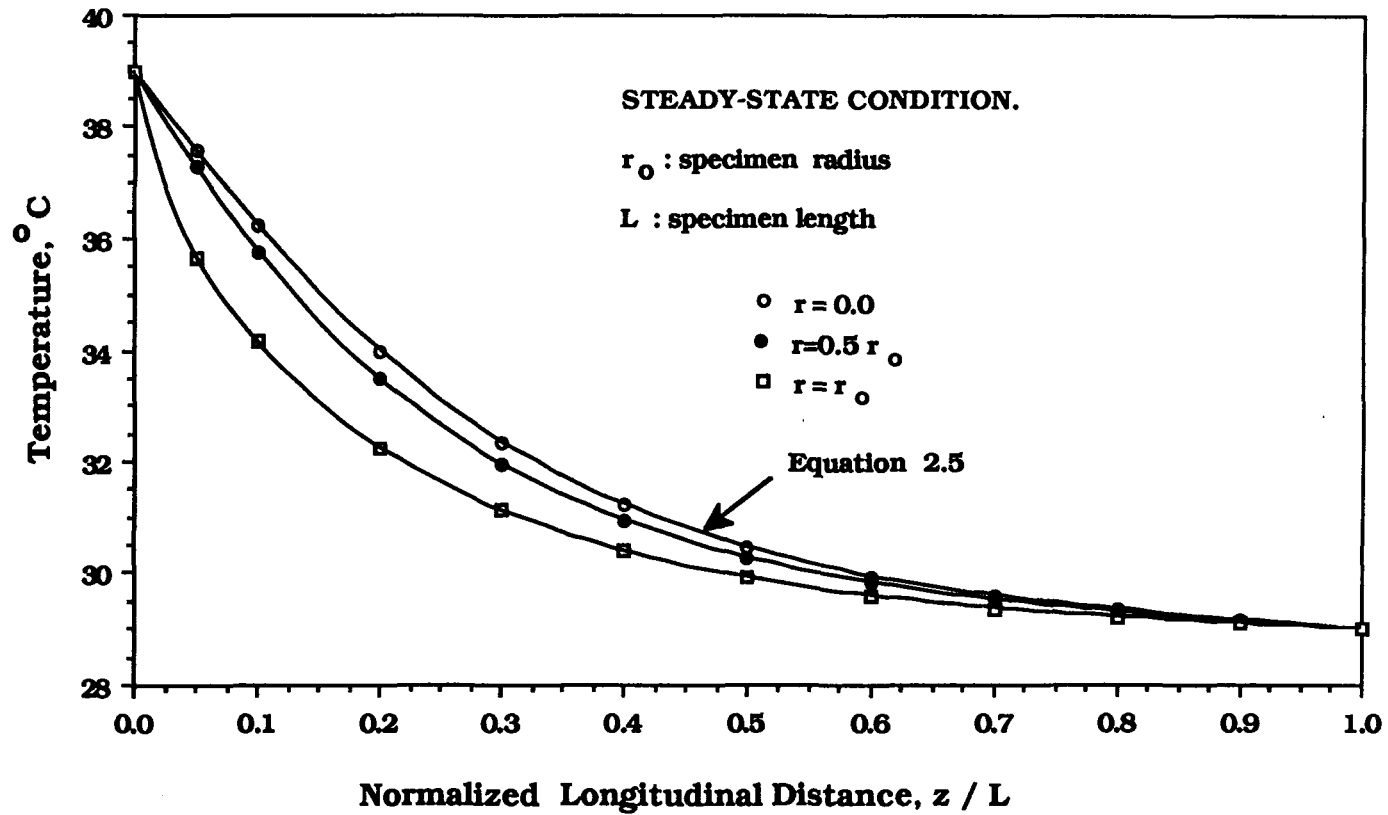


Figure 3.22 : Predicted temperature variation in soil at steady state.

these curves is a good indication that, for the 10 °C temperature difference between the two ends of the specimen the assumption of uniform flow may be warranted. For this case the largest difference between the temperatures at the center and at the radius of the specimen is approximately 2 °C, which is not significant. Due to the triaxial confinement the tendency for radial flow was probably released by upward flow which strengthens the assumption of uniform flow in one direction.

After the establishment of a constant 10 °C temperature difference between the two ends of the specimen, inflow and outflow standpipe readings were taken until the rate of flow reached a steady state and the difference in flow rate readings between the two standpipes was below 1 %. Once again, tests with two different boundary conditions were conducted and coefficient of permeabilities were calculated for each case.

In the " DRAINED BOUNDARY " case, using the equation 2.13, set  $H_a = H_b = C_a = C_b = 0$  and  $T_a \neq T_b \neq 0$ , measure  $Q_h$  and  $t$ , then :

$$Q_h = k_{ht} \cdot \frac{\log(T_a / T_b)}{L} \cdot A \cdot t$$

rearranging

$$k_{ht} = \frac{Q_h}{A \cdot t} \cdot \frac{L}{\log(T_a / T_b)}$$

In the " UNDRAINED BOUNDARY " case, using equation 2.13, set  $Q_h = 0$  and  $H_a = H_b = 0$ ,  $C_a = C_b = 0$ , and  $T_a = T_b = 0$ , measure  $U_a$  and  $U_b$ , then :

$$\Delta H = \frac{(U_a - U_b)}{\gamma_w} = - \frac{k_{ht}}{k_{hh}} \cdot t$$

rearranging

$$k_{ht} = \frac{(U_a - U_b)}{\gamma_w} \cdot \frac{1}{k_{hh} \cdot \log(T_a / T_b)}$$

#### 4- EXPERIMENTS UNDER MULTIPLE GRADIENTS

This constituted the second phase of the experiments. The "multiple gradients" mean the combined application of more than one gradient simultaneously. The specimens would be conditioned by the same procedure discussed under soil sample preparation with slurry prepared with 0.65 M NaCl solution as the mixing water. The experiments were conducted according to the following steps: 1) the top platen was filled with the same concentration solution as in the mixing water of the specimen while the bottom platen was filled with a higher concentration solution of the same salt, 2) the hydraulic gradient was applied by increasing the bottom platen pressure, and 3) the temperature gradient was applied by increasing the temperature at the bottom of the specimen.

In multiple gradient experiments only drained boundaries condition was applied. The flow per unit time was measured and experiments were ended after a steady state flow was achieved with less than 1% difference in the measured flow rates in inflow and outflow tubes. Once again the confining pressure was varied from 100 kPa to 200 kPa with samples consolidated under the respective consolidation pressures.

## 5. UNDRAINED TRIAXIAL SHEAR STRENGTH

Triaxial (CIU) shear tests were conducted on the specimens as soon as the flow (drained or undrained boundary) tests were terminated. The termination criterion for the drained boundary tests was the establishment of steady state flow with less than 1% difference between the measured rates of flow in the inflow and outflow tubes. The termination criteria for the undrained boundary case was establishment of constant pore water pressures at the ends of the specimens. Obviously the latter tests took much less time the former ones which were continued up to 30 days.

The triaxial tests were conducted according to ASTM specifications in D 4767. The load, deformation and pore water pressure at the top and bottom ends were measured with time. The strain was adjusted to 0.00075 cm/min. When testing the specimens which were subjected to pore water pressure built up initially by the temperature or chemical potentials, these pressures were not released prior to the triaxial testing. Therefore, these samples possessed an average initial pore water pressure.

### D. COMPRESSIBILITY

The pore pressure measurements during triaxial testing prompted the following analysis. There appeared to be a typical lag time between the measured pore pressures at the bottom and the top during triaxial shear test of the specimens subjected to different potentials. The rate of migration of water pressure from the top where the load is applied, to the bottom of the specimen appeared to be influenced by the physical changes induced with the potential applications. This observation prompted the idea to develop a quick and fairly consistent method of estimating the coefficient of consolidation ( $C_v$ ) for these soils, which would probably be very difficult to do by conventional methods without physically disturbing the soil specimens. Before discussing the actual procedure of determination of  $C_v$  proposed in this dissertation, a short review of the pertinent theoretical background will be presented below.

## 1. TERZAGHI'S ONE DIMENSIONAL CONSOLIDATION THEORY

Terzaghi made the following assumption to develop his theory of one-dimensional consolidation :

1. The soil is homogeneous and 100% saturated.
2. Drainage is provided at both the top and the bottom of the compressible layer.
3. Darcy's law is valid.
4. The soil grains and water are incompressible.
5. Compression and flow are one dimensional.
6. The small load increment applied produces essentially no change in thickness ( that is, small strain ), and coefficient of permeability,  $k$  and compressibility,  $a_v$  remain constant.
7. There is unique linear relationship between the volume change and the effective stress.

Basically, Terzaghi's one-dimensional equation ( Equation 3.1 ) is a form of the diffusion equation. He adopted the closed form solutions for heat transfer problems to the consolidation problem, such that :

$$C_v \frac{\partial^2 u}{\partial z^2} = \frac{\partial u}{\partial t} \dots\dots\dots( 3.2 )$$

where ,  $z$  : distance

$u$  : pore pressure

$t$  : time

$C_v$  : coefficient of consolidation

The boundary and initial conditions for the case of one dimensional compression as follows :

1. There is complete drainage at the top and bottom of the compressible

layer.

- The initial excess hydrostatic pressure  $u_i$  is equal to the applied increment of stress at the boundary.

These boundary and initial conditions can be written as :

at  $z=0$  and at  $z=2H$ ,  $u=0$

when  $t=0$ ,  $u = u_i = (\sigma_1 - \sigma_3) = \text{deviatoric stress.}$

The general solution of Equation 3.1 when the initial excess pore pressure

$u_i$  is a function of the depth  $z$ , is :

$$u = \sum_{n=1}^{\infty} \left( \frac{1}{H} \int_{z=0}^{z=2H} u_i \sin \frac{n\pi z}{2H} dz \right) \sin \frac{n\pi z}{2H} \exp \left( \frac{-c_v t n^2 \pi^2}{4H^2} \right) \dots\dots\dots (3.3)$$

where  $u_i$  : pore pressure at step  $i$ ,

$H$  : drainage length of specimen,

$n=1,2,\dots$

When  $u_i$  is constant or varies linearly with depth, the solution becomes

$$u = (\sigma'_3 - \sigma'_1) \sum_{n=0}^{\infty} \frac{4}{(2n+1)\pi} \sin \left( \frac{2n+1}{2} \pi \frac{z}{H} \right) \exp \left[ \frac{-(2n+1)^2 \pi^2 c_v t}{4H^2} \right] \dots\dots\dots (3.4)$$

The solution of Equation 3.4 provides the instantaneous value of the pore water pressure  $u$  at any specified time and point in the soil mass. The only part of Equation 3.4 that is a function of the soil properties is  $c_v$ , the coefficient of consolidation.

2. DETERMINATION OF THE COEFFICIENT OF CONSOLIDATION,  $C_v$   
FROM ONE-DIMENSIONAL CONSOLIDATION TEST

One dimensional consolidation is performed by compressing a soil specimen in a device called an oedometer. During the consolidation test, vertical deformation measurements are made in time under a sustained load. The coefficient of consolidation,  $C_v$  is determined from the time - deformation data. There are a few methods that can be used to determine the value of  $C_v$ . One of them is Casagrande's logarithm of time method. In this method, the deformation measurements are plotted versus the logarithm of time. The time corresponding to 50 % consolidation of the soil sample is used to calculate the coefficient of consolidation by equation 3.5.

$$C_v = \frac{T_{50} H_{dr}^2}{t_{50}} \dots\dots\dots (3.5)$$

where,  $T_{50}$  : dimensionless time factor (= 0.197)  
 $H_{dr}$  : the maximum drainage length (= 1/2 specimen height)  
 $t_{50}$  : the time for 50 % consolidation.

3. DETERMINATION OF COEFFICIENT OF CONSOLIDATION,  $C_v$  FROM  
PORE PRESSURE DATA OBTAINED USING THE NEW TESTING SYSTEM

During the CIU triaxial strength tests, pore water pressures were measured at the the top and the bottom ends of the specimens. One important phenomenon observed was that a particular magnitude of pore pressure generated at top end of the specimen transferred to the bottom of the specimen at a certain rate for each type of specimen tested. The elapsed time for each measured magnitude of pressure to arrive to the bottom end is related to the compressibility



characteristics of the specimen during the triaxial shear. Based on the laboratory information and Terzaghi's equation for consolidation an attempt to calculate the coefficient of consolidation,  $C_v$ , was made with the following assumptions:

1. Because of the small strain constraint of consolidation theory, only pore pressures measured below 1 % strain level are used for  $C_v$  calculation.
2. The pore pressure distribution is assumed linear along the specimen below 1 % strain.
3. pore pressure migration rate is assumed constant below 1 % strain.

### 3.1 CALCULATION OF $C_v$

Considering Equation 3.4, all the parameters in that equation except  $C_v$  are known in time steps from the triaxial shear tests. Based on the assumption of constant rate of migration of pore pressure at small strains, the elapsed time for each measured value of the pore pressure to reach to the middle of the specimen was taken as half the time it would require to reach the bottom. The deviatoric stress in Equation 3.4 was taken as the vertical stress corresponding to the top end pore water pressure.

Using an iterative numerical approach and trial and error, the coefficient of consolidation values were calculated for each specimen tested. The  $C_v$  values calculated using this method were compared to those values obtained from conventional consolidation tests for distilled water mixed samples. These showed good agreement as will be discussed in the next chapter. Based on this finding, the  $C_v$  values were also calculated for the soil specimens subjected to potentials using the same method.

## CHAPTER IV

### EXPERIMENTAL RESULTS

#### A. INTRODUCTION

In the previous chapter, a detailed description of the equipment, methods for testing and sample preparation were presented. In this chapter, the results for the two sets of comparative flow experiments which are characterized by the consolidation pressure of soil samples are presented. Also reported are the results pertaining to the use of the new test system in predicting the coefficient of compressibility for saturated clay subjected to coupled flow of water.

The first set of results reported in this Chapter are those obtained from the coupled flow experiments under single or combined potentials. The isolated gradient experiments were performed with either hydraulic, chemical, or temperature gradients on two sets of specimens consolidated at 100 and 200 kPa pressures. The flow boundary conditions were also varied. The experiments performed under hydraulic gradient using distilled water mixed clay, are called "the base tests". These were conducted to calibrate the equipment and to fine-tune the testing procedures. They yielded useful information on the physical quality of the prepared samples, degree of consolidation, average duration of testing, and also the degree of repeatability of data using the test system. The past effective

pressures of the one dimensionally consolidated samples were determined from conventional consolidation tests which revealed slight underconsolidation with OCR values ranging from 0.95 to 0.90. The isotropic consolidation data showed approximately 91 % degree of consolidation for the 100 kPa pressure specimens, and 86 % for the 200 kPa pressure specimens.

The second set of experiments were performed under multiple potentials, varying the sample consolidation pressure. A flow chart of the overall testing program and the testing conditions was given in Chapter 3.

## B. FLOW UNDER ISOLATED GRADIENTS

This group of tests were conducted to calibrate the equipment, to check the repeatability of the tests and mainly to measure the coupled coefficient of permeability for each potential. Good repeatability of data was obtained in these flow tests as indicated in the tables 4.1 and 4.2.

Two sets of samples were prepared, one consolidated under the vertical load of 100 kPa (1 kg/cm<sup>2</sup>) and the other under 200 kPa (2 kg/cm<sup>2</sup>). They were then consolidated isotropically in the triaxial cell under the confining pressures of 100 kPa and 200 kPa, respectively. After isotropic consolidation and saturation, each specimen was subjected to one potential only. At the completion of each test the specimen was discarded even though the flow tests are essentially assumed to be non-destructive type of tests. This was done to assure no interference from possible changes in soil physical parameters on the subsequent flow measurements.

The measured flow of water under different potentials are plotted against time at the consolidation pressures of 100 kPa and 200 kPa in Figures 4.1 and 4.2, respectively. Both figures show that the highest flow rate occurred under the applied hydraulic gradient and the lowest flow rate occurred under the applied chemical gradient. This is not necessarily significant by itself, since the flow rate is directly proportional to the magnitude of the gradient. As the consolidation pressure increases the flow rates decrease probably due to the densification of the soil and reduction of the void space. The significant finding is that, with increasing

**Table 4.1: Summary of hydraulic flow results under isolated gradients for specimens consolidated at 100 kPa pressure.**

	NUMBER OF TESTS	WATER CONTENT $\omega$ , %	VOID RATIO $e$	DRY DENSITY $g/cm^3$	AVERAGE FLOW RATE $cm^3/sec.$	AVERAGE COUPLED COEFFICIENT OF HYDRAULIC PERMEABILITY
BASE TEST WITH DISTILLED WATER						
	2	47 - 49	1.22-1.27	1.21-1.18	$1.2 \times 10^{-4}$	$6.07 \times 10^{-8}$ cm/sec
HYDRAULIC GRAD. 700 / 14, cm/cm						
69 CLAY MIXED WITH SALT SOLUTION						
	4	48 - 50	1.25-1.29	1.19-1.17	$1.02 \times 10^{-4} \pm 1.8 \times 10^{-5}$	$5.16 \times 10^{-8} \pm 2.0 \times 10^{-9}$ cm/sec
HYDRAULIC GRAD. 700 / 14, cm/cm						
CLAY MIXED SALT						
	1	48	1.25	1.19	$0.965 \times 10^{-6}$	$5.15 \times 10^{-7}$ cm <sup>2</sup> /sec
SALT SOLUTION CHEMICAL GRAD. $\log(175/38) / 14, cm^{-1}$						
CLAY MIXED WITH SALT SOLUTION						
	1	49	1.27	1.18	$7.34 \times 10^{-6}$	$2.03 \times 10^{-5}$ cm <sup>2</sup> /sec
TEMP. GRADIENT $\log(39^\circ C/29^\circ C) / 14, cm^{-1}$						

**Table 4.2: Summary of hydraulic flow results under isolated gradients for specimens consolidated at 200 kPa pressure**

	NUMBER OF TESTS	WATER CONTENT W, %	VOID RATIO e	DRY DENSITY g/cm <sup>3</sup>	AVERAGE FLOW RATE cm <sup>3</sup> /sec.	AVERAGE COUPLED COEFFICIENT OF HYDRAULIC PERMEABILITY cm/sec
BASE TEST WITH DISTILLED WATER	4	48 - 49	1.25-1.27	1.19-1.18	$7.93 \times 10^{-5} \pm 4.5 \times 10^{-6}$	$4.01 \times 10^{-8} \pm 8 \times 10^{-9}$
HYDRAULIC GRAD. 700/14 cm/cm						cm/sec
CLAY MIXED WITH SALT SOLUTION HYDRAULIC GRAD. 700/14 cm/cm	4	46 - 47	1.21-1.22	1.212-1.207	$7.18 \times 10^{-5} \pm 7 \times 10^{-6}$	$3.63 \times 10^{-8} \pm 6.5 \times 10^{-9}$
						cm/sec
CLAY MIXED WITH SALT SOLUTION CHEMICAL GRAD. $\log(175/38) / 14 \text{ cm}^{-1}$	1	46	1.21	1.212	$3.22 \times 10^{-7}$	$1.72 \times 10^{-7}$
						cm <sup>2</sup> /sec
SALT SATURATED (38 g/lt) SAMPLE TEMP. GRADIENT $\log(39^\circ\text{C}/29^\circ\text{C}) / 14 \text{ cm}^{-1}$	1	46.5	1.215	1.209	$3.43 \times 10^{-6}$	$0.95 \times 10^{-5}$
						cm <sup>2</sup> /sec

70

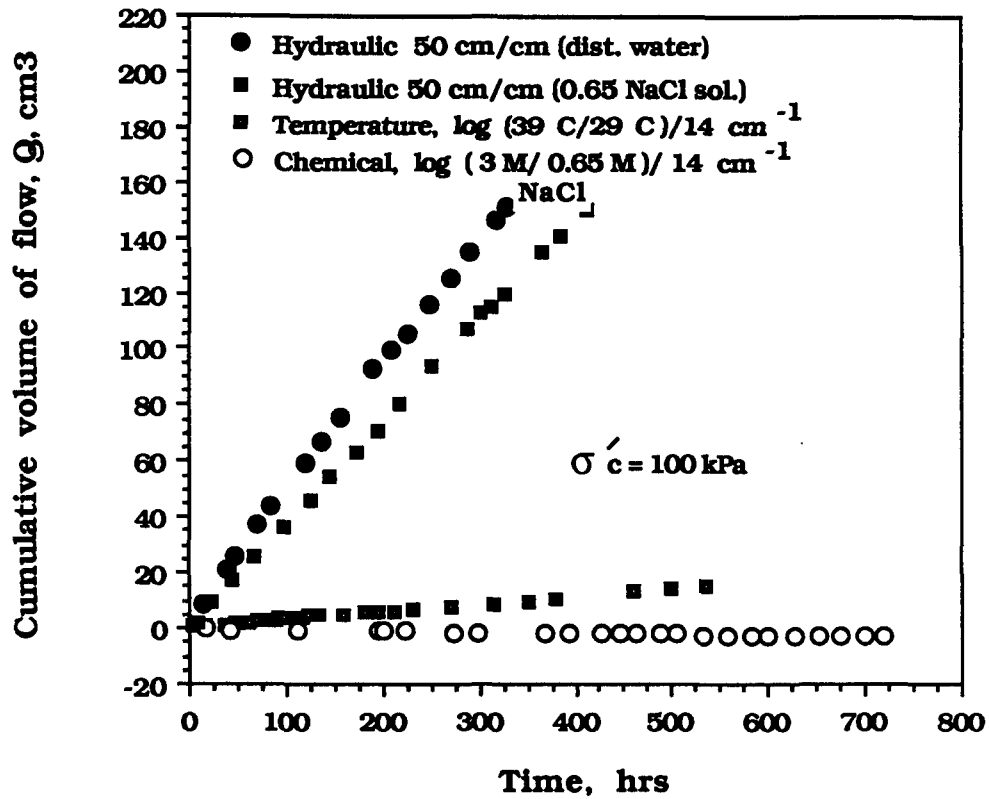


**Figure 4.1 : Time variation of cumulative volume of flow under isolated gradients,  $\sigma'_c$  : consolidation pressure.**

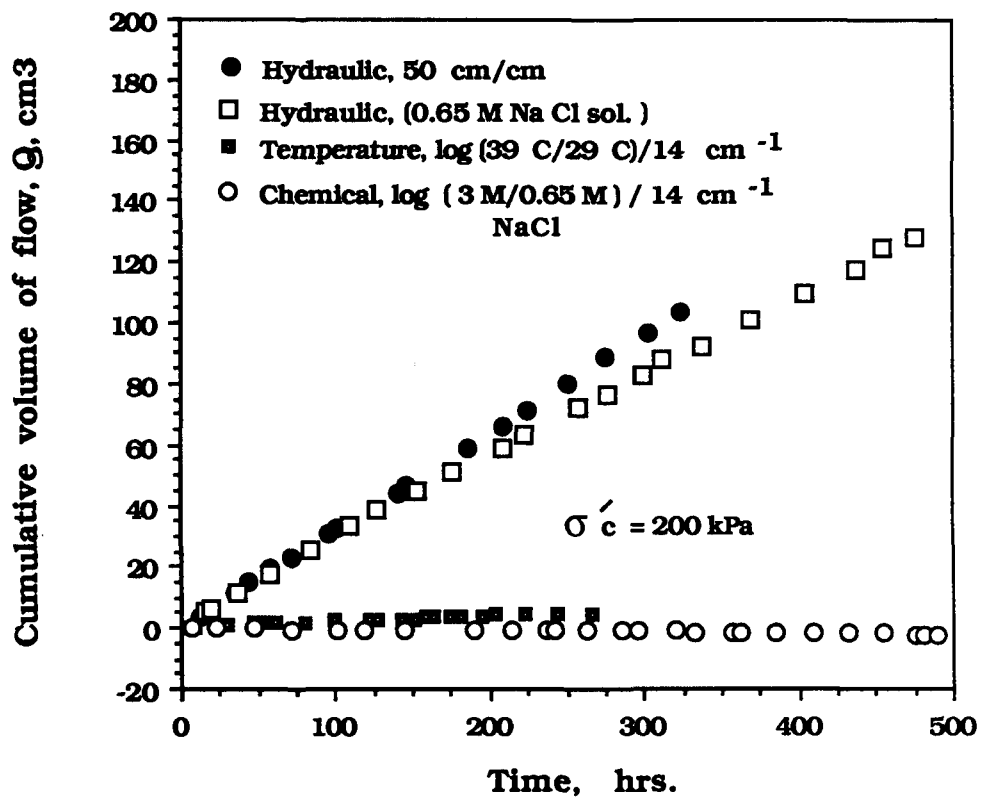


**Figure 4.2 :** Time variation of cumulative volume of flow under isolated gradients,  $\sigma'_c$  : consolidation pressure.

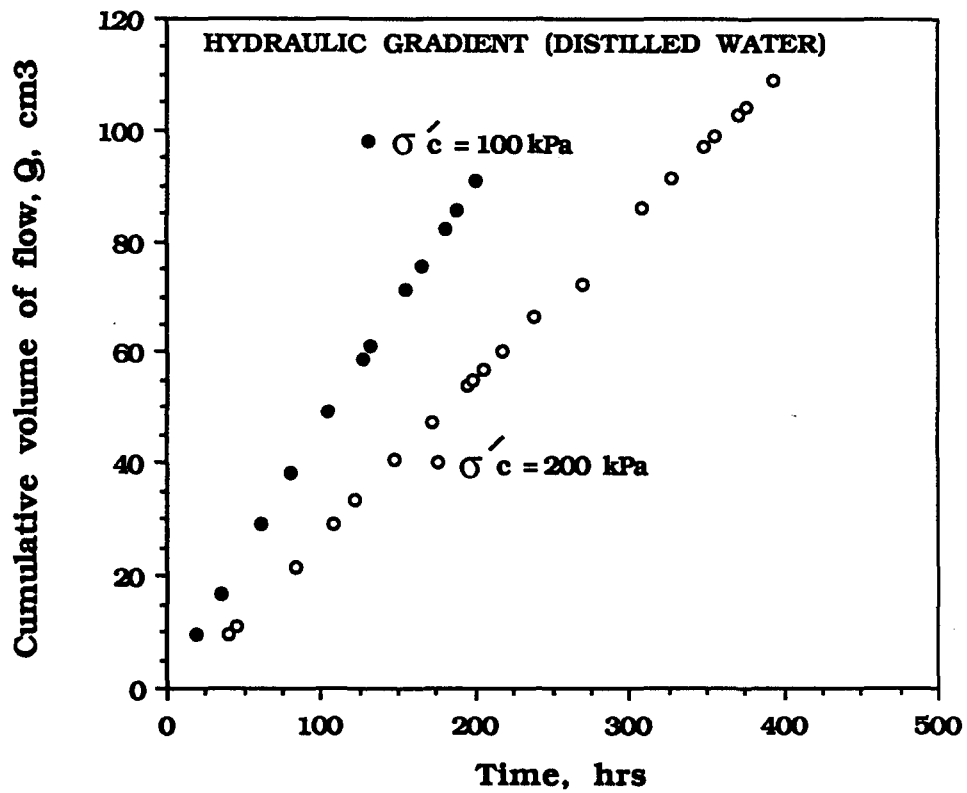
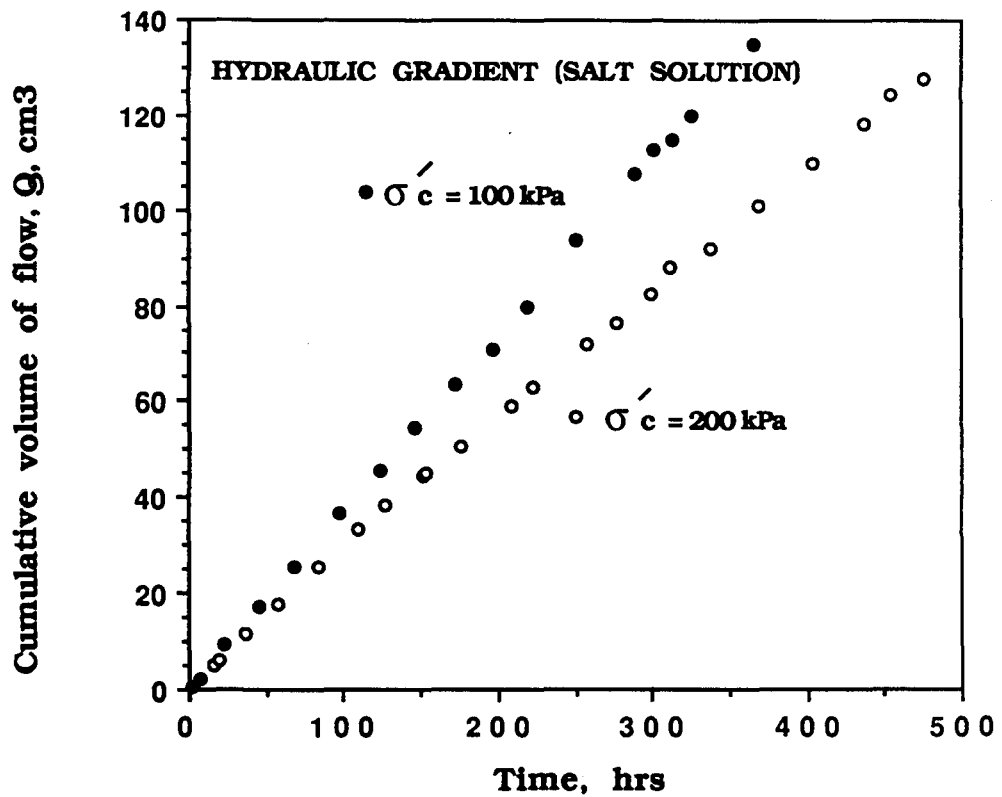


Figure 4.3 : Time variation of cumulative volume of hydraulic flow (average of replicate tests with error band approximately the size of a data point).





**Figure 4.4 : Time variation of cumulative volume of hydraulic flow (average of replicate tests with error band approximately the size of a data point).**

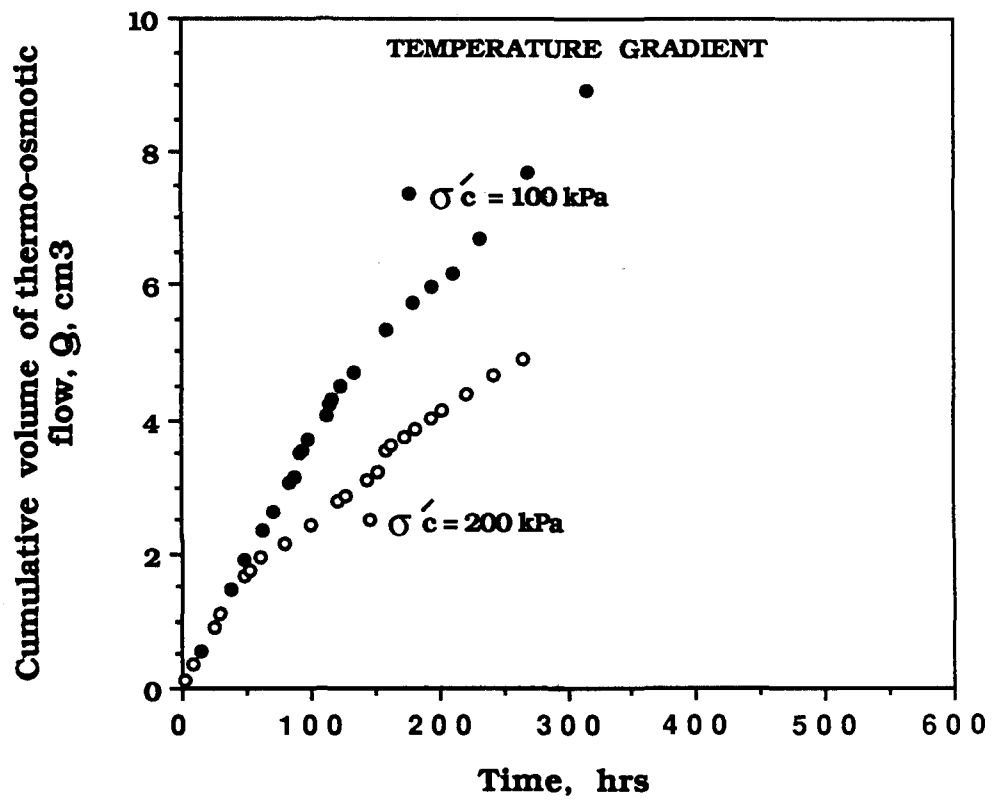
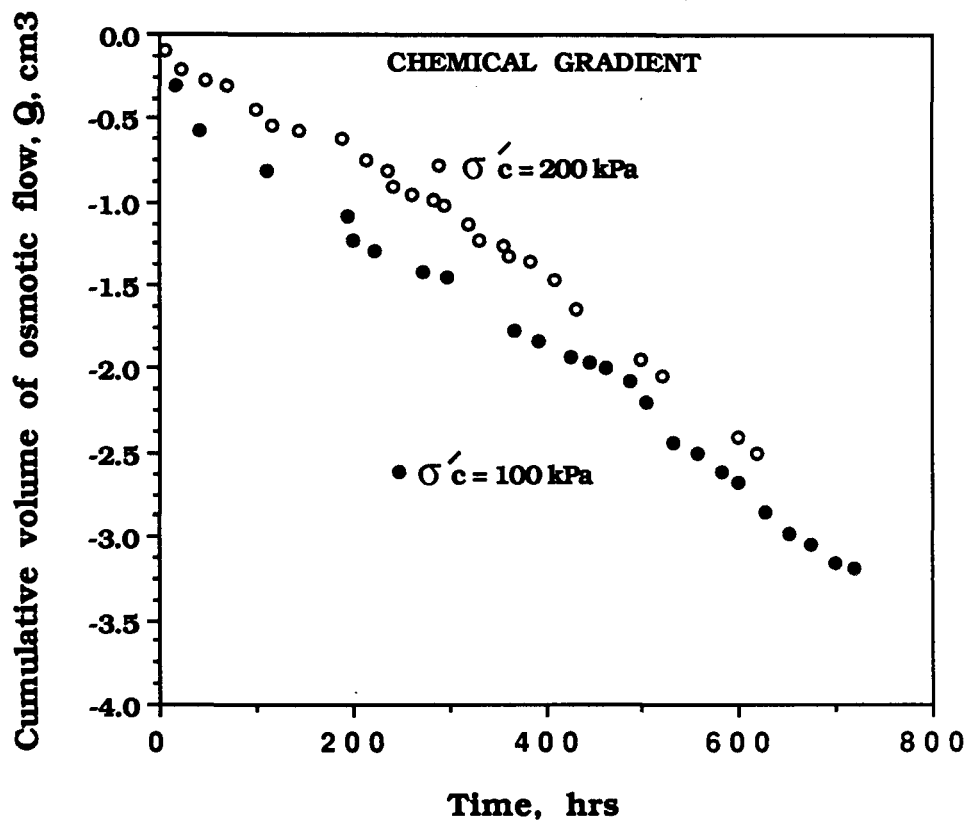


Figure 4.5 : Time variation of cumulative volume of thermo-osmotic flow.



**Figure 4.6 : Time variation of cumulative volume of osmotic flow.**

consolidation pressure the magnitudes of thermo-osmotic and osmotic flows appear to decrease more rapidly than the hydraulic flow. The hydraulic flow with salt solution show the least change with increasing pressure. This is, actually, only slightly lower than that of distilled water specimen permeated with distilled water. Figures 4.3 through 4.6 show the cumulative flow with time of the two consolidation pressure specimens for hydraulic, thermo-osmotic, and osmotic flows separately.

Figures 4.7 through 4.12 show the time variation of coupled coefficients of hydraulic permeability for the three different gradients at consolidation pressures of 100 kPa and 200 kPa. Figures 4.7 and 4.8 show the expected decrease in coefficient of hydraulic permeability with time until a steady state flow condition is reached within the soil. The time lag to achieve the steady state flow is attributed to saturation, and / or, consolidation due to the seepage forces.

With the application of temperature gradient, the thermo-osmotic coefficient of permeability also decrease with time and achieve a steady value, as shown in Figures 4.9 and 4.10. This is expected since consolidation takes place due to the temperature increase at the lower end of the specimen. Elapsed time for this transient range for effective pressure of 100 kPa is twice as much as it is for the effective pressure of 200 kPa. This is probably due to the lower density of the 100 kPa specimens subjected to a larger volume change than the 200 kPa specimens by the same increment in temperature.

Figures 4.11 and 4.12 show that as the concentration of salt solution decreases in the bottom reservoir, so does the osmotic coefficient of permeability. The arrows on these figures indicate the times of refilling of the higher concentration salt solution of NaCl (3 M) in the bottom reservoir. The change in the concentration of the salt solution occurs due to the counter flow of water from the soil into this reservoir. When the reservoir is replenished with 3M NaCl solution the osmotic coefficient increases also. Table 4.3 summarizes the coupled coefficients of permeability obtained from the single gradient tests with drained and undrained boundaries.

At the completion of the chemical gradients tests, two samples, one from each consolidation pressure set, were sliced into 12 discs.

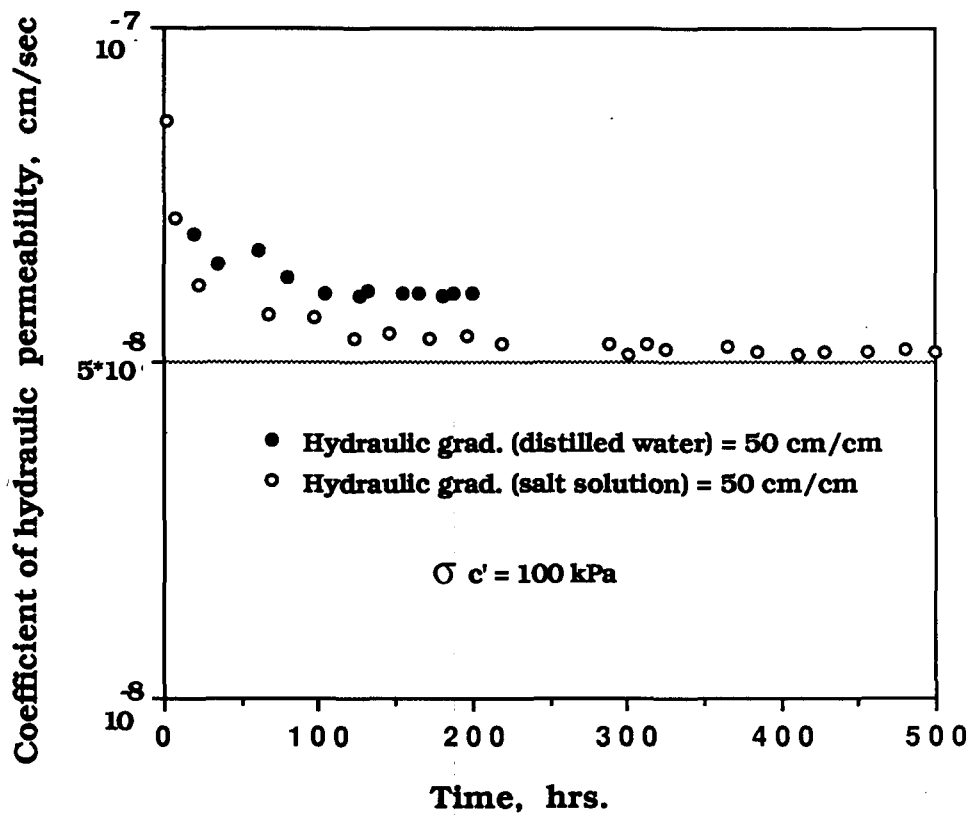
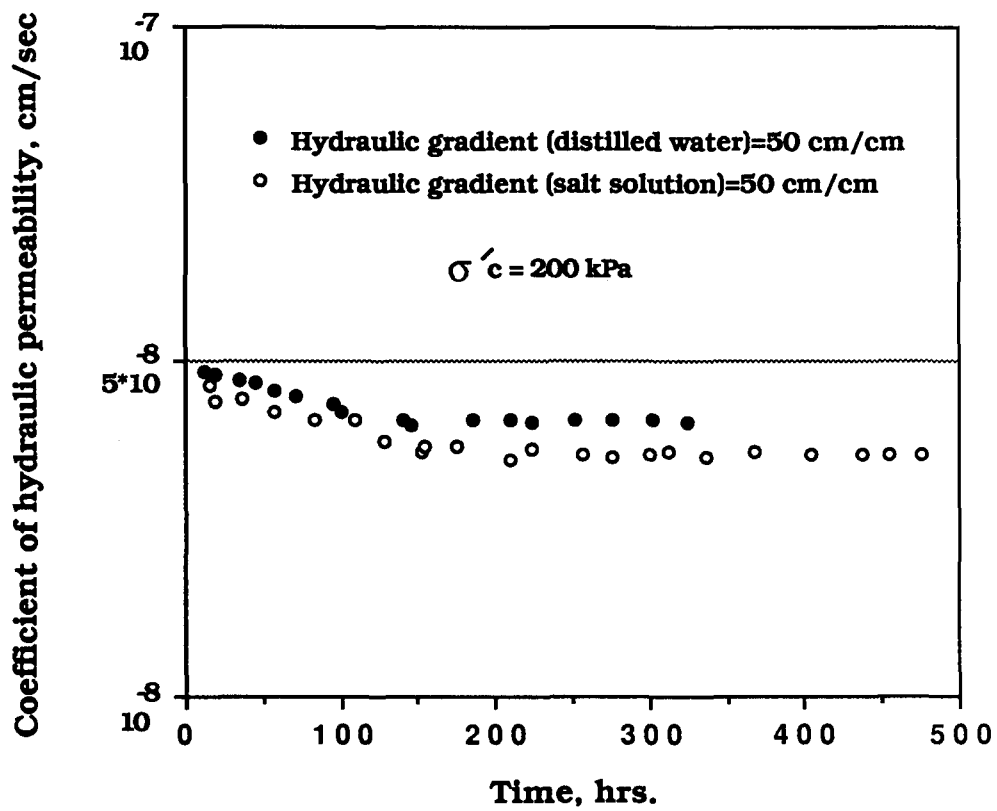


Figure 4.7 : Time variation of coefficient of hydraulic permeability.



**Figure 4.8 : Time variation of coefficient of hydraulic permeability**

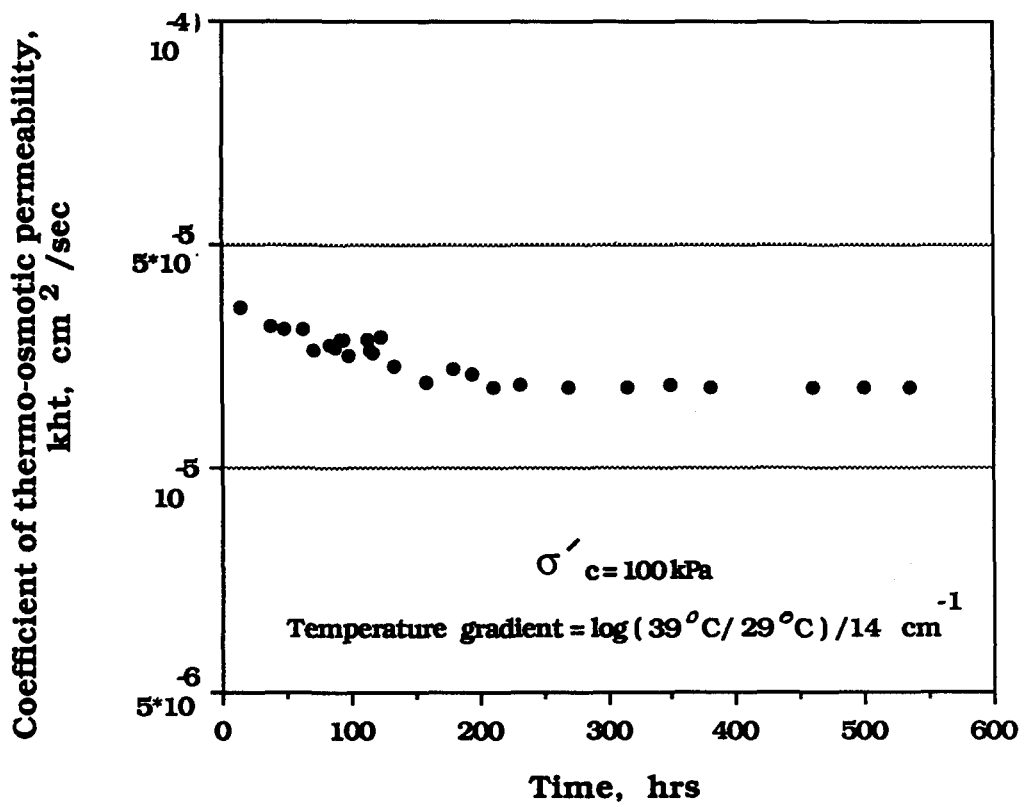


Figure 4.9 : Time variation of thermo-osmotic permeability.

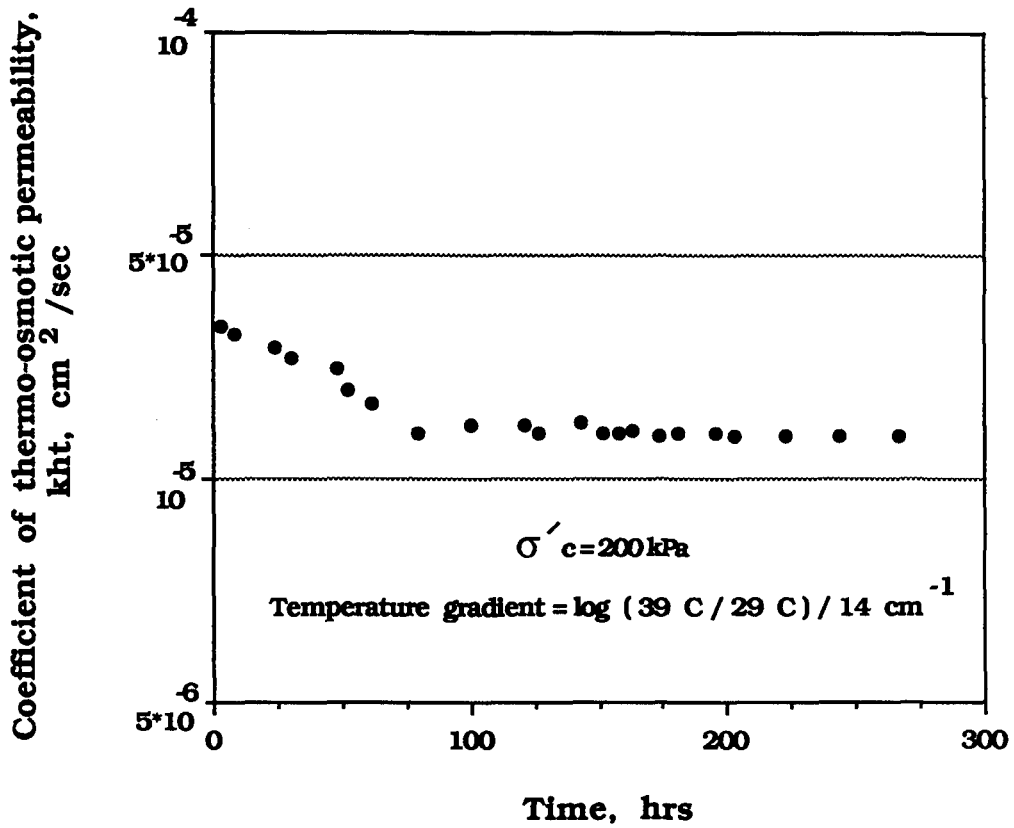
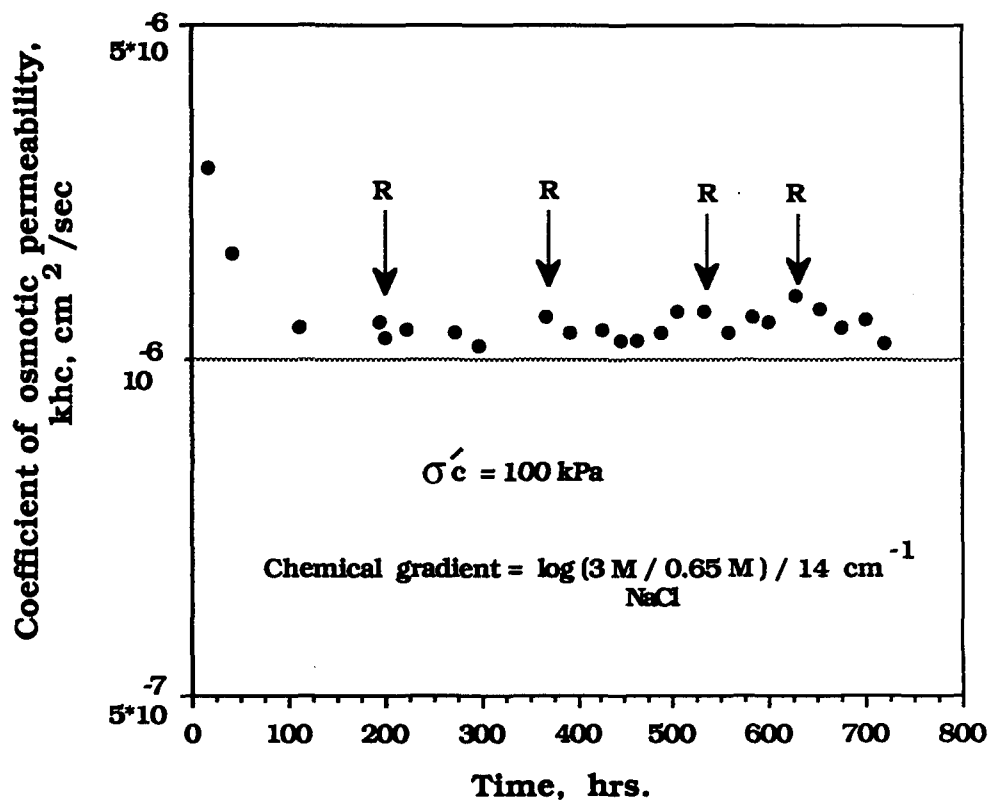
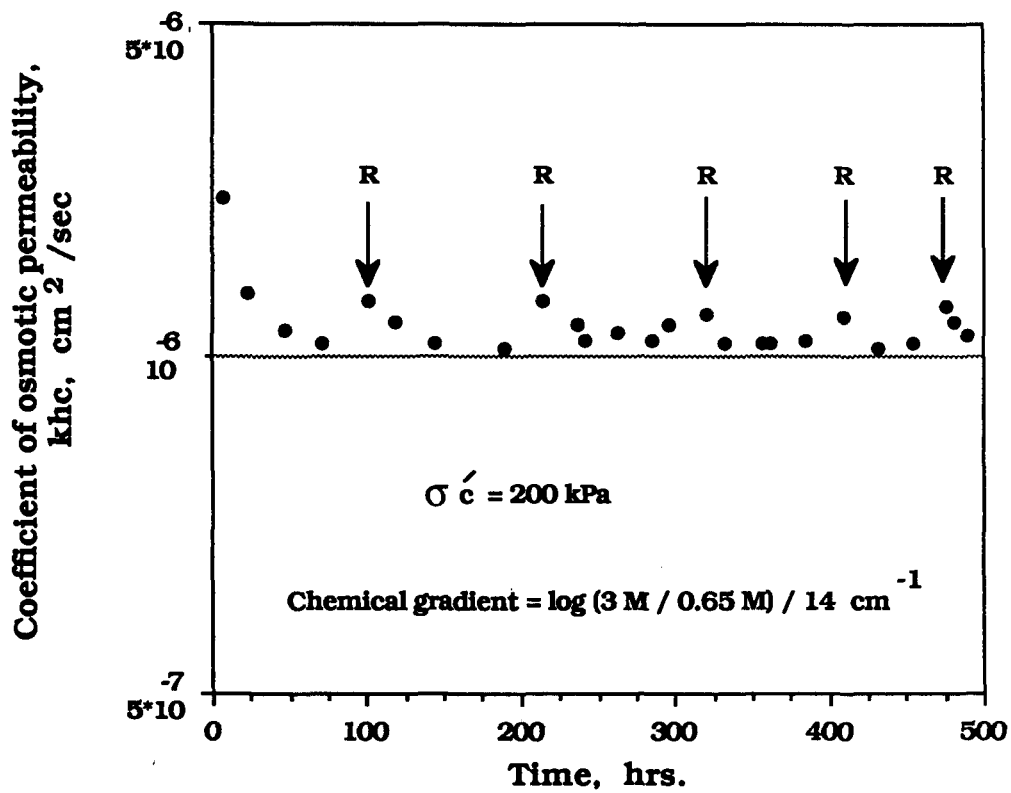


Figure 4.10 : Time variation of thermo-osmotic permeability.





**Figure 4.11: Time variation of osmotic permeability under chemical gradient [R= refilling the bottom platen reservoir with NaCl solution of original concentration = 3.0 M (175 g/lit)]**



**Figure 4.12: Time variation of osmotic permeability under chemical gradient. [R = refilling the bottom platen reservoir with NaCl solution of original concentration = 3.0 M (175 grt)]**

**Table 4.3: Summary of the coupled coefficients of hydraulic permeabilities**

	Consolidation pressure = 100 kPa		Consolidation pressure = 200 kPa	
	Drained	Undrained	Drained	Undrained
	Boundary	Boundary	Boundary	Boundary
<hr/>				
$k_{hh}$ (cm/sec)				
Hydraulic	$6.07 \times 10^{-8}$	-----	$4.02 \times 10^{-8}$	-----
Distilled Water				
<hr/>				
$k_{hh}$ (cm/sec)				
Hydraulic	$5.16 \times 10^{-8}$	-----	$3.62 \times 10^{-8}$	-----
Salt				
<hr/>				
$k_{hc}$	$5.15 \times 10^{-7}$	$4.0 \times 10^{-6}$	$1.72 \times 10^{-7}$	$2.21 \times 10^{-6}$
( $\text{cm}^2/\text{sec}$ )				
<hr/>				
$k_{ht}$	$2.03 \times 10^{-5}$	$1.44 \times 10^{-4}$	$0.95 \times 10^{-5}$	$1.0 \times 10^{-4}$
( $\text{cm}^2/\text{sec}$ )				
<hr/>				

Soil samples taken from the center of each disc were analyzed for sodium concentration. The distribution of sodium concentration in soil after 30 days of ionic diffusion is presented along with the analytical model prediction in Figure 4.13. The analytical model used represents the form of **Fick's second law** for time-dependent transport of solutes in soil as given in Chapter II ( Equation 2.3 ).

Equation 2.3 was solved numerically using effective diffusion coefficients,  $D^*$ , of  $1 \times 10^{-6}$  cm<sup>2</sup>/sec and  $5 \times 10^{-6}$  cm<sup>2</sup>/sec. As observed from figure 4.13 the measured values of Na<sup>+</sup> concentration for the 100 kPa and 200 kPa effective stress specimens agree well with the theoretical predictions. The approximate diffusion coefficients for the tested specimens were back calculated using the same numerical scheme . These coefficients were determined as  $2.7 \times 10^{-6}$  cm<sup>2</sup>/sec for the 100 kPa effective stress specimen, and  $2 \times 10^{-6}$  cm<sup>2</sup>/sec for the 200 kPa effective stress specimen. Using these diffusion coefficients and the numerical solution of Equation 2.3, the first, the 10 th, and the 30 th day concentration profiles of Na<sup>+</sup> were determined for the two specimens. These profiles are given in Figures 4.14 and 4.15, respectively. Using the analytical model, the time it would require to obtain a uniform profile of high salt concentration for the 100 kPa and 200 kPa effective stress specimens were predicted to be 1600 and 1900 years, respectively.

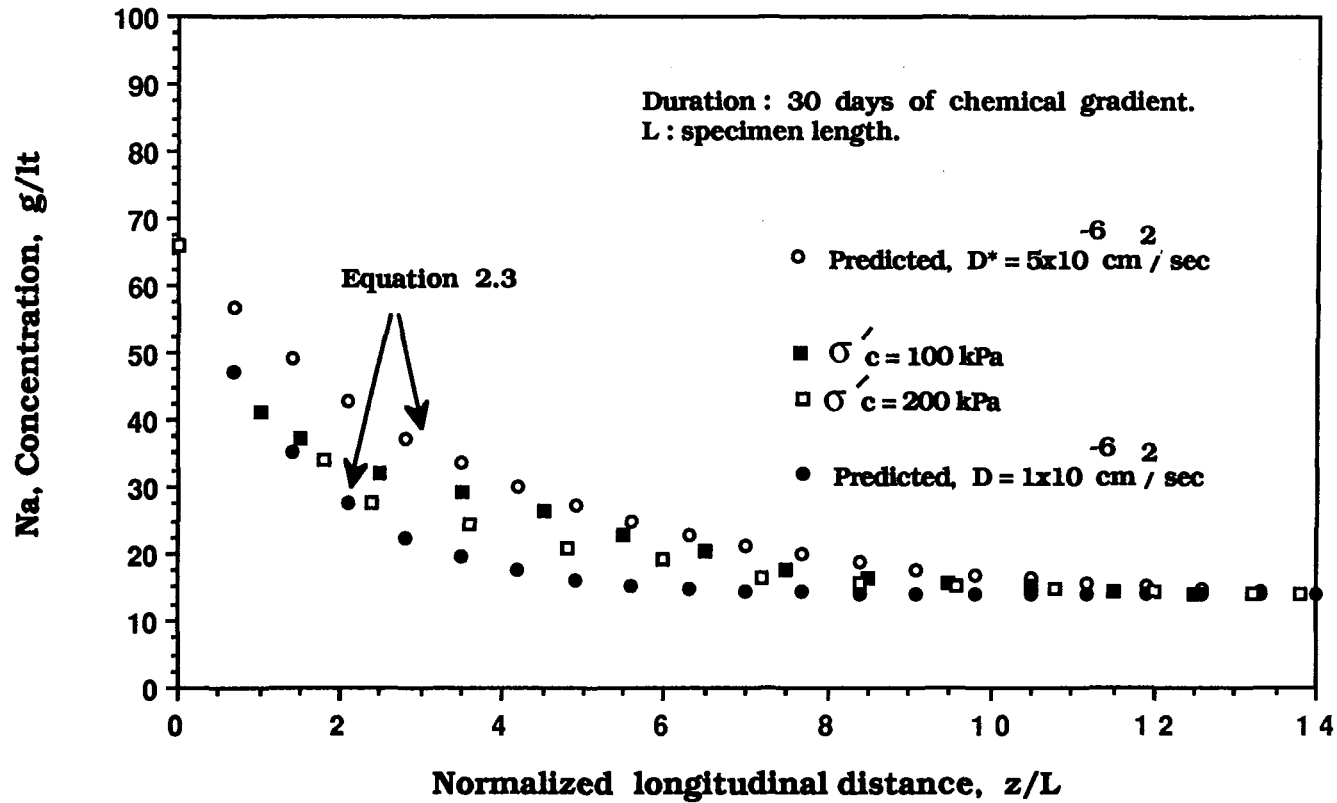


Figure 4.13 : Variation of predicted and measured Na concentration in soil in 30 days ( $D^*$  : effective diffusion coefficient).

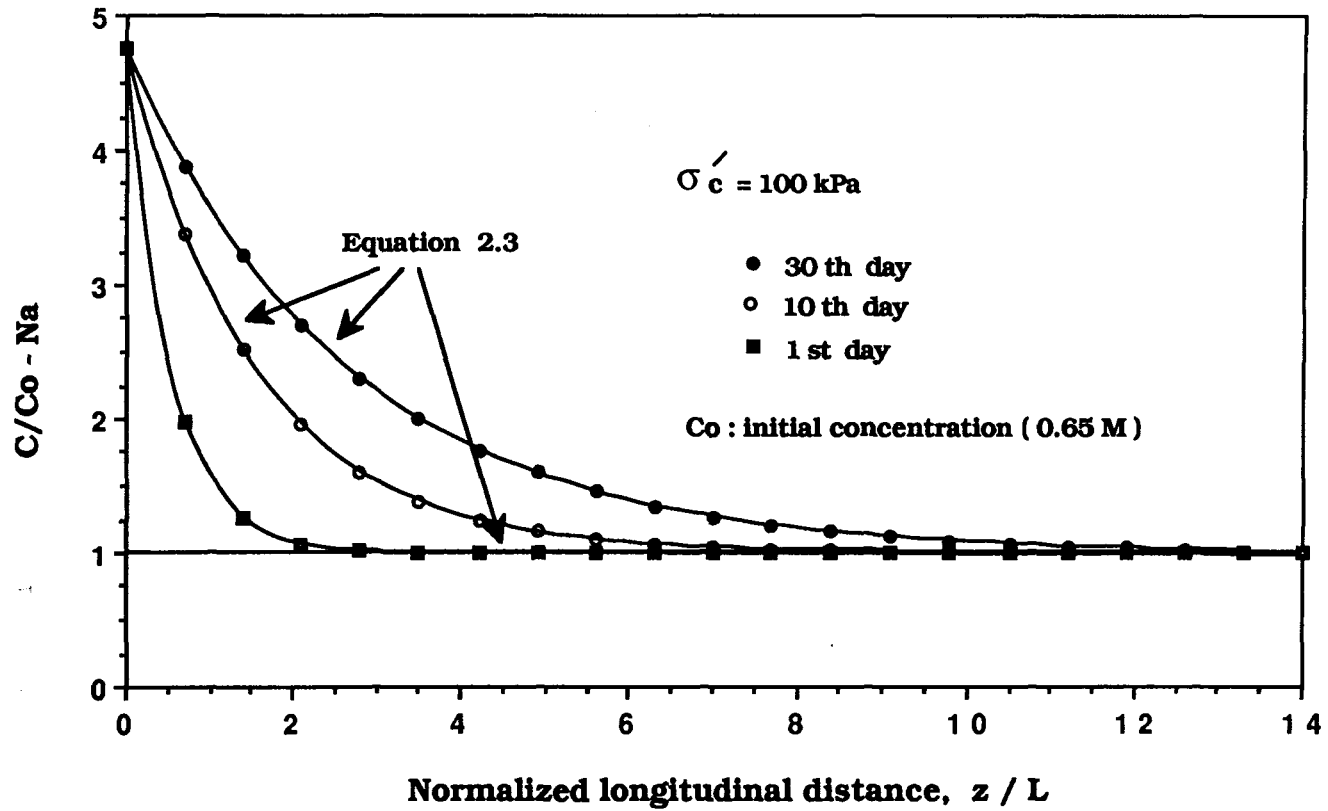


Figure 4.14 : Variation of normalized Na concentration profiles with time using calculated effective diffusion coefficient.

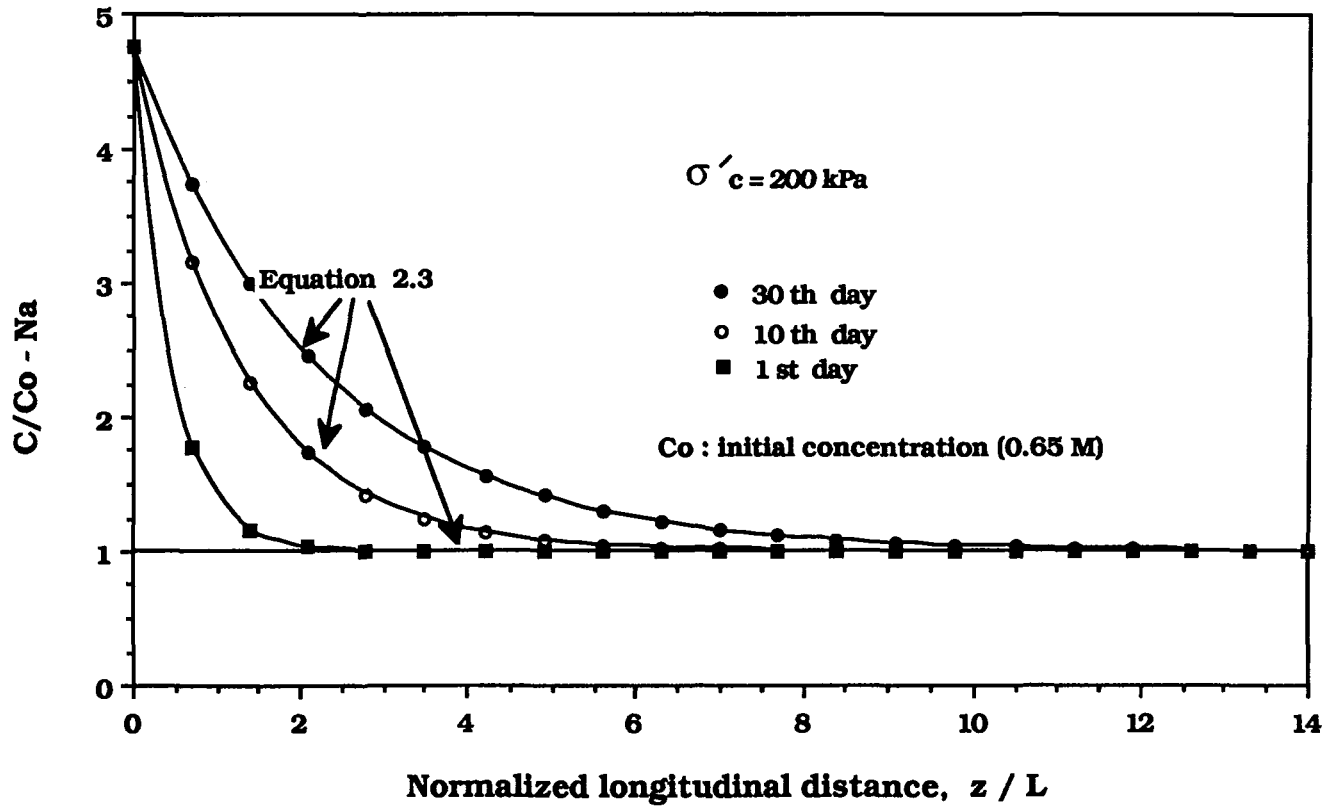


Figure 4.15 : Variation of normalized Na concentration profiles with time using calculated effective diffusion coefficient.

### C. MEASUREMENT OF COUPLED COEFFICIENT OF HYDRAULIC PERMEABILITY UNDER DRAINED AND UNDRAINED BOUNDARY CONDITIONS

The isolated gradient applications were conducted using two types of boundary conditions at the two ends of the specimens. These were discussed in Chapter III as the "drained boundary" and "undrained boundary" cases of flow.

In the "drained boundary" case, the results of which are given in the previous section, the gradients would be applied and the drainage valves at both ends of the specimen would be kept open to achieve a steady state flow. Flow would be measured in time and the test terminated some time after the steady state flow is achieved. The measured flow per unit time at steady state is used to calculate the coupled coefficient of hydraulic permeability. This is discussed in Chapter III also.

In the "undrained boundary" case, the drainage valves would be closed at the specimen boundaries, the potentials applied, and the pore water pressure build up is measured over time. The constant values of pore water pressures are used to calculate the coupled coefficients of hydraulic permeability as discussed in Chapter III.

Table (4.3) summarizes the coupled coefficients of hydraulic permeabilities for the individual gradient applications using the drained and undrained boundary conditions. The  $k_{ht}$  and the  $k_{hc}$  are calculated with either temperature or chemical gradients expressed in logarithms of the temperature or concentration ( $\log (T_a/T_b)/L$  or  $\log(C_a/C_b)/L$ ).



#### D. FLOW UNDER MULTIPLE GRADIENTS

The second group of tests were performed under multiple gradients at consolidation pressures of 100 kPa and 200 kPa. In each case flow was measured in time. Using the coupled coefficient of permeability values obtained from the tests with isolated gradients, equation 2.13 was solved for flow. The computed and the measured variations of cumulative flow for simultaneous application of multiple gradients were compared.

Table 4.4 summarizes the soil sample properties and resulting flow rates under multiple gradients.

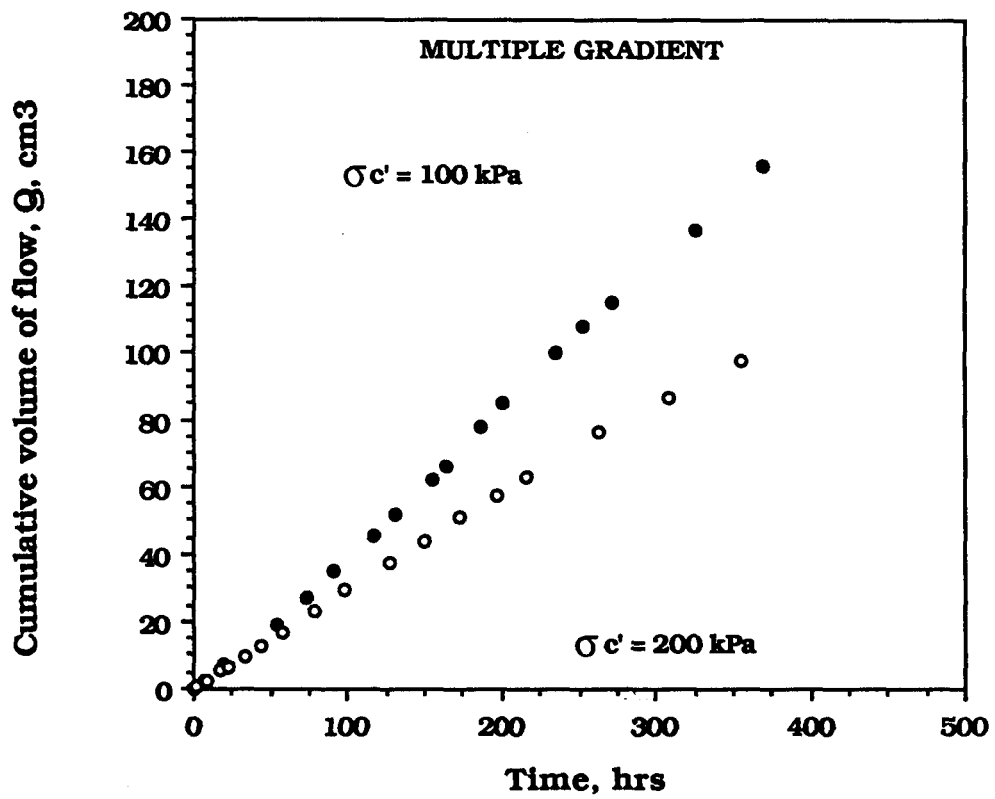
**Table 4.4: Summary of flow measuring tests results**

	NUMBER OF TESTS	WATER CONTENT W, %	VOID RATIO e	DRY UNIT WEIGHT gr/cm <sup>3</sup>	AVG. RATES OF FLOW cm <sup>3</sup> /sec.
CONSOLIDATION PRESSURE : 100 kPa					
SALT SATURATED (38 gr/lt) SAMPLE					
	1	49	1.27	1.180	1.08x10 <sup>-4</sup>
MULTIPLE Gradient					
CONSOLIDATION PRESSURE : 200 kPa					
SALT SATURATED (38 gr/lt) SAMPLE					
	1	47	1.22	1.207	0.745x10 <sup>-4</sup>
MULTIPLE Gradient					

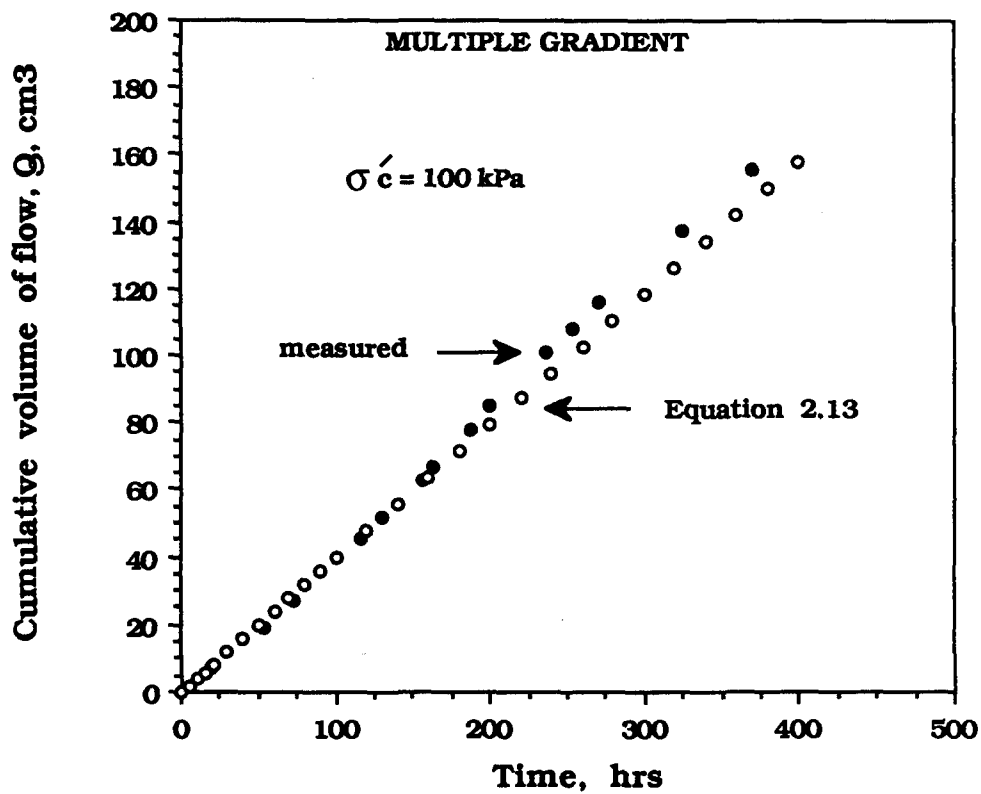
Figure 4.16 shows the measured flow rate is reduced as the consolidation stress increases. Comparing the flows in this figure with the hydraulic potential flows in Figures 4.1 and 4.2, it can be observed that for the same duration of time the cumulative flows under multiple potentials are slightly less than the cumulative flows under hydraulic potential, alone, for both the 100 kPa and 200 kPa effective stress specimens. This may be attributed to the backward flow caused by the chemical diffusion and the consolidation effect of the thermo-osmotic and the osmotic flux. However, when the average flow rates are compared from tables 4.1, 4.2, and 4.3, at steady state of water flux,  $q$  for the multiple gradient application is approximately the same as the  $q$  for hydraulic gradient application in salt solution mixed specimen. It should be noted that the composition of the specimens and the permeants are same in both of these cases.

Figures 4.17 and 4.18 show the measured and the calculated results of flow under multiple gradients with drained boundary conditions for the 100 kPa and 200 kPa consolidation pressures, respectively. There is good agreement between the experimental and predicted values as observed from these figures.

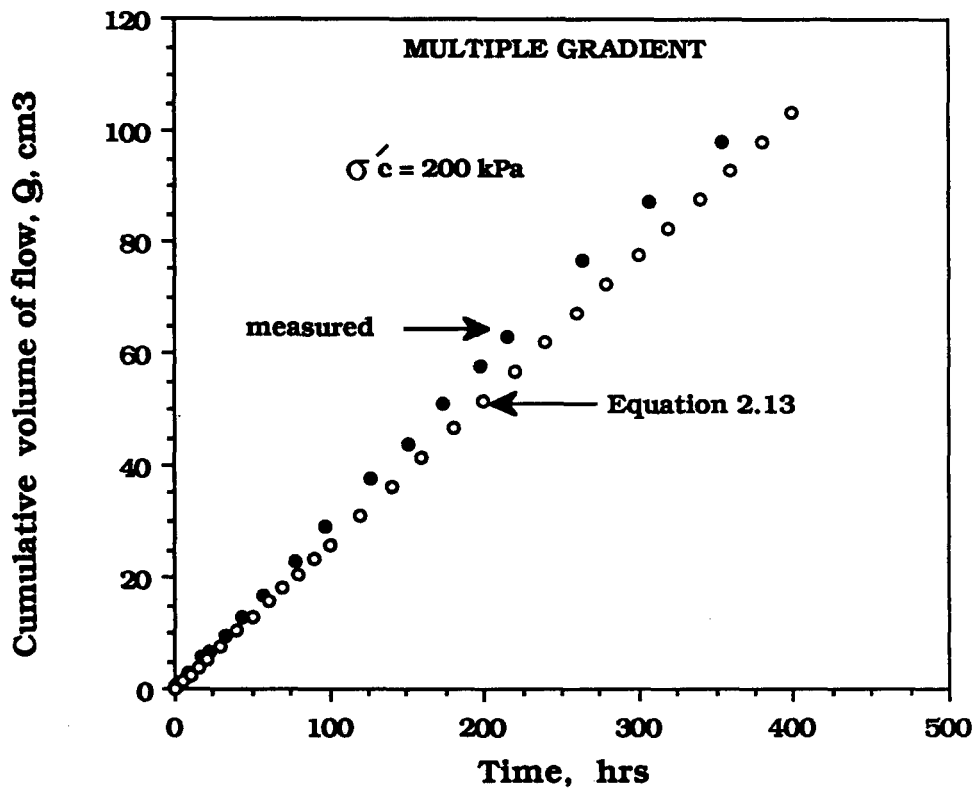
Figure 4.19 shows the correlation between the measured and the predicted cumulative flow for the drained boundary case of testing. As observed there is a very close one-to-one relationship between the two flows.



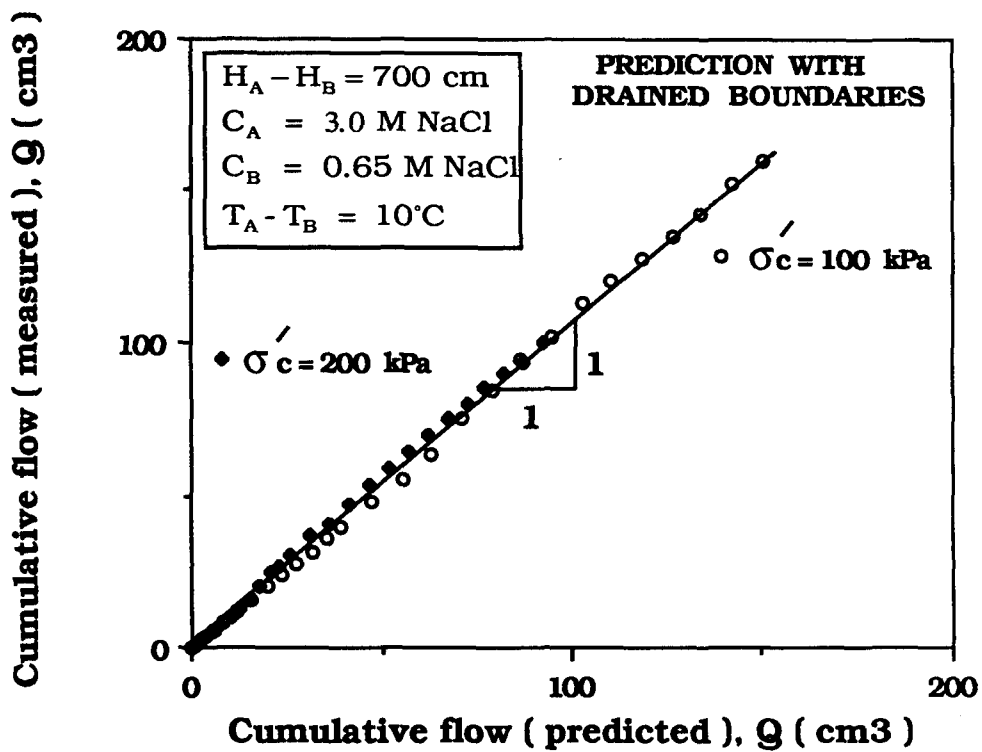
**Figure 4.16 : Time variation of measured cumulative volume of hydraulic flow under the combined effect of multiple gradients with drained boundaries.**



**Figure 4.17 : Time variation of measured and predicted cumulative volume of hydraulic flow under the combined effect of multiple gradients with drained boundaries.**



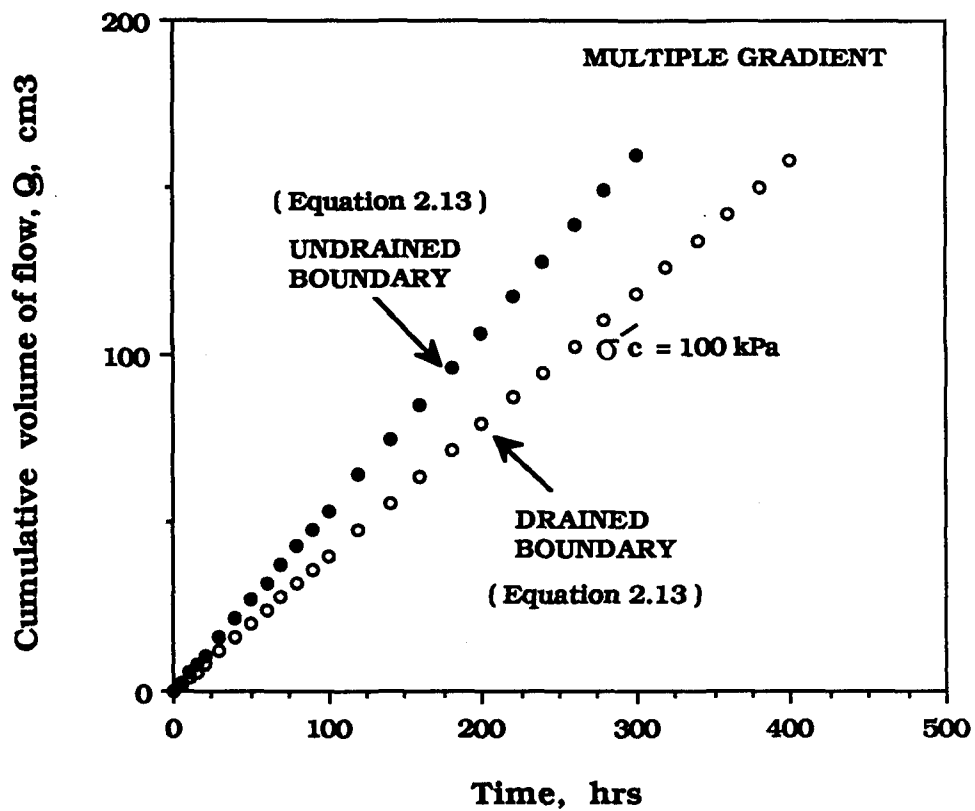
**Figure 4.18 : Time variation of measured and predicted cumulative volume of hydraulic flow under the combined effect of multiple gradients with drained boundaries.**



**Figure 4.19 : Predicted cumulative flow vs. measured cumulative flow under the combined effect of multiple gradients. ( Drained boundaries )**

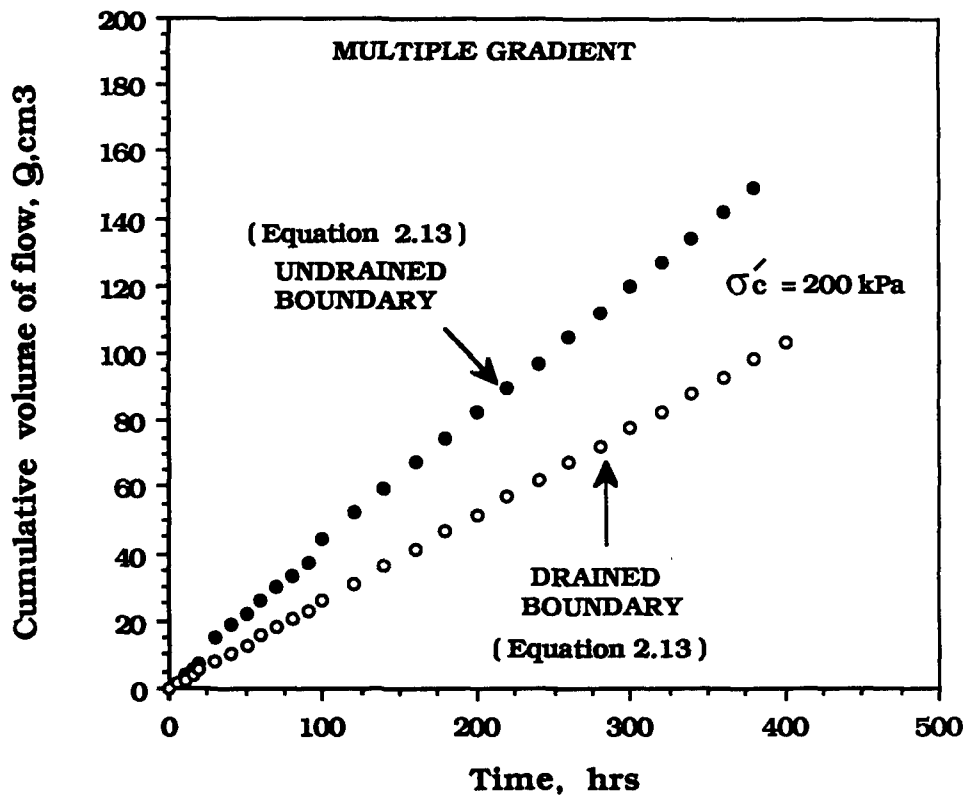
Figures 4.20 and 4.21 show the comparison of the predicted cumulative flows with the drained and the undrained boundaries for the 100 kPa and 200 kPa consolidated specimens, respectively. As observed, the undrained boundary prediction over estimates the flow when compared with the drained boundary case.

Figure 4.22 shows comparison of the predicted cumulative flow using the coefficients calculated from undrained boundary tests with the measured cumulative flow. The previously observed (Figure 4.19) one-to-one agreement is not observed in here. The overprediction of flow with the undrained boundary coefficients arises from the disclusion of the consolidation and densification effects of the thermo-osmotic and osmotic flux of water.



**Figure 4.20 : Comparison of predicted volume of hydraulic flow under the combined effect of multiple gradients with drained and undrained boundaries.**





**Figure 4.21 : Comparison of time variation of predicted volume of hydraulic flow under the combined effect of multiple gradients with drained and undrained boundaries.**

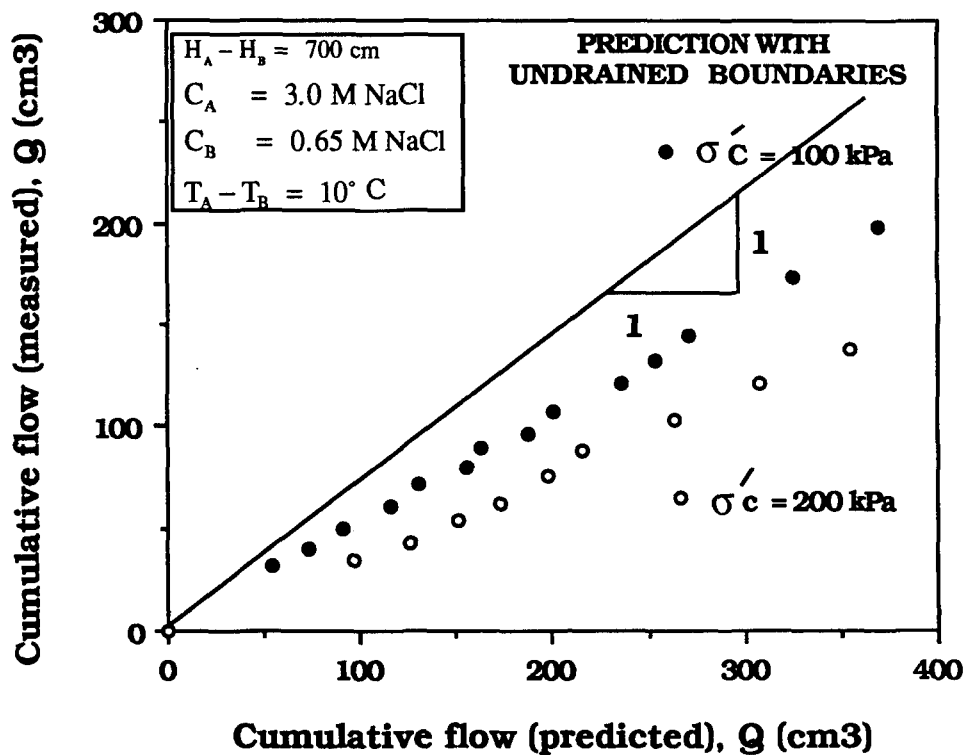


**Figure 4.22 : Predicted cumulative flow vs. measured cumulative flow under the combined effect of multiple gradients. (Undrained boundaries)**

## E. ISOTROPICALLY CONSOLIDATED-UNDRAINED (CIU) TRIAXIAL TESTS

### 1. STRESS-STRAIN RELATIONSHIP

At the completion of each flow test, the specimens were subjected to undrained triaxial shear test. Due to the low hydraulic conductivity of soil, tests were conducted in the undrained condition and pore water pressures were measured at the top and the bottom of each specimen. In these tests the strain rate was constant at 0.00075 cm/min (ASTM 4767-88). The following data were acquired electronically with time:

- 1) Deviatoric or vertical stress measured using a load transducer
- 2) Axial or vertical strain measured using an LVDT.
- 3) Pore water pressure at the bottom end of specimen using a pressure transducer.
- 4) Pore water pressure at the top end of specimen using a pressure transducer.

The summary of these measurements are given in Tables 4.5 and 4.6 for the 100 kPa and 200 kPa consolidated specimens, respectively.

The elastic and the plastic moduli of each specimen were calculated from the stress-strain graphs using a simple bilinear representation as shown schematically on a typical relationship in Figure 4.23. The elastic moduli were determined graphically from the initial straight line portion of the stress-strain relationships. The so called "plastic modulus" was determined by extending the longest straight line portion of the stress-strain relation behind the maximum deviatoric stress point. This was also done graphically. The intersection of the two straight lines was taken as the location of the yield strain. This procedure was adopted from Von-Mises material model for elastic-plastic materials. Although the soil tested did not necessarily behave like a Von-Mises material, but more like Mohr-Coulomb material, the elastic-plastic assumption was made for the prefailure part of the stress-strain behavior to be able to consistently determine yield strain for each material. Each one of these parameters namely,  $E$ ,  $E_p$ , and

**Table 4.5: Summary of measured parameters from CIU triaxial tests of specimens consolidated at 100 kPa**

	NUMBER OF SPECIMENS	STRAIN AT	PORE WATER PRESSURE		
		MAXIMUM STRESS %	MAXIMUM STRESS kPa	TOP kPa	BOTTOM kPa
DISTILLED WATER					
MIXED SPECIMEN	1	9.34	119	30	20
HYDRAULIC GRAD. 50					
SALT WATER MIXED (38 g/lit) SPECIMEN					
HYDRAULIC GRAD.	1	9.25	108	23	19
UNDRAINED BOUNDARY 50					
SALT WATER MIXED (38 g/lit) SPECIMEN					
CHEMICAL GRAD.	1	10.29	134	31	27
Log(175/38)/ 14 cm					
SALT WATER MIXED (38 g/lit) SPECIMEN					
TEMP. GRADIENT	1	9.56	95	34	31
LOG(39 C/29 C) / 14 cm					
SALT WATER MIXED (38 gr/lit) SPECIMEN					
MULTIPLE GRAD.	1	9.40	123	36	28

**Table 4.6: Summary of measured parameters from CIU triaxial tests of specimens at consolidated at 200 kPa**

	NUMBER OF SPECIMENS	STRAIN AT		PORE WATER PRESSURE	
		MAXIMUM STRESS %	MAXIMUM STRESS kPa	MAXIMUM TOP kPa	MAXIMUM BOTTOM kPa
<b>DISTILLED WATER</b>					
MIXED SPECIMEN	2	10.52	182	66	51
HYDRAULIC GRAD.					
50					
<b>SALT WATER MIXED</b>					
(38 gr/lit) SPECIMENS					
HYDRAULIC GRAD.	1	9.95	192	73.9	51.7
50					
<b>SALT WATER MIXED</b>					
(38 g/lit) SPECIMEN					
CHEMICAL GRAD.	1	10.13	213	55	43.5
Log (175/38) / 14 cm					
<b>SALT WATER MIXED</b>					
(38 g/lit) SPECIMEN					
TEMP. GRADIENT	1	10.76	181	70	54
LOG (39 C/29 C) / 14 cm					
<b>SALT WATER MIXED</b>					
(38 g/lit) SPECIMEN					
	1	10.90	181	80.4	49.6
MULTIPLE GRAD.					

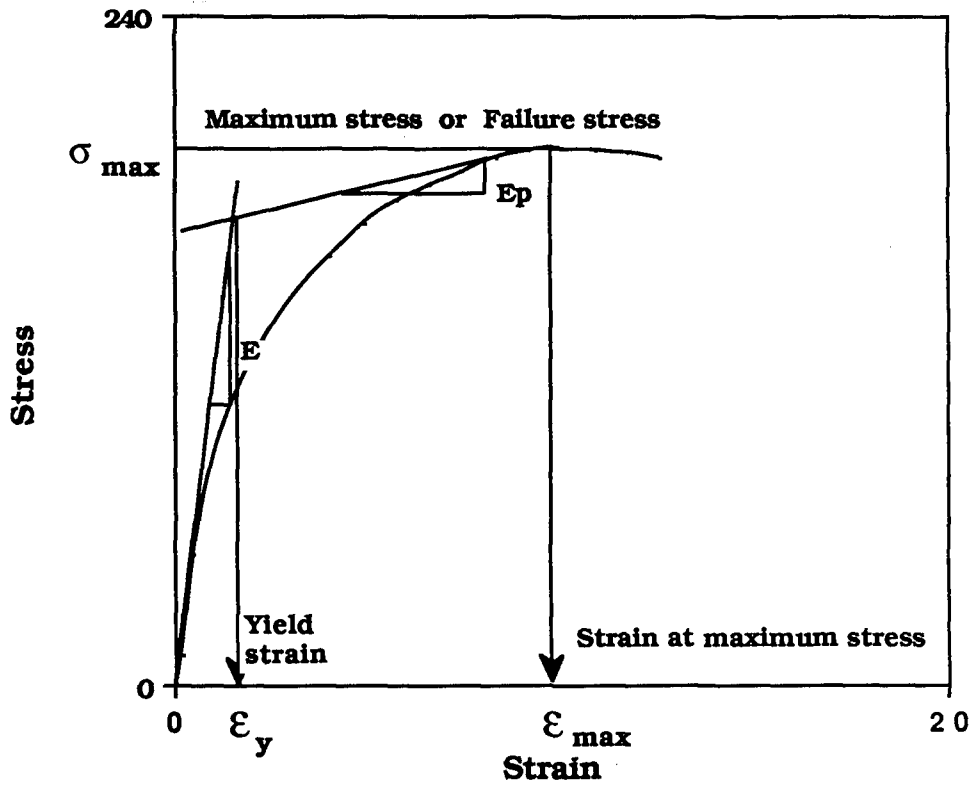


**Figure 4.23 : Bilinear representation of stress-strain relation.**

$\epsilon_y$ , were used to better characterize the differences between the mechanical behaviors of these soil specimens subjected to different flow experiments. Table 4.7 lists these parameters.

Since all the specimens were determined to be at near normal consolidation state, their shear strengths were expected to be a function of only the normal stress on the shearing plane and the internal friction angle. For normally consolidated soils the ratio of maximum deviatoric stress by the effective consolidation pressure is a constant,  $K$ , according to Hvorslev's hypothesis and Skempton and Bishop (1954):

$$\frac{(\sigma_1 - \sigma_3)_f}{2\sigma'_c} = K = \text{Constant}$$

Where  $(\sigma_1 - \sigma_3)_f$  = deviatoric stress at failure,

$\sigma'_c$  = effective consolidation pressure.

Table 4.8 lists the calculated average  $K$  values obtained from the CIU tests. Also listed in Table 4.8 are the calculated effective internal friction angle and the shear strength of the soil specimens consolidated at the two different pressures.

As observed from tables 4.5, 4.6, 4.7, and 4.8 the mechanical properties of the specimens change with the applied potentials over time. The thermo-osmotic potential reduce the strength and stiffness and increase the yield strain. The osmotic potential increase the strength but do not affect the elastic and plastic properties significantly. The inclusion of salt in the pore fluid, however, decreases the stiffness when compared with that of distilled water specimens. The reduction of  $K$  value for the thermo-osmosis subjected specimens may indicate under consolidated behavior, whereas the increase of  $K$  for osmosis subjected specimens may indicate slightly overconsolidated behavior.

The stress-strain variation of the so called "base specimens" (slurried with distilled water, permeated with distilled water) are presented in Figure 4.24. These are for consolidation and confining pressures of 100 kPa and 200 kPa. The

Test I and Test II indicated on the graph pertain to the replicate specimens of 200 kPa pressure consolidated samples. The closeness of these curves illustrate the repeatability of the tests. As expected, the compressive strength of 200 kPa pressure consolidated specimens are higher than that of the 100 kPa pressure consolidated specimens.

Figures 4.25 and 4.26 show the stress-strain variations of the specimens subjected to chemical potentials. In Figure 4.25, it is the stress-strain relation of those specimens for which the boundaries were drained, or flow was allowed. Whereas, in Figure 4.26 it is the stress-strain relation of those specimens for which pore pressure build up took place with no flow allowed under the applied chemical potential.

The undrained boundaries case exhibits lower strength and stiffness probably due to the initial pore water pressure built up. The specimens permeated with high concentration salt solution showed higher strength, probably due to the intrusion of salt into pore space.

Figure 4.27 presents the stress-strain relations for the specimens subjected to temperature gradients with drainage. These exhibit plastic behavior whereas the others show strain softening. This is probably due to the induced volume change and consolidation by the temperature gradients such that when the sample is sheared it behaves like an underconsolidated material.

Figure 4.28 shows the stress-strain diagrams for specimens subjected to multiple gradients. The shape of the curves for the 100 kPa and 200 kPa pressure consolidated specimens are similar to each other, both exhibiting a distinctive characteristic of strain hardening prior to failure.

Figure 4.29 and 4.30 show the combination of the stress-strain diagrams for specimens subjected to isolated and multiple gradients at 100 kPa and 200 kPa consolidation, respectively. In both cases the maximum strength was achieved with specimens subjected to intrusion of high concentration salt solution. The lowest strengths were achieved when specimens were subjected to temperature gradients. The behavior of the 100 kPa specimens appeared to be more influenced by the temperature gradients. This is readily observed comparing Figures 4.29 and 4.30,



**Table 4.7: Summary of the plastic and elastic parameters determined from bilinear representation of stress-strain diagrams.**

	ELASTIC MODULUS		PLASTIC MODULUS		YIELD STRAIN	
	E, kPa		E <sub>p</sub> , kPa		ε <sub>y</sub> %	
	FOR 100 kPa	FOR 200 kPa	FOR 100 kPa	FOR 200 kPa	FOR 100 kPa	FOR 200 kPa
DISTILLED WATER						
MIXED SPECIMEN	16000	17500	400	500	1.0	1.5
HYDRAULIC GRAD.						
50						
SALT WATER MIXED						
(38 g/lt) SPECIMEN						
HYDRAULIC GRAD.	6500	8666	667	667	1.3	1.7
UNDRAINED						
BOUNDARY						
50						
SALT WATER MIXED						
(38 g/lt) SPECIMEN						
CHEMICAL GRAD.	6333	9000	545	1250	1.5	1.6
Log(175/38) / 14 cm						
SALT WATER MIXED						
(38 g/lt) SPECIMEN						
TEMP. GRADIENT	2500	7000	429	636	3.2	2.1
LOG(39C/29 C) / 14 cm						
SALT WATER MIXED						
(38 gr/lt) SPECIMEN						
MULTIPLE GRAD.	3250	5000	692	750	2.5	2.6

**Table 4.8 : Summary of strength parameters.**

	K	INTERNAL FRICTION ANGLE		COMPRESSIVE STRENGTH	
		$\Phi'$		$\tau_f$ , kPa	
		FOR 100 kPa	FOR 200 kPa	FOR 100 kPa	FOR 200 kPa
DISTILLED WATER MIXED SPECIMEN HYDRAULIC GRAD. 700/14, cm/cm	0.525	39.1	43.7	18.1	20.6
SALT WATER MIXED (38 g/lit) SPECIMEN CHEMICAL GRAD. Log(175/38)/ 14 cm UNDRAINED BOUNDARY	0.510	20.8	18.8	15.3	20.8
SALT WATER MIXED (38 g/lit) SPECIMEN CHEMICAL GRAD. Log(175/38)/ 14 cm	0.601	25.1	20.6	22.3	28.8
SALT WATER MIXED (38 g/lit) SPECIMEN TEMP. GRADIENT LOG(39 C/29 C) / 14 cm	0.460	18.7	17.5	10.0	17.9
SALT WATER MIXED (38 gr/lit) SPECIMEN MULTIPLE GRAD.	0.534	23.6	17.4	18.2	17.4

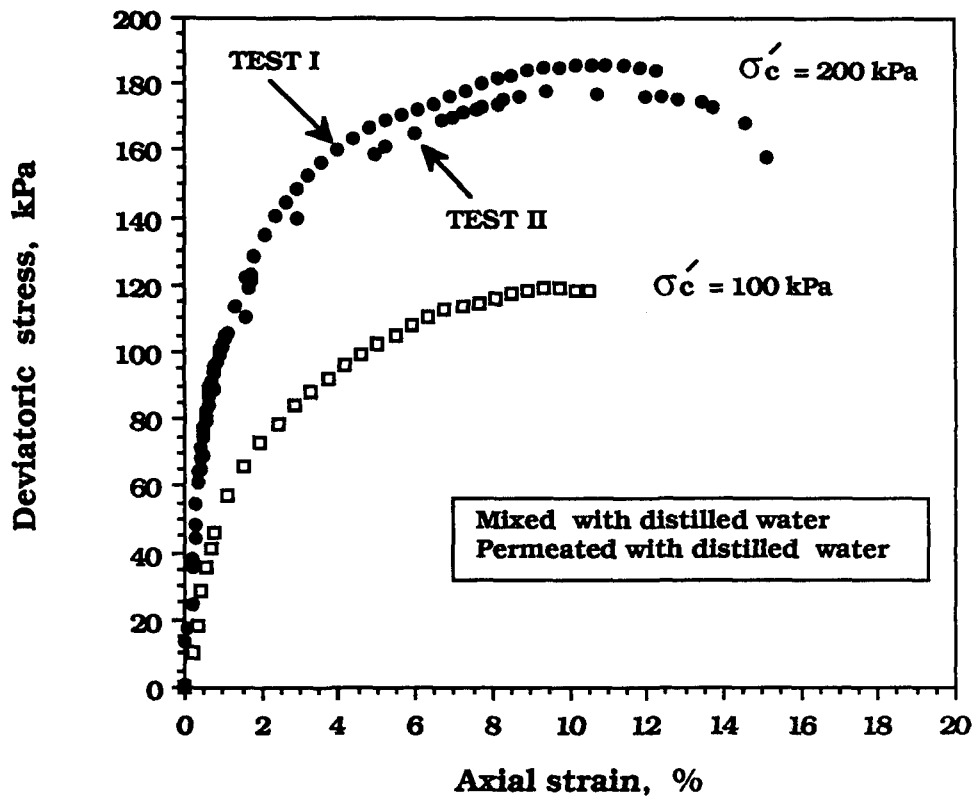


**Figure 4.24 : Axial strain vs. deviatoric stress variation of base specimens following hydraulic permeation with distilled water under hydraulic gradient.**

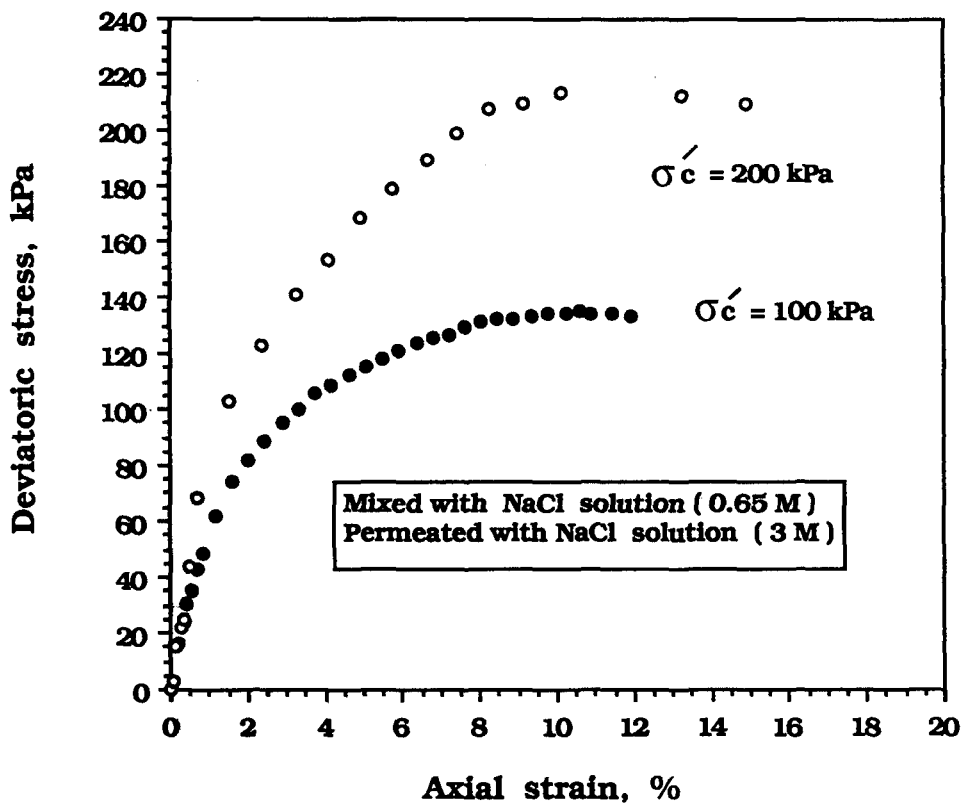


**Figure 4.25 : Axial strain vs. deviatoric stress variation of salt solution mixed specimen following permeation with high concentration of salt solution under chemical gradient.**

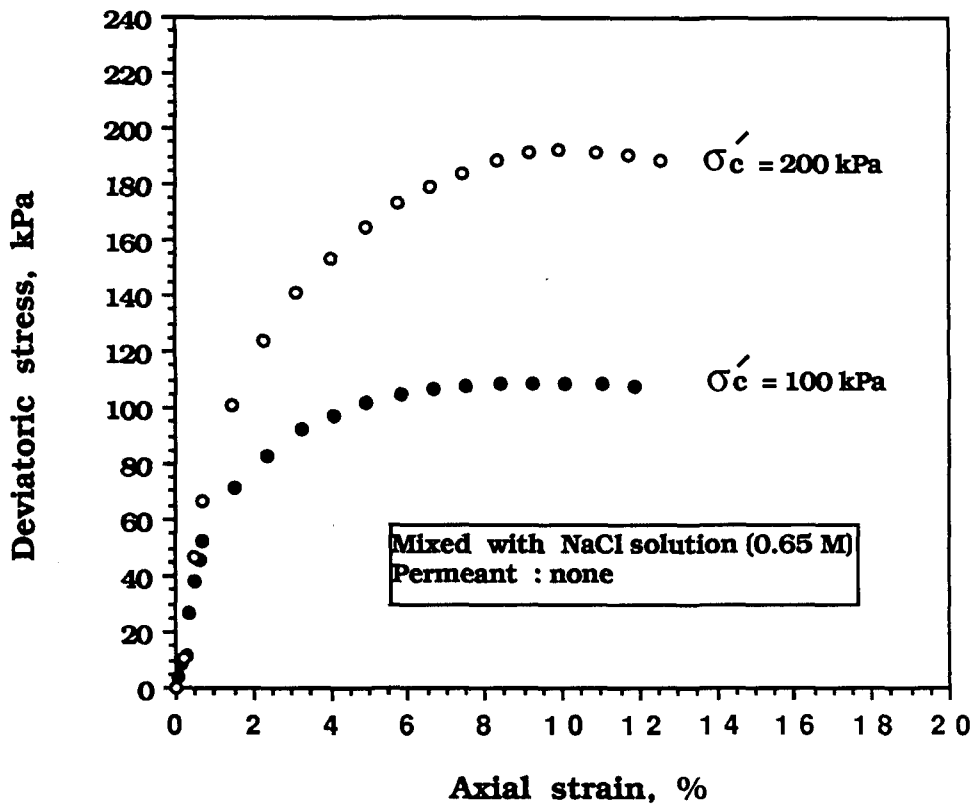


**Figure 4.26 : Axial strain vs. deviatoric stress variation of salt solution mixed specimens following the pore pressure built up due to chemical gradient.**

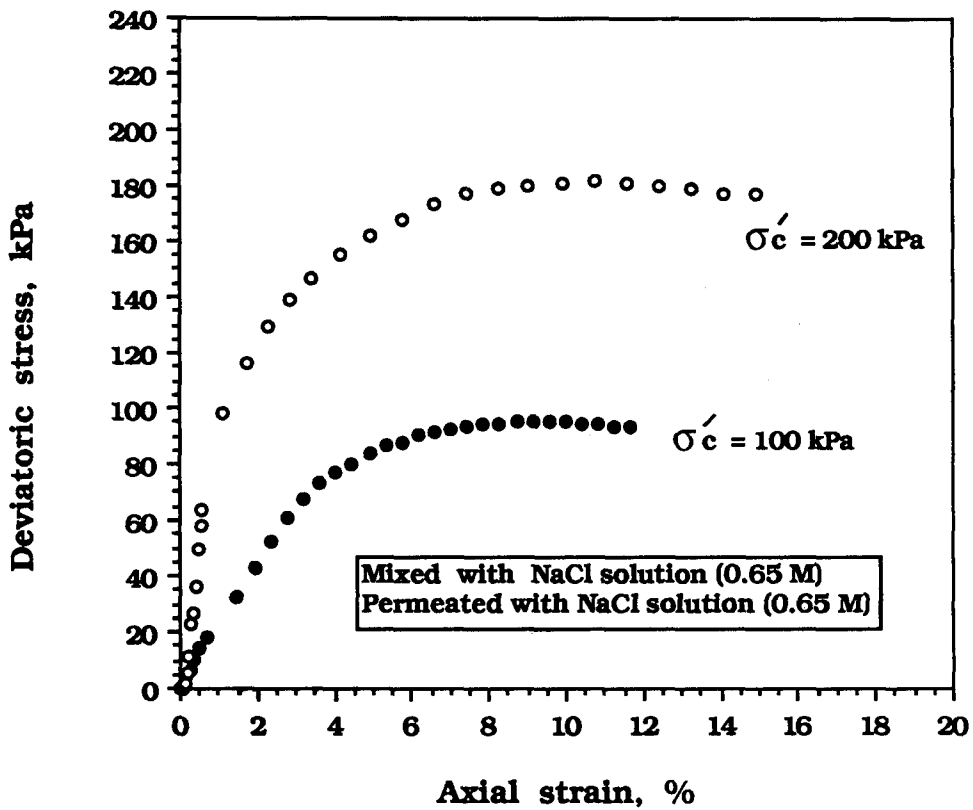


**Figure 4.27 : Axial strain vs. deviatoric stress variation of salt solution mixed specimens following permeation with salt solution under temperature gradient.**

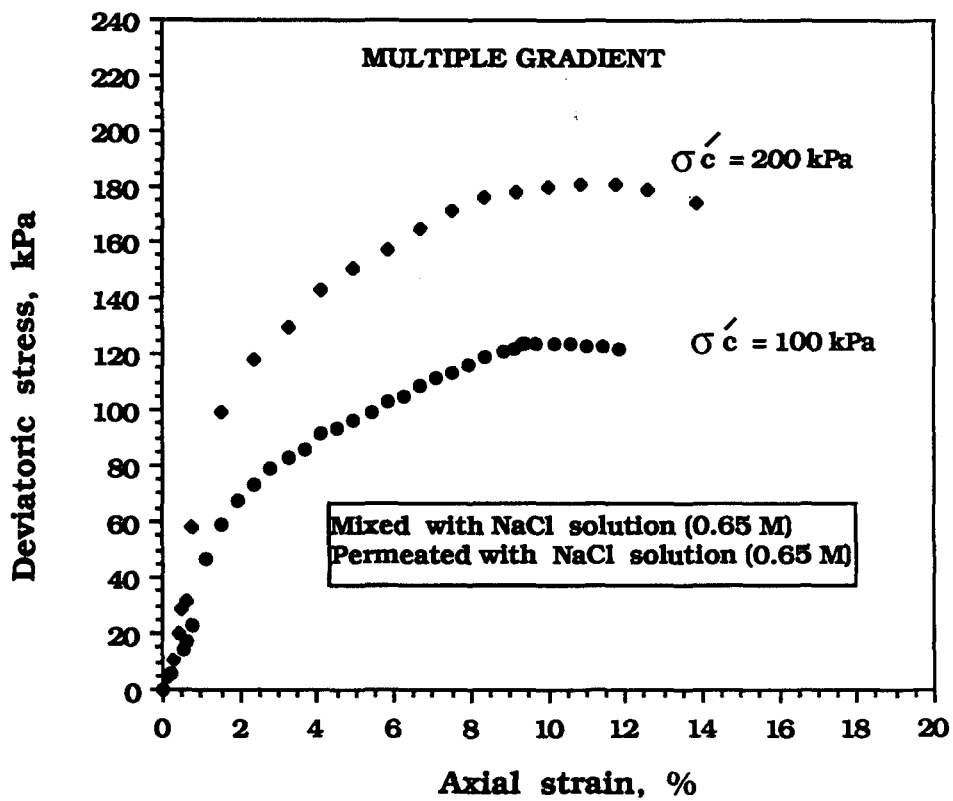


**Figure 4.28 : Axial strain vs. deviatoric stress variation of salt mixed specimens following permeation with salt solution under multiple gradients.**

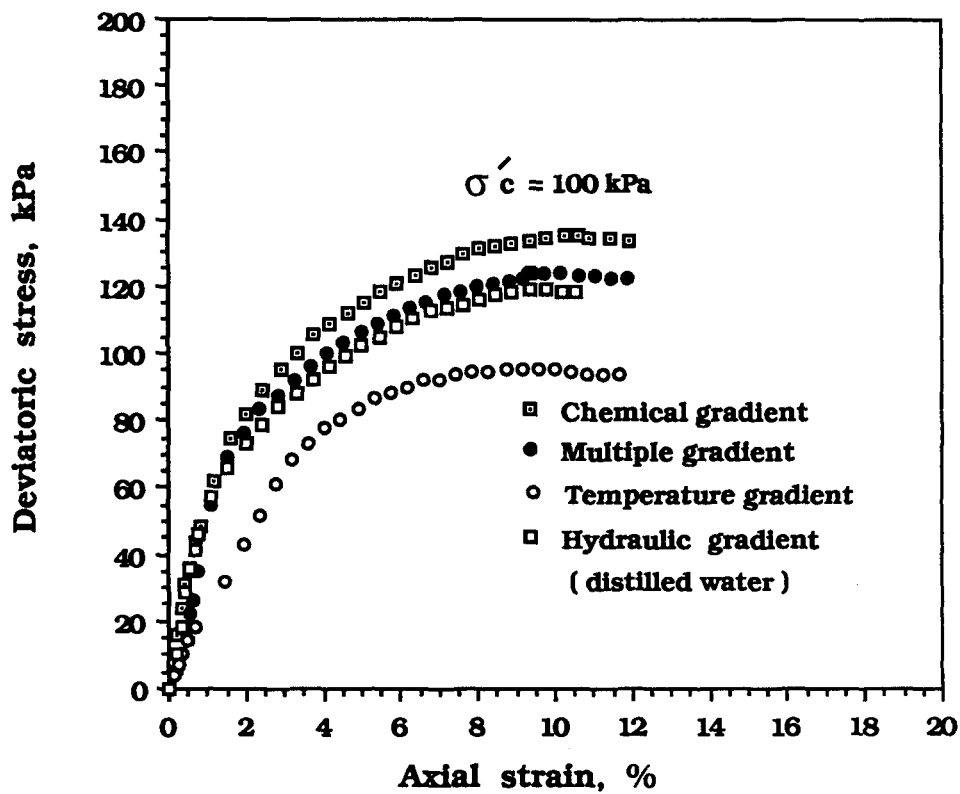


**Figure 4.29 : Combined graphs of axial strain vs. deviatoric stress variation of the salt solution mixed specimens following permeation with salt solution under isolated and multiple gradients.**



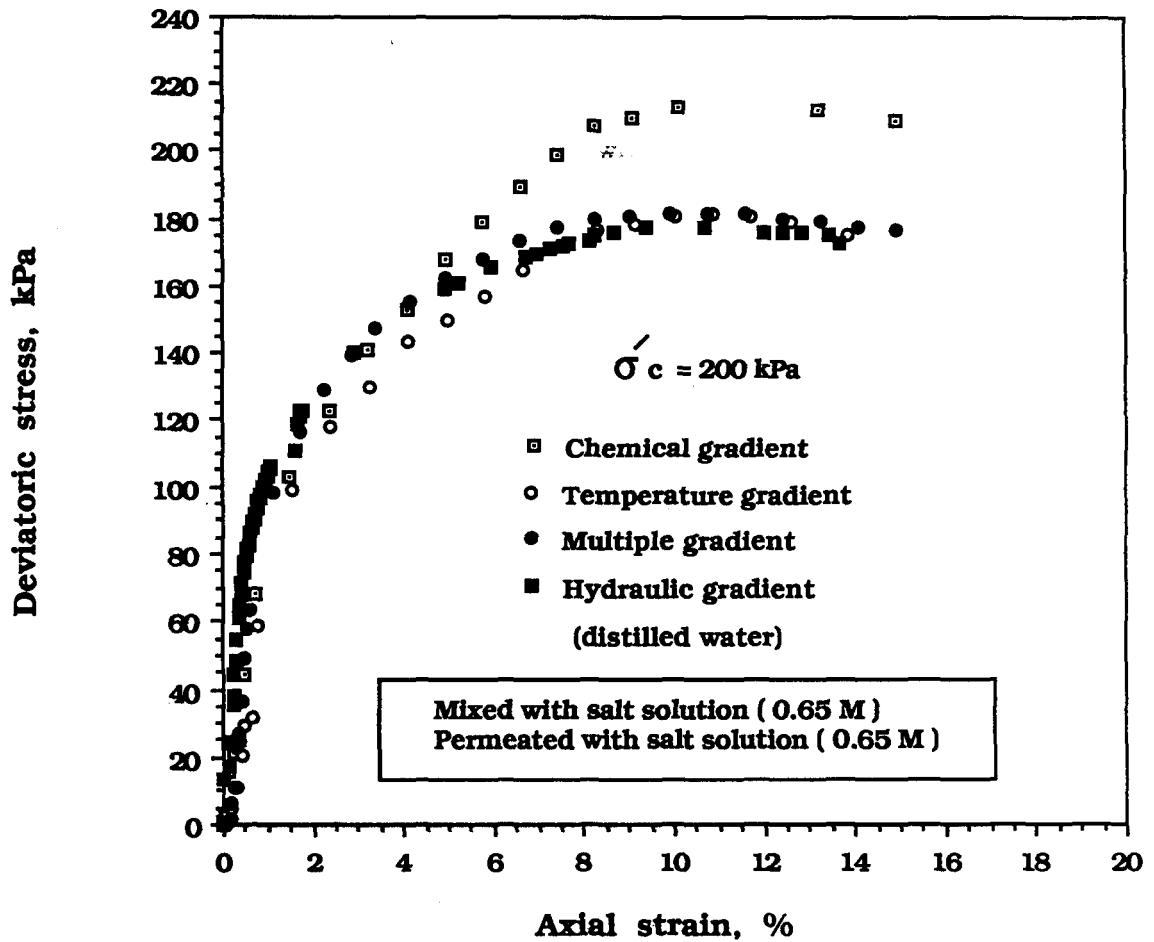


**Figure 4.30 : Combined graphs of axial strain vs. deviatoric stress variation of the salt solution mixed specimens following permeation with salt solution under isolated and multiple gradients.**

in which the strength decrease is more evident with temperature gradient in the 100 kPa pressure consolidated specimen.

## 2. PORE WATER PRESSURE

The pore water pressures were measured at the top and the bottom of the specimens with separate transducers calibrated in the same manner. The original reason for this practice was to check the uniformity of pore water pressure distribution throughout the specimen at the constant strain rate applied ( 0.00075 cm/min ) according to ASTM D 4767-88.

The strain versus pore water pressure response of the specimens tested under the isolated and the multiple gradients are presented in Figures 4.31 through 4.35. As observed throughout these graphs, the pore pressures are not uniformly distributed along the length of the specimens, the bottom pore pressure response lagging behind the top one. The magnitude of the time lag , or the difference between the pore water pressure responses at the top and the bottom at a certain magnitude of axial strain appear to be affected by the previous conditioning ( potential application ) of the specimens. The lower pressure consolidated specimens appear to respond more uniformly with respect to pore water pressure distributions than the higher pressure consolidated specimens. The differences also appear to increase with chemical and temperature gradients which is most likely due to the non-uniform physical changes that occur through the length of the specimens. In all the cases, the pore water pressure response at the top and the bottom of the specimen appear to converge at strain levels in excess of 10 to 12 %, except for the specimens subjected to multiple gradients. This is observed in Figure 4.35 in which the pore water pressure responses do not appear to converge as fast. This is probably due to the increased level of non-uniform changes in the soil specimens with the combined effect of all three potentials applied together.

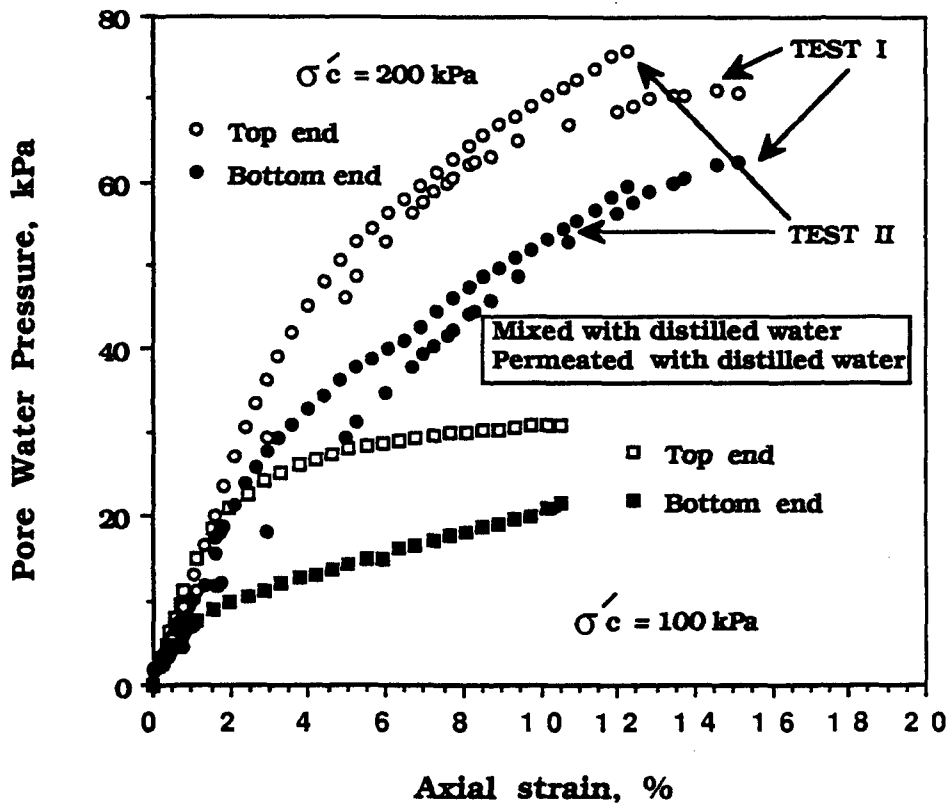


**Figure 4.31 : Axial strain vs. pore water pressure response of base specimens in triaxial shear following hydraulic permeation with distilled water.**

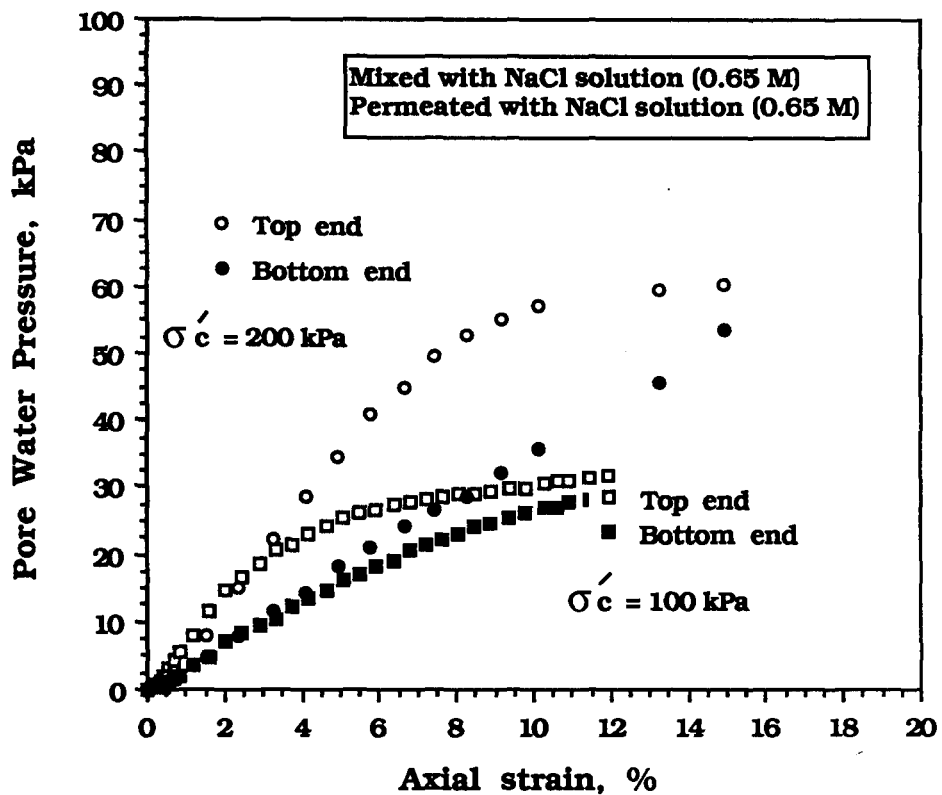


**Figure 4.32 : Axial strain vs. pore water pressure response of salt solution mixed specimens in triaxial shear following permeation with high concentration of salt solution under chemical gradient.**

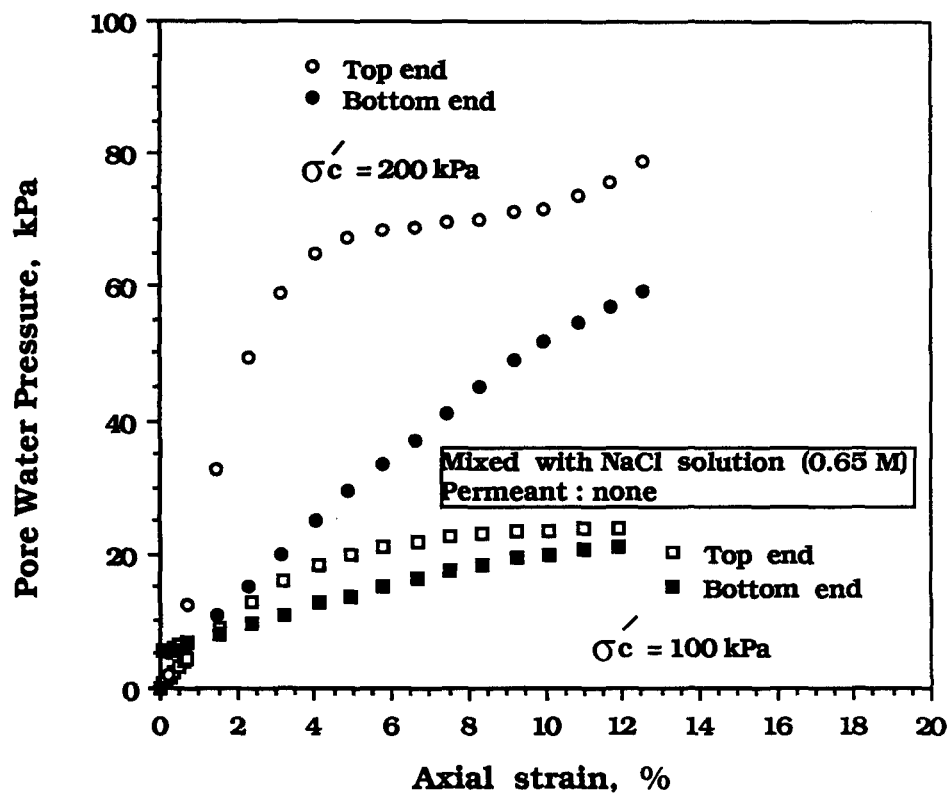


**Figure 4.33 : Axial strain vs. pore water pressure response of salt solution mixed specimen in triaxial shear following pore pressure built up due to chemical gradient. (Initial pressure at bottom = 5 kPa)**

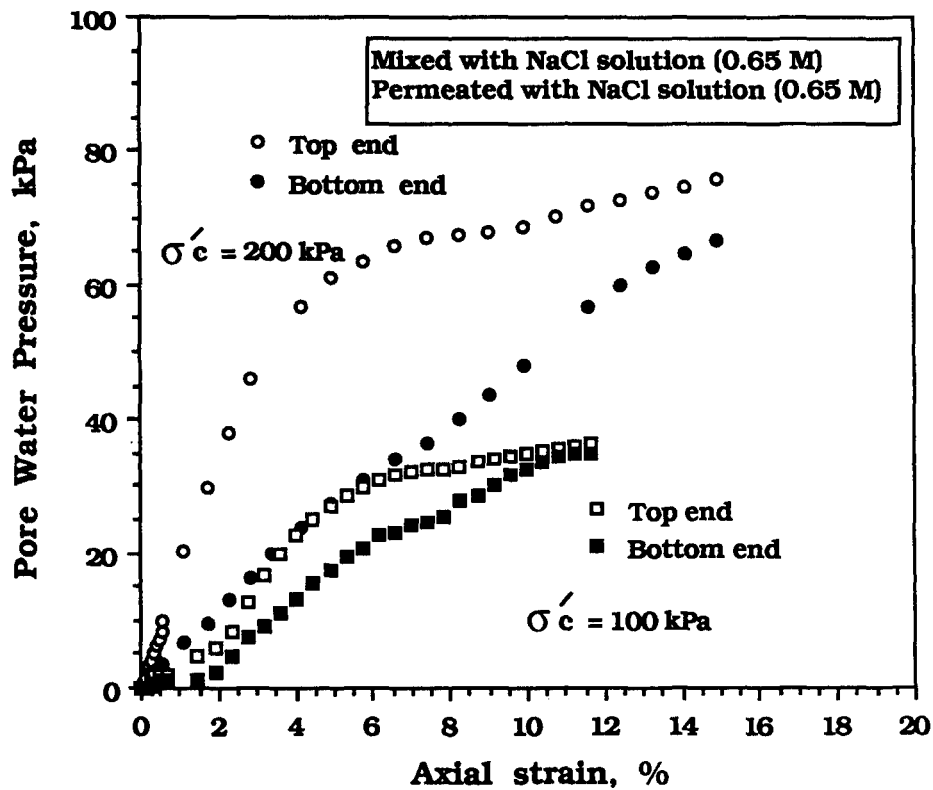
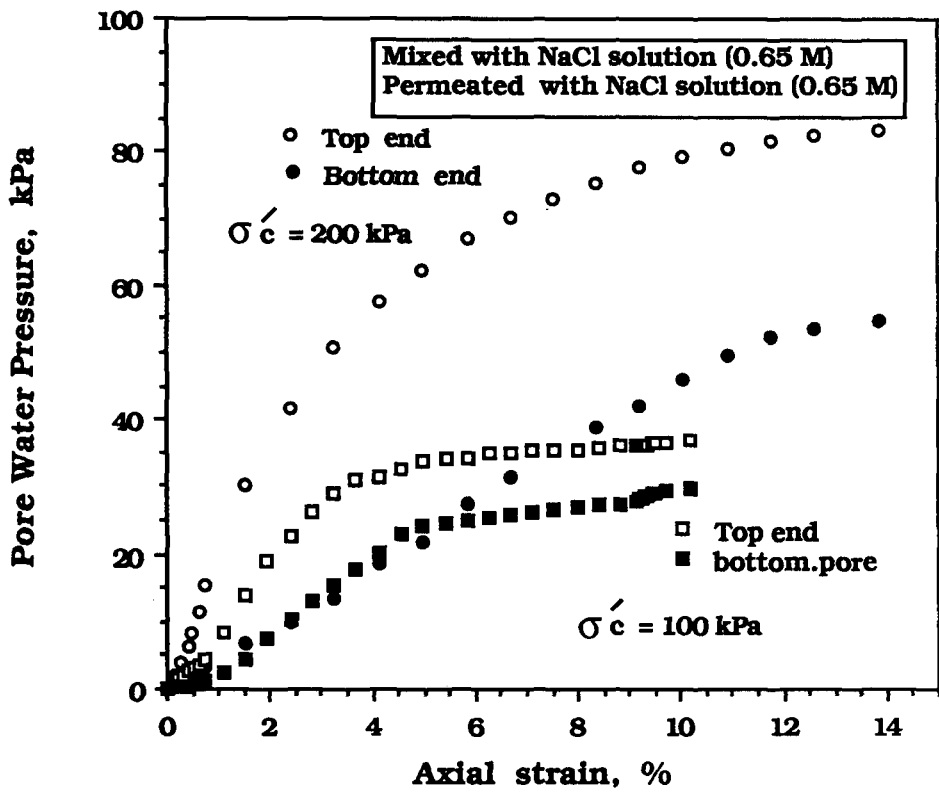


Figure 4.34 : Axial strain vs. pore water pressure response of salt solution mixed specimens in triaxial shear following permeation with salt solution under temperature gradient.



**Figure 4.35 : Axial strain vs. pore water pressure response of salt solution mixed specimens in triaxial shear following permeation with salt solution under multiple gradients.**

## F. COMPRESSIBILITY

Coefficient of consolidation,  $C_v$  values were calculated using the consolidation equation given in section D in Chapter 3. Consolidation tests were performed on 100 kPa and 200 kPa pressure consolidated distilled water mixed specimens.  $C_v$  values obtained from those consolidation tests and the calculated ones using Equation 3.4 are very similar as shown in Table 4.8. Therefore, the other calculated values of  $C_v$  using the corresponding pore pressure data obtained from tests of osmotic, thermo-osmotic, and multiple potential permeability tests are assumed to be reliable values for those specimens. It is difficult and probably impossible to obtain these values in tests using available conventional consolidation equipment. The coefficient of consolidation values calculated using Equation 3.4 are summarized in Table 4.9.

As shown in Table 4.9, the lowest coefficient of consolidation,  $C_v$  was obtained for the specimens test under temperature potential. The compressibility slightly decreased with the intrusion of salt. The interesting finding is the lowered compressibility of the temperature gradient subjected specimens. This does not agree with the findings of compressive strength of these specimens since they exhibited the lowest strengths and also showed more plastic behavior. The lowering of the compressibility is probably due to the overall consolidation of the specimens with the increased temperatures initially. The lowered strength and the apparent plastic behavior may be due to the large differences between the pore water pressures between the ends of the specimens at the strain levels larger than 1% below which the  $C_v$  values were determined from. As the strains increase, the pore water pressure generated would now be emphasized by the pore water pressures developed at the hot end of the specimen since the drainage valves would be closed during the test. The overall increased pore water pressures in the specimen would then give rise to lower strengths and plastic behavior. Therefore, the  $C_v$  values obtained in here reflect the condition of the specimens immediately



conditions. The overall effect of multiple gradients in this case is the lowering of the compressibility probably dominated by the temperature effect.

**Table 4.9: Experimental determined Cv using the proposed method.**

Cv ( cm <sup>2</sup> / min )				
Consolidation Test	No Gradient	Chemical Gradient Drained	Temperature Gradient Drained	Multiple Gradient Drained
Consolidation pressure = 100 kPa				
0.179	0.183	0.173	0.089	0.104
Consolidation pressure = 200 kPa				
0.110	0.109	0.98	0.058	0.073

## CHAPTER V

### DISCUSSION OF RESULTS

In the previous chapter short discussions on the test results and predictions were presented. In this chapter these discussions are expanded and significance of the findings are illustrated by hypothetical field examples, the conditions of which can be simulated in the laboratory using the new system.

#### A. COUPLED FLOW AND STRESS-STRAIN

Figures 4.1 and 4.2 show that the selected hydraulic potential produces the largest flow rate because of the higher energy. The osmotic and thermo-osmotic flow rates are small compared to the hydraulic one. However the physical changes caused by these potentials, as demonstrated by the measurement of changes in mechanical properties in this work, may be irreversible and their effects larger than the hydraulic potential in long term. Olsen (1972) observed a similar effect through his investigations where he emphasized the need to consider non-hydraulic potentials in prediction of liquid transport in soils, especially in deep formations. The consolidation pressure was found to be an important parameter effecting the results with respect to the flow under different gradients in this investigation also. It can be observed from Figures 4.1 and 4.2 that the higher the

consolidation pressure is, the lower the differences among the flow curves under different potentials. This is probably because, the lower effective stress may allow a larger degree of physical and microstructural changes to take place due to more void space.

There is similarity between the plots in Figures 4.7 and 4.8 with respect to the hydraulic permeability under different consolidation pressures. This behavior has been observed by Michaels and Lin (1955) also. Coefficient of hydraulic permeability of distilled water mixed specimens is higher than that of salt solution mixed specimens in both figures. It should be noted that the permeants are different in each case, distilled water in the former and salt solution in the latter one. At first glance, these results might be unexpected because one would expect salt to induce flocculation and therefore larger permeability. However taking into consideration the sample preparation and the difference in the viscosities of the permeants, the results are viable. Since all of the specimens are consolidated, the initial microstructure of the clay solids in slurry form would either be destroyed during consolidation or the new structure would be dominated by the magnitude of the vertical pressure and not the interparticle forces. Therefore salt containing or not, the final structure of a compacted system should not vary much. According to Poiseuille's law, the average velocity of fluid flow through a round capillary of radius  $R$  is inversely proportional to the viscosity of the fluid. Since salt solution would have slightly higher viscosity than distilled water, reduction in permeability should be expected.

In Figures 4.9 and 4.10 there are sharp decreases in  $k_{ht}$ 's until the steady state condition. This is due to fast consolidation with temperature increase. Campanella and Mitchell (1968) made similar observations of consolidation taking place with increasing temperature in soils. Houston et al. (1985) also found that soil density increased when the temperature was increased under drained conditions. The elapsed time until steady state is approximately twice as high at 100 kPa as it is at 200 kPa effective stress. This indicates a linearity between the effective stress and the time required to achieve the induced volume change by the constant temperature increase.

Specimens subjected to temperature potential exhibited the lowest maximum deviatoric stress as shown in Figures 4.29 and 4.30. The same effect

has been observed by others also ( Campanella and Mitchell ( 1968 ), Naik et al., ( 1987 ) ). The main reason behind this is probably the generation of pore water pressures with increased temperature. Other factors such as changing density and viscosity of pore fluid and dissolution of more salt in pore fluid may also influence the strength behavior.

In the case of chemical gradient with drained boundaries, the flow is the reverse direction. Chemical moves in the direction of the gradient and produces water flow in the opposite direction because of molecular diffusion. In this analysis good agreements between experimentally measured and numerically computed values were obtained. Furthermore, effective diffusion coefficient,  $D^*$  was obtained by back calculation using the same numerical solution. The results are  $2 \times 10^{-6}$  and  $2.7 \times 10^{-6}$   $\text{cm}^2/\text{sec}$  for the 100 kPa and 200 kPa pressure consolidated specimens, respectively. These values compare well with  $3 \times 10^{-6}$   $\text{cm}^2/\text{sec}$  as given by Mitchell and Yeung ( 1991 ) for kaolinite clay, as shown in Figure 5.1. The specimens subjected to chemical gradient exhibited the highest maximum deviatoric stress, as shown in Figures 4.29 and 4.30. Clay has a large surface area by volume ratio and clay mineral surfaces carry negative charges. Due to the intrusion of salt (NaCl), concentration of anions increase which gather at the edges of the clay particles. This results in reduced repulsion between the particles. But the specimen is already at a compact state and is under confinement. Therefore, no significant change in the microstructure of the specimen is expected at this state. Because of the reduction of interparticle repelling, however, strength of the soil increases, probably acting more like a slightly over consolidated clay with cohesion. The dry density of soil might have increased slightly which would have contributed to the increased strength, also.

Figures 5.2 and 5.3 show scanning electron microscope pictures of the kaolinite specimens. Figures 5.2.a and 5.2.b show the horizontal and vertical orientation of pure kaolinite particles, respectively. Figures 5.3.a and 5.3.b show the orientation of kaolinite particles with salt after the application of the osmotic gradient. As observed in these Figures, particles are in agglomerations in face to face orientation mostly. There is no evidence of change in microstructure toward flocculation with the intrusion of the salt.

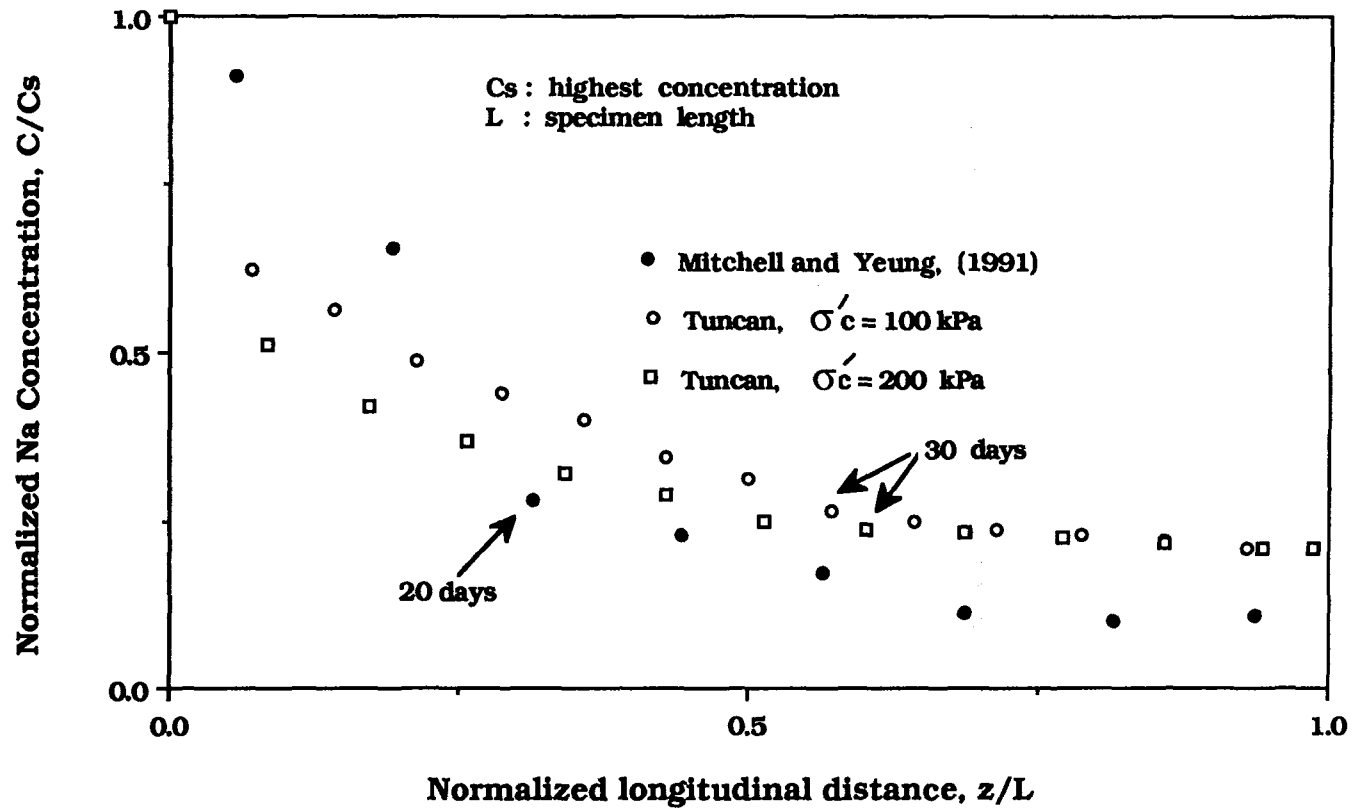


Figure 5.1 : Sodium diffusion into saturated kaolinite under chemical potential

## B. COUPLED FLOW UNDER MULTIPLE GRADIENTS

Figures 4.17 and 4.18 show that there is good agreement between measured data and computed data when Equation 2.13 is used with coupled flow coefficients measured under drained boundary conditions. The significance of this finding is that the coupled coefficients of hydraulic flow appear to preserve their constancy when the potentials are present simultaneously. Obviously, this is valid for the duration, magnitudes and types of the potentials tested in this work. However, it can be argued that this validation may apply to most natural field cases, since the relative magnitudes of the potentials selected in this work are realistic with respect to field cases. The individual magnitudes of these potentials are much larger than typical field potentials, probably simulating extreme situations encountered in the field.

The constancy of the coupled coefficients indicate that the soil constancy and composition is also preserved. This is rather disproved by the variation in the mechanical properties and behavior the soil subjected to the potentials. Although the individual coefficients might have been influenced by the presence of other potentials in the system, the net flow does not change. Therefore, superpositioning the thermo-osmotic, osmotic, and hydraulic forces producing the flow, as given in equation 2.13, is valid.

Cumulative flows under the multiple gradients is less than those under hydraulic gradients. The retardation is caused by a combination of osmotic and thermo-osmotic consolidation. The consolidation induced by potentials over a period of time also becomes a significant factor in estimation of coupled coefficients by the measurement of pore water pressures at the potential sites. This obviously is a faster method of estimating the coupled coefficients of permeability. However, the method over estimates these coefficients and thus flow. The coupled coefficients of permeability should be measured at steady - state when the induced consolidation by the various potentials are more or less completed. The pore water pressure method estimates a higher coefficient prior to completion consolidation and steady state condition. If proper formulations are developed to incorporate the effect of consolidation in the predicted coefficients, the pore pressure method to determine flow under multiple gradients should be

advantageous. Its advantage over the former method would obviously be that it would be a rapid and non-destructive testing.

### C. COMPRESSIBILITY

Comparison of the coefficient of consolidation values obtained from conventional consolidation tests and from the pore pressure measurements in the low strain range of triaxial shear testing yielded very good agreement. The same method was used to predict  $C_v$ 's for the specimens subjected to various gradients. The results show the expected which can be explained readily.

The significant reduction in the compressibility of the heated specimens demonstrated the influence of thermo-osmotic consolidation. Observing the pore pressure response in triaxial shear of the specimens subjected to temperature potential ( Figure 4.3 ), there is a sharp increase of pressure at the top end initially, whereas the bottom end pressure increases smoothly. This may be attributed to a densified or consolidated zone near the bottom end which quickly transmits the heat generated pore pressure upward once the drainage valve at the bottom is closed for the undrained shear. The transmitted pressure then enhances the pore pressure generated at the top which results in a sharp increase initially, until all bottom pressure is transmitted. The bottom pressure response is probably influenced by the densified zone also.

The new system can potentially be used to measure  $C_v$  fairly quickly, without conducting the triaxial shear test. This capability was not tested for this work but is recommended for future work. It can be performed as follows: After establishing the desired gradient or gradients, specimen would be vertically loaded at a constant pressure similar to one dimensional consolidation test. Improvements can be made in the equipment to control the lateral expansion at this state. Then the pore water pressures would be observed until the pore pressure value at the opposite end of the specimen attain to the maximum value of pore pressure measured at the loaded end. The time it takes for this pressure to travel from top to bottom is measured and then used in the calculation of  $C_v$  ( Equation 3.5 ) for the particular soil specimen. The suggested procedure, when developed, may have benefits in over others for it would be a rapid and non-destructive

technique.

#### D. USE OF NEW EQUIPMENT

The new equipment developed in this dissertation made the tests discussed above possible. It is the author's assessment that this equipment essentially widened the window of experimental environmental geotechnology. Using this equipment, it is probably possible to simulate a wider range of field situations related to environmental problems. The following examples are representations of possible use of the equipment to simulate some field conditions.

**Case 1:** A factory site mostly consisting of fine grained materials and limestone is confined with retaining walls on the sides. There is a concrete slab on the ground surface and the soil is underlain by rock. The concrete slab supports three cylindrical acid tanks. There is a tower between the main factory buildings and the tanks. The problem is differential rising of the tower on one corner. The reason causing this situation was found to be acid leakage from the tanks and also oils from the factory over the years. These materials had permeated in to the ground. The chemical reactions between acid and limestone had increased the pore water temperature up to 60 °C which caused large pore water pressures to develop. Drainage was inhibited by oily layers of soil and confining structures around the site, therefore the excess pressure pushed up the concrete slab and the nearby structures. In here, probably the so called "undrained boundaries" condition was created over the years. This situation could be simulated in the laboratory with several different combinations of possible potentials, such as temperature and chemical, using the new system. The results drawn from those experiments could be used to first understand the magnitude of the pore water pressures and the volume of flow induced. This information can then be used in subsequent remediation as well as preventive actions at the site.

**Case 2:** Power cables and nuclear power plants are continuous source of heat potentials. This situation can be simulated in the laboratory in two different ways. One is the large area simulation (unconfined boundaries) which means that there would be a long term constant temperature gradient on the specimen. The



other one is the simulation of relatively small area (confined boundaries) which indicates uniform distribution of heat in soil. This would be an example of consolidation under uniform temperature application.

**Case 3:** Determining the engineering behavior of marine sediments under hydraulic, chemical, temperature, and electrical gradients may be an interesting application of the new system. Often due to the low consolidation pressures and the underconsolidated states of marine sediments, application of multiple gradients that produce coupled flow should bring about more detectable changes in their physico-chemistry and micro-structure. There may be several scenarios, taking in to consideration near shore and coastal soils : 1) salt water diffusion into land soils. and 2) flow due to the lateral and vertical temperature differences in marine floor.

It seems that the above-mentioned examples did arise because of the wide capability of the equipment developed in this dissertation. One of the important finding of this work is that the new system is potentially a non-destructive test equipment to measure coupled coefficients of permeabilities and also the coefficient of consolidation for soils under different potentials.

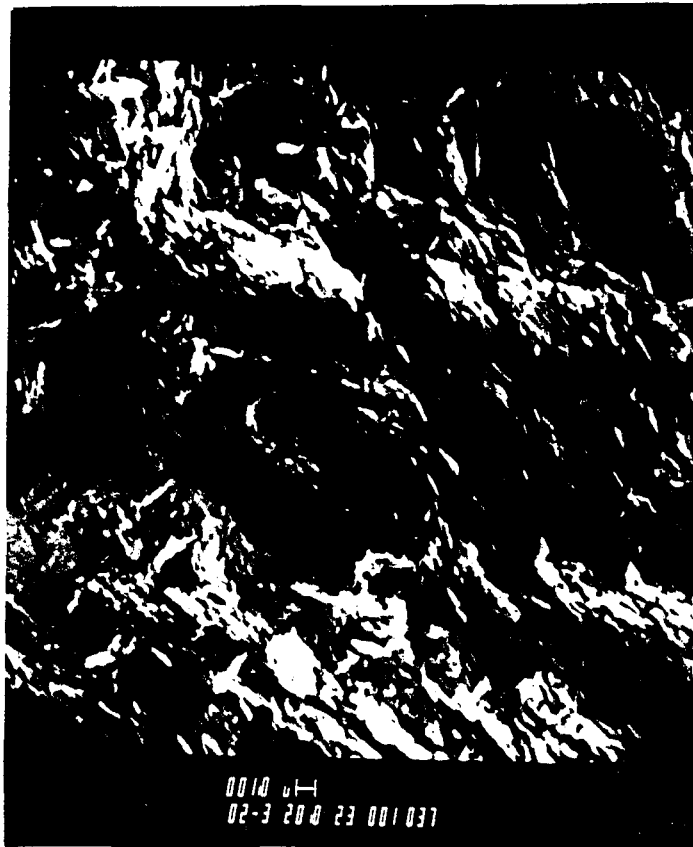


Figure 5.2. a : SEM micrograph of pure kaolinite specimen consolidated at  $2 \text{ kg/cm}^2$ , [ horizontal cross-section ].



Figure 5.2. b : SEM micrograph of pure kaolinite specimen consolidated at 2 kg/cm<sup>2</sup>, [ vertical cross-section ].



Figure 5.3. a: SEM micrograph of kaolinite specimen consolidated at  $2 \text{ kg/cm}^2$  and subjected to the salt gradient, [horizontal cross-section].



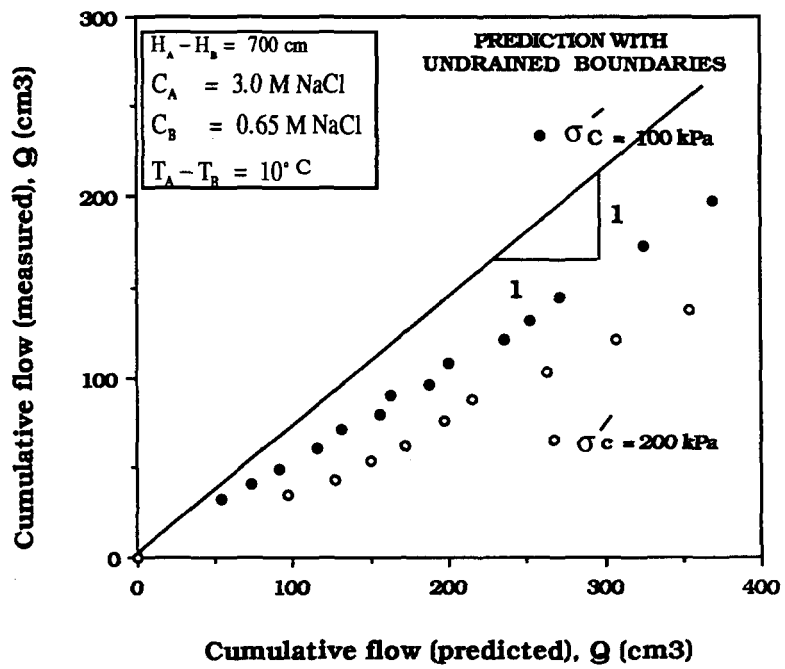
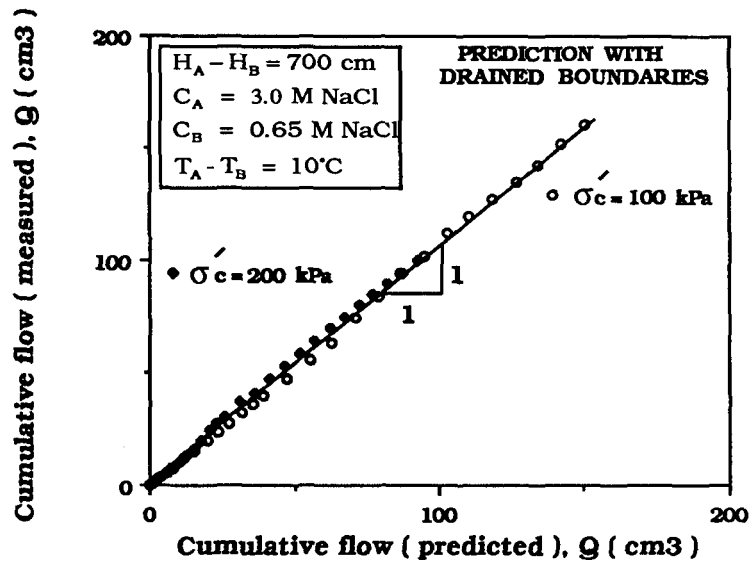
Figure 5.3. b : SEM micrograph of kaolinite specimen consolidated at  $2 \text{ kg/cm}^2$  and subjected to the salt gradient, [vertical cross-section].

## **CONCLUSIONS AND RECOMMENDATIONS**

### **A. CONCLUSIONS**

The objectives of this study were two-fold : 1) the development of a new laboratory equipment to measure the flow of water through saturated clay soil under single and multiple gradients, 2) determination of the accuracy and validity of a phenomenological coupled flow equation which includes multiple gradients. Overall, good agreement between experimental findings and the theoretical equation was achieved when coupled flow coefficients predicted from " drained boundary " experiments were used in the predictions. Agreement was not achieved when parameters predicted from " undrained boundary " experiments were used in the equation.

When the constancy and composition of the soils were checked by direct and indirect methods, it was found that soil properties did change with the applied osmotic, thermo-osmotic and hydraulic potentials. However neither these changes nor the inter-dependence of coupled coefficients of flow invalidated the use of the theoretical Equation 2.13. When the coupled coefficients were calculated from pore pressures induced at the potential application sides, the net flow was over estimated.



The significance of these findings are:

- 1) The superpositioning of the forces that cause flow of water in saturated soil is valid provided that the coupled coefficients are determined at steady state flow under constant potentials.
- 2) Determination of the coupled flow coefficients using the pore water pressure built up at the potential sites is faster than direct determination from flow measurements. However, if these coefficients are used in prediction of flow, it is necessary to modify equation 2.13 to incorporate the effects of osmotic, thermo-osmotic and hydraulically induced consolidation prior to steady state flow.

The following specific conclusions emerged from this study:

- 1) The triaxial test system developed in this study has been proven by its stable performance and good repeatability of water conduction and triaxial shear data on replicate specimens.
- 2) As the consolidation pressure increased the coupled flow rates decreased due to the densification of the soil. Larger changes occurred in the flow rates and coupled coefficients of permeabilities for osmotic and thermo-osmotic potentials than those for hydraulic potential with consolidation pressure.
- 3) With the application of thermo-osmotic potential, the coupled coefficient of hydraulic permeability decreased sharply with time before achieving a steady value.  
This was attributed to thermo-osmotic consolidation.  
The elapsed time for this transient range was twice as much for 100kpa, as for 200 kPa effective stress.
- 4) The coupled coefficient of osmotic permeability was influenced the most



with effective stress. This coefficient decreased to about one third of its original value than the consolidation pressure was doubled.

- 5) The measured values of sodium concentration distribution for the 100 kPa and 200 kPa pressure consolidated specimens agreed well with the theoretical predictions. The approximate effective diffusion coefficients were calculated as  $2 \times 10^{-6} \text{ cm}^2/\text{sec}$  and  $2.7 \times 10^{-6} \text{ cm}^2/\text{sec}$  for the 100 kPa and 200 kPa effective stress specimens, respectively.
- 6) For the same duration of time the cumulative flows under multiple gradients were less than the cumulative flows under hydraulic gradient alone. This is attributed to the backward flow caused by the chemical diffusion and the consolidation effects of temperature and chemical potentials.
- 7) The specimens which were subjected to chemical potential with pore pressure build up at the boundaries exhibited lower strengths and stiffness probably due to the initial pore water pressure build up. The specimens subjected to permeation of high concentration salt solution showed increased strength.

The specimens subjected to temperature potential exhibited plastic behavior and lowered strengths. This was attributed to the induced volume change by the temperature gradients such that when the sample was sheared it behaved like an underconsolidated material.

- 8) The proposed procedure to determine the coefficient of consolidation from pore water pressure responses during triaxial shear may be a viable method which can potentially be developed into a non-destructive test.

## **B. RECOMMENDATIONS**

The following recommendations are made for the continuation of this work:

- 1) Addition of electrical potential capability to the equipment.
- 2) Experimental study of specific inter-relationships between the coupled coefficients of permeabilities by :
  - a) changing one gradient at a time, while keeping the others constant,
  - b) changing the surrounding temperature of the soil specimen from room temperature of 24 °C.
- 3) Study and testing of better insulation around the specimen to prevent the heat loss and establish linear distribution of temperature at steady state.
- 4) Study of after test properties of the soil such as density, and water content distribution along the length and across the radius of the specimen.
- 5) Study of flow when the potentials are applied at different combinations of flow directions.
- 6) Develop the non-destructive testing potential of the equipment by :
  - a) Modifying the coupled flow equation (Equation 2.13) to include the

effects of consolidation such that values of pore water pressures generated at the potential application sites can be used reliably to predict flow.

b) Conduct adequate number of tests to determine if of the proposed method of applying a constant vertical stress and measuring the migration rate of pore water pressure from top to bottom of a specimen can be used reliably to predict coefficient of consolidation,  $C_v$ .

## REFERENCES

- Abd-El-Aziz M. H., and Taylor S.A. ( 1965 ), " Simultaneous Flow of Water and Salt Through Unsaturated Porous Media: I. Rate Equations," Soil Science Society Proceedings, pp. 141-143.
- Abdel-Hadi O. N., and Mitchell J. K. ( 1981 ), " Coupled Heat and Water Flows Around Buried Cables," The Journal of the Geotechnical Engineering Division, ASCE, Vol. 107, No. GT11, pp. 1461 - 1481.
- Baldi G., Borsetto M., and Hueckel T. ( 1986 ), " Thermally Induced Strains and Pore Pressures in Clays , " International Symposium on Environmental Geotechnology, pp. 391- 402.
- Barbour S. L., and Fredlund D. G. ( 1989 ), " Mechanism of Osmotic Flow and Volume Change in Clay Soils, " Canadian Geotechnical Journal, Vol. 26, pp. 551 - 562.
- Beziat A., and Gabis B. ( 1988 ), " Effect of Compaction Pressure and Water Content on the Thermal Conductivity of Some Natural Clays, " The Clay Minerals Society, Vol. 36, No. 5, pp. 462 - 466.

- Biggar J. W., and Neilsen D. R. (1960), " Diffusion Effects in Miscible Displacement Occuring in Saturated and Unsaturated Porous Materials, " Journal of Geophysical Research, Vol. 65, NO. 9, pp. 2887 - 2895.
- Bjerrum L. Moum J., and Eide O. (1967), "Application of Electro-osmosis on a Foundation Problem in Norwegian Quick Clay , " Geotechnique, Vol. 17, pp. 214 - 235.
- Campanella R. J., and Mitchell, J. K. (1968), " Influence of Temperature Variations on Soil Behavior, " Journal of the Soil Mechanics and Foundation Division, Division, ASCE, Vol. 94, No. SM3, pp. 709 - 734.
- Casagrande L. (1952), " Electro-Osmotic Stabilization of Soils, " Journal of Boston Society of Civil Engineers, Vol. XXXIX, No. 1, pp. 1941-1953.
- Cassel D. K., Neilsen D. R., and Biggar J. W., (1968), " Soil Water Movement in Response to Imposed Temperature Gradients," Soil Science Society of America, Proceeding, Vol. 33, pp. 493- 500.
- Esrig M. I. (1968), " Pore Pressures, Consolidation, and Electrokinetics, " Journal of the Soil Mechanics and Foundations Division, ASCE, No. SM4, Vol. 94, pp. 899 -921.
- Evans J. C. and Fang H. Y. (1986), " Triaxial Equipment for Permeability Testing with Hazardous and Toxic Permeants, ASTM Geotechnical Testing Journal , Vol. 9, No. 3, pp. 126-132.
- Evgin E. and Svec O. J. (1988), " Heat and Moisture Transfer Characteristics of Compacted Mackenzie Silt," Geotechnical Testing Journal, GTJODJ, Vol. 11, No. 2, June, pp. 92 - 99.

- Fang H. Y. ( 1986 ), " Introductory Remarks on Environmental Geotechnology, " Environmental Geotechnology, Proceedings, International Symposium on , ed. by H.Y. Fang ; Envo Publishing Co., Bethlehem, pp.1-14 .
- Fang H. Y. and Pamukcu S., editors ( 1989 ), 2nd International Symposium on Environmental Geotechnology, Proceedings, Envo Publishing Co., Bethlehem, V.1, 550p.
- Fang H.Y. ( 1989 ), " Particle Theory - A Unified Approach for Analyzing Soil Behavior, in proceedings, 2nd International Symposium on Environmental Geotechnology, ed. by H.y. Fang and S. Pamukcu; Envo Publishing Co., Bethlehem, V.1., pp. 167-194.
- Fisher K.M. ( 1991 ), " The Influence of Organic Carbon Flux on the Deposition of Clays in the Marine Environment: Implications with Respect to Microstructure," Microstructure of Fine- Grained Sediments from Mud to Shale, Benett, R.H., Bryat, W.R., and Hulbert M.H., Springer-Verlag, New York, pp. 147-160
- Goodall and Quicgly R. M. ( 1977 ), " Pollutant Migration from Two Sanitary Landfill Sites Near Sarnia, Ontario, " Canadian Geotechnical Journal, Vol. 14, pp. 223 - 236.
- Geraminegad M., and Saxena S. K., ( 1986 ), " A Coupled Thermoelastic Model for Saturated - Unsaturated Porous Media, " Geotechnique 36, No. 4, pp. 539-550.
- Graham J., Fensury H., and Shields D. H. ( 1988 ), " The Thawed Strength of Soil Compacted While Frozen, " Geotechnical Testing Journal, GTJODJ, Vol. 11, No. 2, pp. 125 - 131.
- Gray D. H. ( 1968 ), " Thermo - Osmotic and Thermoelectric Coupling in Saturated Soils, " pp. 66 - 77.

- Gray D. H., and Mitchell J. K. (1967), "Fundamental Aspects of Electro-Osmosis in Soils," *Journal of Soil Mechanics and Foundations Division*, Proceedings of the ASCE, Vol. 93, No. SM6, pp. 209 - 235.
- Gurr C. G., Marshall T. J., and Hutton J. T., (1952), "Movement of Water in Soil Due to a Temperature Gradient," *Soil Science* Vol. 74, pp. 335 - 345.
- Houston S. L., Houston W. N., and Williams N. D. (1985), "Thermo - Mechanical Behavior of Seafloor Sediments," *Journal of Geotechnical Engineering*, ASCE, Vol. 111, No. 11, pp. 1249 - 1263.
- McCarthy, D. F. (1988), "Essentials of Soil Mechanics and Foundations," Prentice Hall, Englewood Cliffs, New Jersey 07632.
- Michaels A. S., and Lin C. S. (1955), "Effects of Counterelectro - Osmosis and Sodium Ion Exchange on Permeability of Kaolinite," *Industrial and Engineering Chemistry*, Vol. 47, No. 6, pp. 1249 - 1253.
- Miller, D.G. (1960), "Thermodynamics of Irreversible Processes . The Experimental Verification of the Onsager Reciprocal Relations," *Chemical Review*, pp. 15-37.
- Mitchell J.K., Greenberg J.A., and Witherspoon P.A. (1973), "Chemico-Osmotic Effects in Fine-Grained Soils," *Journal of the Soil Mechanics and Foundations Divisions*, ASCE, Vol. 99, No. SM4, pp. 307-321.
- Mitchell, J. K. (1976), "Fundamentals of Soil Behavior," John Wiley & Sons, Inc. New York, pp. 341- 342.
- Mitchell J. K. and Yeung A. T. (1991), "Electro - kinetic Flow Barriers in Compacted Clay," *Transportation Research Board* 1288, pp. 1 - 9.

- Naik D., (1986), "Effect of Temperature and Pore Fluid on Shear Characteristics of Clay," *International Symposium on Environmental Geotechnology*, pp. 382 - 390.
- Olsen H. W. (1972), "Liquid Movement Through Kaolinite Under Hydraulic, Electric, and Osmotic Gradients," *The American Association of Petroleum Geologist Bulletin*, Vol. 56, No. 10, pp. 2022 - 2028.
- Pamukcu S., and Tuncan M., (1991) "Influence of Some Physicochemical Activities on Mechanical Behavior of Clays," *Microstructure of Fine- Grained Sediments from Mud to Shale*, Bennett, R.H., Bryat, W.R., and Hulbert M.H., Springer-Verlag, New York, pp. 241-255.
- Pamukcu S., Tuncan M., and Fang H.Y., (1990) "Influence of Some Environmental Activities on Mechanical Behavior of Clays," in *Physico-Chemical Aspects of Soil and Related Materials*, ASTM STP 1095; Philadelphia, American Society for Testing and Materials, pp. 91-107.
- Penrod E. B., Walton w. w., and Terrell D. V. (1958), "A Method to Describe Soil Temperature Variation," *Journal of the Soil Mechanics and Foundation Division, Proceedings of the ASCE*, vol. 84, No. SM1, pp. 1537.1 - 8.
- Radhakrishna H. S., Lau Ka-C., and Crawford A. M. (1984), "Coupled Heat and Moisture Flow Through Soils," *Journal of Geotechnical Engineering, ASCE*, Vol.110, No. 12, pp. 1766 - 1784.
- Salomone L. A., Kovacs W. D., and Kusuda T. (1984), *Thermal Performance of Fine-Grained Soils*, " *Journal of the Geotechnical Engineering, Proceeding of the ASCE*, Vol. 110, No. 3, pp. 359 - 373.
- Segall B. A., O'Bannon C. E., and Matthias J. A. (1980), "Electro - Osmosis Chemistry and Water Quality," *Journal of the Geotechnical Engineering Division, Proceedings of the ASCE*, Vol. 106, No. GT10, pp. 1148 - 1152.



- Schackelford C. D. ( 1988 ), " Diffusion as a Transport Process in Fine - Grained Barrier Materials, " *Geotechnical News*, pp. 24 - 27.
- Skempton A.W. and Bishop A.W. ( 1964 ), " Soils , " Chapter 10 of *Building Materials , their Elasticity and Plasticity*, ed. M. Reiner, North- Holland Publishers, Amsterdam.
- Taylor S. A., and Cary J. W. ( 1964 ), " Linear equations for the Simultaneous Flow of Matter and Energy in a Continuous Soil System, " *Soil Science Society Proceeding*, pp. 167 - 171.
- Tuncan M., Khan L.I., and Pamukcu S. ( 1988 ), " The Effect of Leachate on Geotechnical Properties of Clay Liners, " in *Hazardous and Industrial Waste, Proceedings, 20 th Mid-Atlantic Industrial Waste Conference*, pp. 133-144.
- Tuncan M. , Pamukcu S., and Hu Z.X., ( 1989 ), " Development of Multipurpose Triaxial Apparatus for Testing of Soils under Coupled Influence of Thermal-Chemical-Hydraulic & Electrical Potential," in *Proceedings, 2nd International Symposium on Environmental Geotechnolgy* , ed. by H.Y. Fang and Sibel Pamukcu; Envo Publishing Co., Bethlehem, V.1, pp. 135-152.
- Tuncan M. ( 1991 ), " Development of Apparatus for Determining Mechanical Behavior of Clay under Multiple Gradients," in *Proceedings, 2nd International Symposium on Environmental Geotechnolgy* , ed. by H.Y. Fang and Sibel Pamukcu; Envo Publishing Co., Bethlehem, V.2, pp. 215-221.

## **APPENDIX A**

### **OPERATION OF MULTIPLE POTENTIAL FLEXIBLE WALL PERMEAMETER USERS' MANUAL**

This system has four units in operation :

- 1) Control panel ( Figure A.1).
- 2) Subcontrol panel ( Figure A.2).
- 3) Heat control panel ( Figure A.3).
- 4) Data acquisition ( Figure A.4).

#### **OPERATION**

After mounting the sample in the triaxial cell, the following steps are taken to operate the permeameter:

##### **A. TRIAXIAL CONSOLIDATION**

1. Fill the tubing connected to the top and the bottom platens, and inflow and outfl standpipes. Make sure there are no air bubbles in tubings or in standpipes.

2. Fill the triaxial cell with distilled water switch (4) on on the SUB CONTROL panel. Make sure that the valve (9) for pressure TRANSFER cell is OFF.
  
3. Adjust cell pressure using pressure regulator (1) on the MAIN CONTROL panel checking the value with pressure gauge (7). To apply the cell pressure, TURN ON (4) on the MAIN CONTROL panel, (9) on the pressure TRANSFER cell, and (3) for Cell.I and (12) for Cell.II on the SUB CONTROL panel.
  
4. To fill the the top and the bottom platens' drainage tubings :
  - 1) For Cell.I TURN (5) on the SUB CONTROL panel clockwise for the top platen and then counter clockwise for the bottom platen. Subsequently, TURN ON (9) and (8) on the MAIN CONTROL panel for the top and the bottom platens, respectively.
  - 2) for Cell.II TURN (14) on the SUB CONTROL panel clockwise for the top platen and then counter clockwise for the bottom platen. Subsequently, TURN ON (18) and (17) on the MAIN CONTROL panel for the top and bottom platens, respectively.
  
5. Application of back pressures : On the MAIN CONTROL pane; 1) for Cell.I, adjust pressure regulators (2) and (3) to the desired pressures for the inflow and outflow standpipes , respectively. Now, make sure the valves (8), (9), (21), and (23) were TURNED OFF!... Then TURN ON (9) and (8) for the top and the bottom platens, respectively. On the SUB CONTROL panel; TURN ON (2) and (3) for the top and the bottom platens, respectively.
  - 2) for Cell.II, adjust pressure regulators (12) and (13) to the desired pressures for the inflow and outflow standpipes, respectively. Now, make sure the valves (17), (18); (22), and (23) were TURNED OFF!... Then TURN (17) and (18) for the top and the bottom platens, respectively. On the SUB CONTROL panel;

TURN ON (10) and (11) for the top and the bottom platens, respectively.

7. Taking the initial readings: For Cell.I; on the MAIN CONTROL panel read standpipe (10) for inflow (11) for outflow.

For Cell.II; on the MAIN CONTROL panel read (19) for inflow and (20) for outflow.

When the rate of flow in both standpipes are equivalent for at least a couple days, this indicates the completion of consolidation under the applied triaxial stress.

## B. APPLICATION OF HYDRAULIC GRADIENT

1. After completion of triaxial consolidation, apply the hydraulic gradient:

1) Cell.I; on the MAIN CONTROL panel, make sure the valves (9) and (8) for the top and the bottom platens are TURNED OFF !... Adjust pressure regulators (3) and (2) for the top and bottom platens, respectively to the desired level. Then TURN ON (9) and (8) on the MAIN CONTROL panel

2) Cell.II; on the MAIN CONTROL panel, make sure the valves (18) and (17) for the top and the bottom platens are TURNED off !... Adjust pressure regulators (13) and (12) for the top and bottom platens, respectively to the desired level. Then TURN ON (18) and (17) on.

2. Readings: Cell.I; read standpipes (10) and (11) for inflow and outflow, respectively on the MAIN CONTROL panel.

Cell.II; read standpipes (19) and (20) for inflow and outflow, respectively on the MAIN CONTROL panel.

## C. APPLICATION OF CHEMICAL GRADIENT

1. Make sure that the inflow and outflow standpipes, and the top and the bottom platen reservoirs are completely emptied !...

2. First , fill reservoir B and the inflow and outflow standpipes with the chemical solution.
  - 1) Cell.I; on the MAIN CONTROL panel TURN OFF ( 9 ) and ( 8 ) , and then open valves ( 21 ) , ( 24 ) , and ( 25 ) by turning them counter clockwise. This will fill the standpipes. After the filling of the standpipes, CLOSE ( 24 ) and ( 25 ) . TURN ON ( 9 ) and ( 8 ) on the MAIN CONTROL panel. Make sure each time to TURN ( 5 ) colockwise and counter clockwise on the SUB CONTROL panel corresponding to the operation of ( 9 ) and ( 8 ) on the MAIN CONTROL panel, respectively.
  - 2) Cell.II; TURN ( 9 ) and ( 8 ) OFF , and then open valves ( 21 ) , ( 24 ) , and ( 25 ) by turning counter clockwise. After the filling of the standpipes, TURN ( 24 ) and ( 25 ) OFF. TURN ON ( 9 ) and ( 8 ) on the MAIN MAIN CONTROL panel Make sure each time to TURN ( 5 ) colockwise and counter clockwise on the SUB CONTROL panel corresponding to the operation of ( 9 ) and ( 8 ) on the MAIN CONTROL panel, respectively.
  
3. If the test is “ DRAINED BOUNDARIES “ case, leave the valves ( 21 ) and ( 23 ) open !... To check the concentration of the chemical solution either in the top or in the bottom platen reservoirs during the test : 1) Cell.I; TURN OFF ( 9 ) or ( 8 ) on the MAIN CONTROL panel and then disconnect the reduction adaptor which connects the smaller diameter drainage tubing inserted in the platens with the larger drainage tubing connected to valve ( 5 ) on the MAIN CONTROL panel . Insert the tubing into the sample container and TURN ON ( 9 ) or ( 8 ) on to take in a small volume of liquid. Then connect the adaptor and carry on the test.
  - 2) Cell.II; TURN OFF ( 18 ) or ( 17 ) on the MAIN CONTROL panel and then disconnect the reduction adaptor which connects smaller diameter drainage tubing inserted in the platens with the larger drainage tubing connected to valve ( 14 ) on the SUB CONTROL panel. Insert the tubing into the sample container and TURN ON ( 18 ) or ( 17 ) to take in a small volume of liquid. Then connect the adaptor and carry on the test.

4. Readings: Cell.I; read standpipes (10) and (11) for inflow and outflow, respectively on the MAIN CONTROL panel.  
Cell.II; read standpipes (19) and (20) for inflow and outflow, respectively on the MAIN CONTROL panel.
5. If the test is "UNDRAINED BOUNDARIES" case: 1) Cell.I; TURN OFF (9) and (8) on the MAIN CONTROL panel. TURN ON (6) and (7) on to measure the pore water pressures.  
2) Cell.II TURN OFF (18) and (17) on the MAIN CONTROL panel  
TURN ON (15) and (16) on to measure the pore water pressures.

#### C. APPLICATION OF TEMPERATURE GRADIENT

1. After completion of triaxial consolidation, heat applied using temperature controllers and veryak. SWITCH the power ON for the heat control panel (Figure A.3).
2. Adjust the veryak (6) or (7) to the desired voltage for either the bottom or top platen thermofoil heaters. A calibration chart is provided with this manual. it is very "IMPOTANT" to know that the maximum applicable voltage for the thermofoil heaters installed in this equipment is 45 volts.
3. Find the peak voltage value by the trial and error to obtain constant temperature. On the HEAT CONTROL panel, observe the heat increase from the temperature controllers (1) and (2) and thermometer (3). (1) is connected to the thermocouples installed in the bottom platen, (2) is connected to the thermocouples installed in the top platen, and (3) is connected to the thermocouple installed in the cell to measure cell water temperature. Set the temperature controllers at least 10 °C ahead

of the temperature being applied to prevent any collapse of the heaters due to possible surges in the supplied voltage.

4. Record the temperature values in time until a steady temperature is read.
5. To switch the veryak's power ON or OFF, use SWITCHES (4) and (5) for the veryaks' (6) and (7), respectively.

#### D. ( CIU ) TRIAXIAL SHEAR TEST

1. Make sure that all the drainage valves connected to the cells are closed.
2. Assemble the cell in the load frame.
3. Select the strain rate range.
4. Place the tip of the LVDT on the raising plate.
5. The signal conditioners ( Figure A.4 ): Pore Pressure Transducers ( 1 ) and ( 3 ) are for the top and the bottom platens, respectively, LVDT ( 2 ), and Load Cell ( 4 ). ( 1 ) and ( 3 ) must be checked and recalibrated at the beginning of each test. This calibration is done as follows:
6. Turn on the computer , type " SAMP2 " , and then press "ENTER" twice to get into the data acquisition program. You will see the following :

\*\*\*\*\* Parameter Selection \*\*\*\*\*

1. Gain selection : channel ( 0 , 1 , 2 , 3 ) = ( 1 , 10 , 1 , 1 )

2. Fast- speed Period : Interval ( sec ) = 2, Samples = 60
3. Mid-speed Period : Interval ( min ) =10 samples = 60
4. Slow-speed Period : Interval ( min ) = 15, samples=190
5. Output file name : Dat.dat, Output image file name: Image.dat
6. AVG points / sample = 1000, Sample\_height = 14.0
7. Data Display Configuration....
8. Display a recorded image :
9. Finish Selection:

\*\*\*\*\*

Enter selection number please : 9

\*\*\*\*\*

Selection ( 1 ) is set for the signal conditioners. Set the " 2 ", " 3 ", and "4" depending upon the length of the test. Reset " 5 " each time a new test is run. If a new file name is no provided all the previous data will be deleted. Do not change image.dat. Do not change " 6 ", " 7 ", and " 8 ". Finally, check 1 through 8 and then write " 9 ". Press enter to start your experiment.

7. Now, four grafigs will be displayed on the screen. These first 4 will be the time vs. voltage of pore pressure transducers, LVDT, and Load cell. Press " N " to see the next four graphs, namely stress vs. strain, sress vs. p.w.p at the bottom end vs stress, p.w.p at the top end vs stress, and p.w. p at the top end vs. strain. Pressing " N " one more time will return screen back to the first graphs. Those are graph plotted in real time which will progress with the duration of the experiment.
8. Computer terminates the program automatically according to the setting given in 2, 3, and 4. At the termination all the data will be stored in the file given in setting number 5.



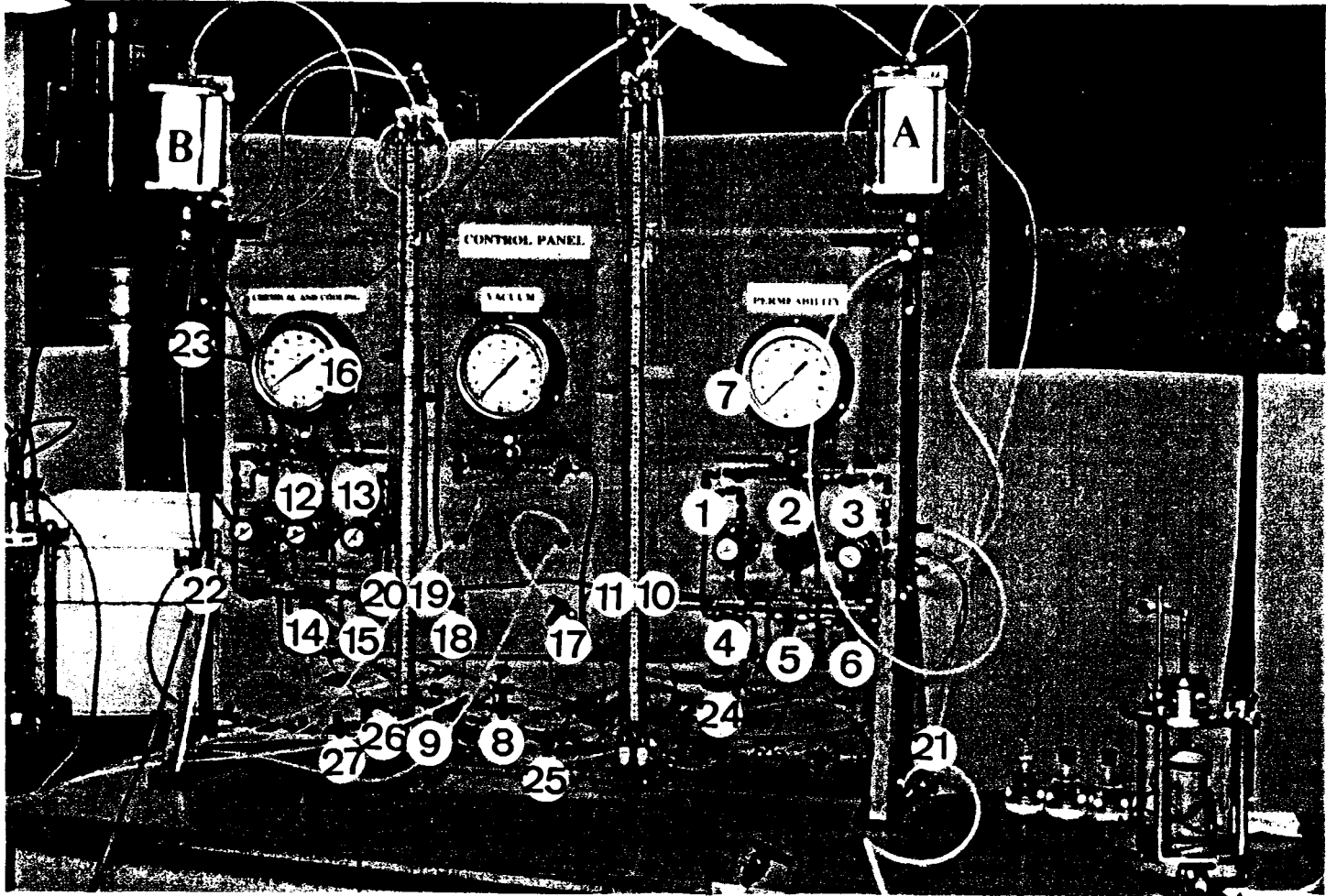


Figure A.1: Photograph of the Main control panel

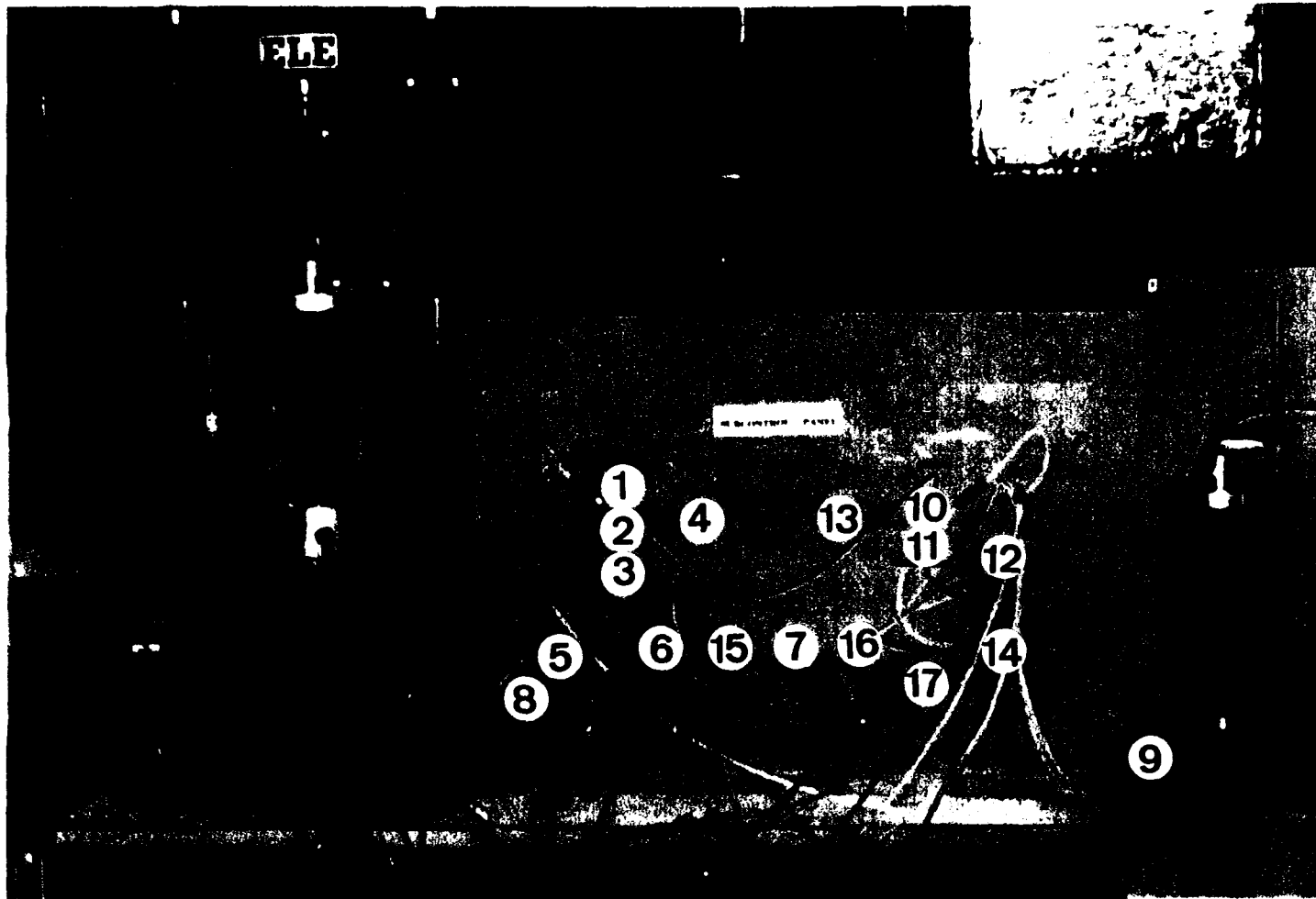


Figure A.2: Photograph of the Sub control panel

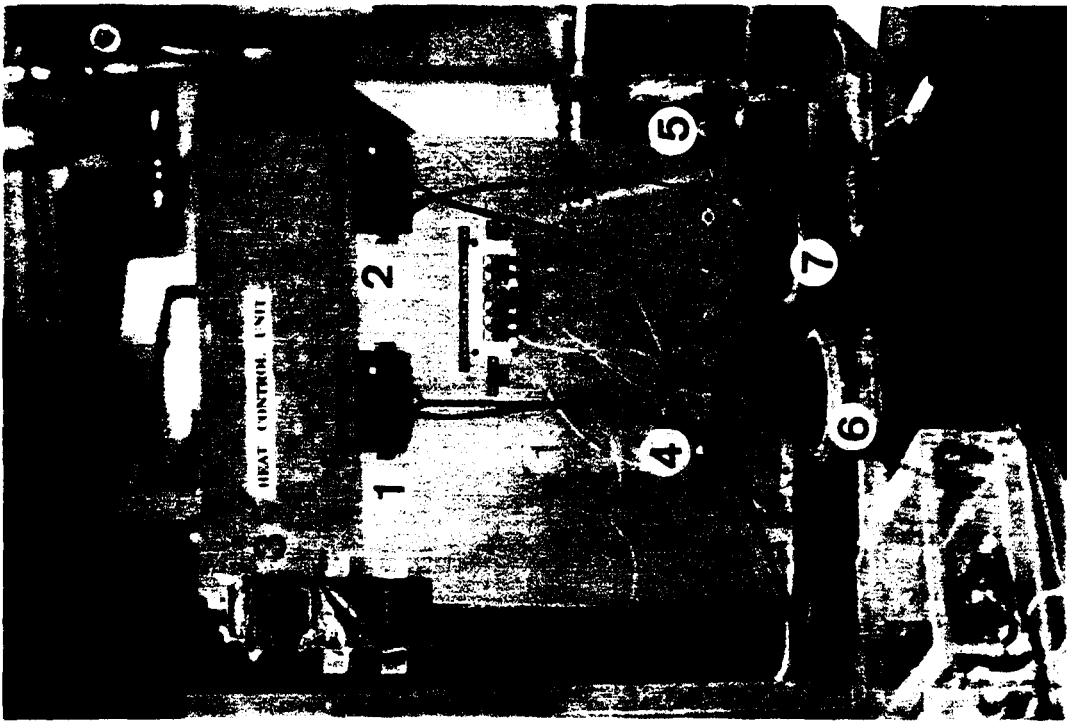


Figure A.3: Photograph of the Heat control panel

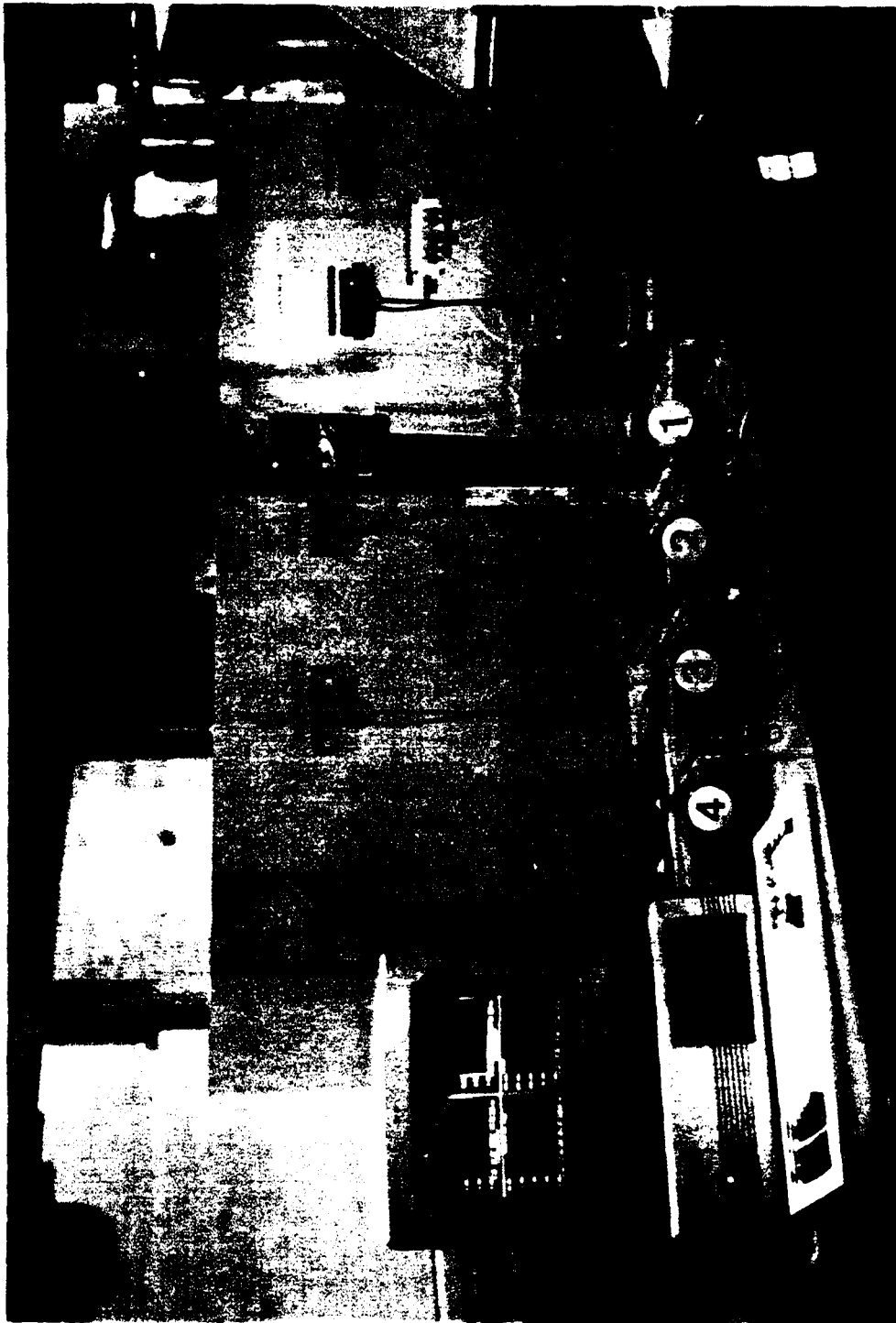


Figure A.4: Photograph of the Data acquisition

APPENDIX B  
DATA ACQUISITION PROGRAM

```
/*-----  
SAMPLING DATA PROGRAM: As data are collect,  
                        they are displayed on realtime.  
  
Designed for Multipurpose Triaxial Testing System.  
  
Designer: MUSTAFA TUNCAN  
          LEHIGH UNIVERSITY  
  
Jan., 1990  
-----*/  
  
/*----- DEFINITIONS SPECIFIC TO LABPAC -----*/  
  
#define MASTER  
#include "labhead.h"  
  
#define INT_TIMER 5  
/* timer 5 and IRQ 3 has been hard wared */  
#define INT_CHAN 3  
#define DMA_SEL 0 /* no DMA in LAB Master */  
/*-----*/  
  
/*----- DEFINITIONS SPECIFIC TO GRAPHICS -----*/  
  
#include <conio.h>  
#include <stdio.h>  
#include <string.h>  
#include <alloc.h>  
#include <graphics.h>  
#include "lablib.h"  
#include "user.h"  
  
extern struct LayoutType wd[8];  
/* the 8 viewports are defined in window.c */  
  
struct EnvironmentType env;  
int *buf;
```

```

/*----- FUNCTION PROTOTYPES -----*/

int  gprintf(int *xloc, int *yloc, char *fmt, ... );
int  AbortGraph(void);
void DisplayData(int, float, float, float, float);
void ReturnToDos(char *);
int  convert_string(char *, float*);
int  emptystring(char *);
void makestring(char *);
void disp_legend(int);
int  sampling(int, struct EnvironmentType *);
int  average_points(int *buf, int avgpoints, int channels);

void display_to_file(FILE *, struct EnvironmentType *);
void disp_msg(void);
void displayinfo(struct EnvironmentType *);
void getparameters(struct EnvironmentType *);
void setupenv(void);

void save_env(void);
void load_env(void);

void displayportsettings(void);
void getportparameters(void);
/*-----*/

main()
{  int i, ch, pg=0;

  disp_msg();

  if (searchpath("config.env")!=NULL) {

      load_env(); /* use environment if exists */
  }
  else { /* use default values */
      setupenv(); /* set the env struction */
      setdefaultwindows1(); /* set the wd[8] structure */
      setdefaultwindows2();
  }
  getparameters(&env);
  setdefaultwindows1(); /* reset the wd[8] structure */

  save_env();
      init_graph();
      setvisualpage(0);
      /* first see the main screen */
}

```

```

        setallwindows();
        /* draw the 8 view ports */
        for (i=0; i<3; i++)
            sampling(i,&env);
        /* three speed sampling */

        setvisualpage(0);

        while((ch=getch())!=ESC){
            if (ch=='n' || ch=='N'){
                setvisualpage(pg=(++pg % 2));
            }
        }
        closegraph();
    }

void save_env(void)
{
    FILE *outfile;
    if ((outfile=fopen("config.env","w+b"))==NULL){
        printf("Error opening file to save environment\n");
        exit(1);
    }
    fwrite(&env,sizeof(struct EnvironmentType),1,outfile);
    fwrite(wd,sizeof(struct LayoutType),8,outfile);
    fclose(outfile);
}

void load_env(void)
{
    FILE *infile;
    if ((infile=fopen("config.env","r+b"))==NULL){
        printf("Error opening file to load environment\n");
        exit(1);
    }
    fread(&env,sizeof(struct EnvironmentType),1,infile);
    fread(wd,sizeof(struct LayoutType),8,infile);
    fclose(infile);

    wd[0].startx=0.0;
    wd[0].endx=env.intervals[0]*env.samples[0]+0.0;

    wd[1].startx=0.0;
    wd[1].endx=env.intervals[1]*env.samples[1]+0.0;
}

```

```

    wd[2].startx=0.0;
    wd[2].endx=env.intervals[2]*env.samples[2]+0.0;
}

void setupenv(void)
{
env.gain[0]=0; env.gain[1]=0; env.gain[2]=0; env.gain[3]=0;
env.chan[0]=0; env.chan[1]=1; env.chan[2]=2; env.chan[3]=3;

env.channels=4;

env.chfactor[0]=96.16; env.chfactor[1]=248.1; env.chfactor[2]=0.50
env.chfactor[3]=96.16;

env.skip[0]=1; env.skip[1]=60; env.skip[2]=60;

env.intervals[0]=1; env.intervals[1]=0; env.intervals[2]=0;

env.samples[0]=60; env.samples[1]=0; env.samples[2]=0;

    strcpy(env.filename, "datafile.dat");
    strcpy(env.imagefile, "image.dat");

    env.avg_points=1;
    /* how many data points used to average to get 1 sample */

env.ports[0]=1; env.ports[1]=1; env.ports[2]=1; env.ports[3]=0;
env.ports[4]=1; env.ports[5]=1; env.ports[6]=1; env.ports[7]=1;

env.Xchannels[0]=0; env.Xchannels[1]=0; env.Xchannels[2]=0;
env.Xchannels[3]=0;
env.Xchannels[4]=2; env.Xchannels[5]=1; env.Xchannels[6]=2;
env.Xchannels[7]=1;

env.Ychannels[0]=0; env.Ychannels[1]=0; env.Ychannels[2]=0;
env.Ychannels[3]=0;
env.Ychannels[4]=1; env.Ychannels[5]=0; env.Ychannels[6]=0;
env.Ychannels[7]=3;

    env.sample_height=14;
}

void display_to_file(FILE *outfile, struct EnvironmentType *en)
{

```



```

    fprintf(outfile,"Sampling Recording Data File:\n\n");
    fprintf(outfile,"Image is stored in %s\n\n",en->imagefile);
    fprintf(outfile,
    "Gain selection : channel(0, 1, 2, 3)=(%d, %d, %d, %d)\n\n",
    translate(en->gain[0]);translate(en->gain[1]),
    translate(en->gain[2]),translate(en->gain[3]));
    fprintf(outfile,"Sample Height : %f\n\n", en->sample_height);
    fprintf(outfile,
    "Number of Points for Averaging = %d\n\n" ,en->avg_points);
    fprintf(outfile,"Fast-Speed Period: Interval(sec)=%d,
    samples=%d\n", en->intervals[0], en->samples[0]);
    fprintf(outfile,"Mid-speed Period: Interval(min)=%d,
    samples=%d\n", en->intervals[1], en->samples[1]);
    fprintf(outfile,"Slow-Speed Period: Interval(min)=%d,
    samples=%d\n", en->intervals[2], en->samples[2]);
}

void condition_data(int *buf, float *ddd,
                    struct EnvironmentType *en)
/* conditioning the data stored in buf,
   2 sweeps are conditioned */

int ii, jj;
for (jj=0; jj<en->channels; jj++){
    ii=translate(en->gain[jj]);
    ddd[jj]=buf[jj]*(en->chfactor[jj]+0.0)/(409.5*ii);
ddd[en->channels+jj]=buf[en->channels+jj]*en->chfactor[jj]/(409.5*ii
}
}

int sampling(int mode, struct EnvironmentType *en)
{
    int    ch, j, i, result, visualpage=0;
    int    colors[4];
    long   ii;
    int    interval,skipp,sweeps;

    FILE   *outfile;
    float  x1,y1,x2,y2, ddd[20];
           /* max 20 channels, currently */

    colors[0]=EGA_LIGHTRED;colors[1]=EGA_YELLOW;colors[2]=EGA_LIGHTGRE
    colors[3]=EGA_BROWN;

```

```

if (mode==0){
if ((outfile=fopen(en->filename,"w+t"))==NULL){
/* clear existing file */
printf("Error Opening Output File!!!");
exit(1); /* jump out if error */
}
else
fclose(outfile);
}

if (en->intervals[mode]==0 || en->samples[mode]==0)
return(0); /* jump out if */

if ((outfile=fopen(en->filename,"a+t"))==NULL){
printf("Error Opening Output File!!!");
exit(1); /* jump out if error */
}

display_to_file(outfile, en);
/* display environment information */

interval=en->intervals[mode];
sweeps=en->samples[mode];
skipp = en->skip[mode]*en->intervals[mode];

switch (mode) {
case 0:
fprintf(outfile,"Fast-Speed Sampling (unit=seconds):\n");
break;
case 1:
fprintf(outfile,"Mid-Speed Sampling (unit=minutes):\n");
break;
case 2:
fprintf(outfile,"Slow-Speed Sampling(unit=minutes):\n");
break;
}

fprintf(outfile,"interval= %d, samples = %d\n\n", interval,
sweeps);
fclose(outfile);

buf=(int*)malloc(sweeps*en->channels*sizeof(int));

/* alloc buffer for sweeping function */

```

```

    result=labpac(RESET); /* reset whole system */
result=labpac(AIINIT, ATOD, en->channels, DMA_SEL, en->gain);
    /* reset analog input channels */
result=labpac(TIINIT, TIMER);
    /* reset all the five timers */
result=labpac(TIIST, INT_TIMER, 15, 25);
    /* 4 Hz interrupt start timer 5 */
result=labpac(SWINIT, INT_TIMER, INT_CHAN);/*
    initialize sweep functions,
    0.5 Hz service, timer 5, interrupt 3 */
result=labpac(AISWST, skipp, sweeps, en->channels, en->chan,
    buf);
/* start sweep funtions, 1 Hz sweeps, returns
    control right away, need further check to see
    progress */
for (i=sweeps; i>0; ) {
result = labpac(AISTAT, sweeps);
    /* no-halt poll sweep status, see
    how many sweeps are left (wait on the sweep number
    given) */

if (result<=(i-1)) { /* new data collected */
average_points(&buf[(sweeps-i)*en->channels],en->avg_points,
    en->channels);
    /* perform average operation if required */
condition_data(&buf[(sweeps-i)*en->channels],ddd,en);

outfile=fopen(en->filename,"a+t");
    /* open file for save */
for (j=0; j<en->channels; j++)
    fprintf(outfile, "%5d %12.7f ",sweeps-i+1,ddd[j]);
fprintf(outfile,"\n");
fclose(outfile);

if (i<sweeps) /* condition 2 sets of data */
    condition_data(&buf[(sweeps-i-1)*en->channels],ddd,en);

for (j=0; j<en->channels ; j++){
    setcolor(colors[j]);
    setlinestyle(1,0,NORM_WIDTH);

if (i<sweeps) { /* drawing starts from second data set */
disp_data(&wd[mode], (sweeps-i)*interval,
    buf[(sweeps-i-1)*en->channels+j]/409.5,
(sweeps-i+1)*interval,buf[(sweeps-i)*en->channels+j]/409.5);
    }
}
}

```

```

if (i<sweeps) { /* display data on different bank */
    for (j=3; j<8; j++){ /* total five data ports */
        if (en->ports[j]!=0)
            setcolor(colors[en->Xchannels[j]]);
disp_data(&wd[j],ddd[en->Xchannels[j]], ddd[en->Ychannels[j]],
dd[en->channels+en->Xchannels[j]],
        ddd[en->channels+en->Ychannels[j]]);
    }
    }
i--; /* wait for next sweep */
}
if (kbhit()) { /* 'N' is used to switch visual page */
    ch = getch();
    switch (ch){
case 0: getch(); /* control function keys */
        break;
case 'n':
case 'N': visualpage = (visualpage+1) % 2;
        setvisualpage(visualpage);
        break;
case ESC:
        closegraph(); /* Change to text mode
        labpac(AISWAB); /* stop sweep functions */
        labpac(TIAB,INT_TIMER); /* stop timer counting */
        exit(0); /* jump out */
    }
}
} /* end of main loop */

if (i==0) {
    labpac(AISWAB); /* stop sweep */
    labpac(TIAB,INT_TIMER); /* stop timer */
}
free(buf); /* free memory allocated */
}
int translate(int sel)
{ int jj;
  switch (sel){
case 0: jj=1; break;
case 1: jj=10; break;
case 2: jj=100; break;
case 3: jj=500; break;
default: jj=1; break;
}
}

```

```

    return(jj);
}
/*
/*          Abort Check:
/*          key is an ESC, then exit program,
/*          else stay in graphic system.
/*
/*
int AbortGraph(void)
{
    int c;

    if (kbhit()){
        c = getch();          /*      Read a character from kbd      */
if( ESC == c ){          /*      Does user wish to leave?      */
    closegraph();          /*      Change to text mode      */
    labpac(AISWAB);          /* stop sweep functions */
    labpac(TIAB,INT_TIMER); /* stop timer counting */
    return(1);          /* Return to calling program */
}
    if( 0 == c ){          /* Did use hit a non-ASCII key? */
        c = getch();          /* Read scan code for keyboard */
    }
}
return(0);          /* no ESC hit, Keep going */
}

/*-----*/
/*GPRINTF: Used like PRINTF except the output is sent to the */
/* screen in graphics mode at the specified co-ordinate. */
/*
int gprintf( int *xloc, int *yloc, char *fmt, ... )
{
    va_list argptr;          /* Argument list pointer      */
    char str[140];          /* Buffer to build sting into  */
    int cnt;          /* Result of SPRINTF for return */

    va_start( argptr, fmt ); /* Initialize va_ functions */
    cnt = vsprintf( str, fmt, argptr );
    outtextxy( *xloc, *yloc, str ); /* prints string to buffer */
}          /* Send string in graphics mode */

```

```

*ylloc += textheight( "H" ) + 2;
/* Advance to next line */

va_end( argptr );
/* Close va_ functions */

return( cnt );
/* Return the conversion count */
}

int convert_string(char *ss, float *array)
{ /* convert a data string into real array */
int ii,count;
char * tmp;

ii=0; count=0;
tmp=ss;
while (tmp[0]!='\x0'){
for (ii=0; tmp[ii]==' '; tmp++);
for (ii=0; (tmp[ii]!=' ' && tmp[ii]!='\x0');ii++);
if (tmp[ii]==' '){
tmp[ii]='\x0';
array[count]=atof(tmp);
count++;
tmp += (ii+1);
}
else{
array[count]=atof(tmp);
count++;
tmp += ii;
}
for (ii=0; tmp[ii]==' '; tmp++);
}
return(count);
}

void makestring(char *ss)
{ /* trim the \r\n chars in a string from fgets() calls */
int ii;
for (ii=0; ss[ii]!='\r'; ii++);
ss[ii]='\x0';
}

int emptystring(char *ss)
{ /* detect an empty string */

```

```

    char *tmp;
    tmp =ss;
    for (;tmp[0]==' ';tmp++);
    if (!(tmp[0]>='0' && tmp[0]<='9'))
        return(1);
    else
        return (0);
}

void ReturnToDos(char *msg)
{
    closegraph();
    printf("%s\n",msg);
    exit(1);
}

int average_points(int *buf, int avgpoints, int channels)
{
    int ii,jj,ttemp, *iptr;
    double aa[20]; /* max 20 channels, currently */
    if (avgpoints==1)
        return (0); /* no need to process average functions */
    for (ii=0; ii<20; ii++) aa[ii]=0.0; /* init. array */
    for (ii=0; ii<avgpoints; ii++) /* for all the points */
        for (jj=0; jj<channels; jj++){ /* for each channels */
            ttemp = labpac(AIRAW, jj);
            aa[jj] += ttemp+0.0;
        }
    for (jj=0; jj<channels; jj++)
        aa[jj] /= avgpoints;
    for (jj=0; jj<channels; jj++)
        buf[jj]=aa[jj];
        /* replace data array with avg. values */
    return (0);
}

```

```

    void disp_msg(void){
        clrscr();
        gotoxy(1,8);
        printf("This program sampels 4 channels of data points.\n\n\n");
        printf( ESC to exit program!\n\n");

        printf(" Hit any key to continue ... \n");
        getch();
        clrscr();
    }

    void displayinfo(struct EnvironmentType *en)
    {
        int ii;
        clrscr();

        printf("***** Parameter Selection *****\n");
        printf("(1)  ");
        for (ii=0; ii<en->channels; ii++) printf("Ch%d: Gain=%d;
            ",ii,translate(en->gain[ii]));
        printf("\n\n");
        printf("(2)  Fast-Speed Period: Interval(sec)=%d,
            samples=%d\n\n", en->intervals[0], en->samples[0]);
        printf("(3)  Mid-speed Period: Interval(min)=%d,
            samples=%d\n\n", en->intervals[1], en->samples[1]);
        printf("(4)  Slow-Speed Period: Interval(min)=%d,
            samples=%d\n\n", en->intervals[2], en->samples[2]);
        printf("(5)  Output file name: %s,
            Output Image file name: %s\n\n", en->filename,en->imagefile);
        printf("(6)  AVG points/sample = %d,
            sample_height = %7.3f\n\n",en->avg_points,en->sample_height);
        printf("(7)  Data Display Configuration...\n\n");
        printf("(8)  Display a recorded image\n\n");
        printf("(9)  Finish Selection \n");
        printf("*****\n\n");

        printf("Enter selection number please: ");
    }

    void getparameters(struct EnvironmentType *en)
    {
        int sel,ch,gg;
        float tt;

        displayinfo(en); /* display the selects first */
    }

```



```

scanf("%d", &sel);
while (sel!=9) {
window(1,23,80,25);
clrscr();
window(1,1,80,25);
switch (sel) {
case 1:
ch=getint(1,23,"Enter channel number? ");
if (ch>=0 && ch<=3)
gg=getint(1,24,"Enter Gain --> 0:Gain=1, 1:Gain=10,
                2:Gain=100, 3:Gain=500 ? ");
        if (gg>=0 && gg<=3)
            en->gain[ch]=gg;
        }
break;
case 2:
ch=getint(1,23,"Enter fast-speed sampling interval,
                in seconds (0:no fast sampling)? ");
if (ch>=0 && ch<=300)
en->intervals[0]=ch;
gg=getint(1,24,"# of samples? ");
if (gg>=0 && gg<=1000)
en->samples[0]=gg;
break;
case 3:
ch=getint(1,23,"Enter mid-speed sampling interval,
                in minutes (0:no mid sampling)? ");
if (ch>=0 && ch<=300)
en->intervals[1]=ch;
gg=getint(1,24,"Enter samples? ");
if (gg>=0 && gg<=1000)
en->samples[1]=gg;
break;
case 4:
ch=getint(1,23,"Enter slow-speed sampling interval,
                in minutes (0:no slow sampling)? ");
if (ch>=0 && ch<=300)
en->intervals[2]=ch;
gg=getint(1,24,"Enter samples? ");
if (gg>=0 && gg<=1000)
en->samples[2]=gg;
break;
case 5:
strcpy(en->filename,getstring(1,23,"Enter output filename? "));
strcpy(en->imagefile,getstring(1,24,"Enter image filename? "));
break;

```

```

case 6:
    gg=getint(1,24,"AVG points/Sample? ");
    if (gg>0)
        en->avg_points=gg;

    tt=getfloat(40,24,"Sample Height? ");
    if (tt>0.0)
        en->sample_height = tt;
    break;

case 7: /* configure display */
    getportparameters();
    break;

case 8: /* display image */
    break;
}
displayinfo(en);
scanf("%d", &sel);
}
en->chfactor[2] = 0.508*100.0/en->sample_height;
}
void displayportsettings(void)
{ /* dispaly current ports assignments */
    int jj;
    clrscr();
    printf("--- Total ports = 8 ----, Detailed information:\n\n");
    for (jj=0; jj<3; jj++){
        printf("Port %1d : Fixed, not configurable \n\n",jj);
    }
    for (jj=3; jj<8; jj++){
        if (env.ports[jj]==0){
            printf("Port %1d : not used. \n\n",jj);
        }
        else{
            printf("Port %1d : xlable = %s, ylabel = %s,
xchannel=%1d, ychannel=%1d\n",jj,wd[jj].xlabel,wd[jj].ylabel,
env.Xchannels[jj],env.Ychannels[jj]);
            printf("xmin=%7.3f, xmax=%7.3f, ymin=%7.3f, ymax=%7.3f\n",
wd[jj].startx, wd[jj].endx, wd[jj].starty, wd[jj].endy);
        }
    }
    gotoxy(20,23);
}
}

```

```

void getportparameters(void)
{ /* change port parameters */
  int yes,jj, sel;
  do {
    displayportsettings();

    yes=isyes(20,22,"Do you want to change anything (Y/N)? ");
  if (yes){
    jj=getint(1,22,"Enter port number? ");
    sel=getint(40,22,"0: Delete Port, 1: Change ? ");

    if (sel==0) env.ports[jj]=0;
    if ( sel==1 && jj>=3 && jj<=7) {
      env.ports[jj]=1; /* use this port */
      strcpy(wd[jj].xlabel,getstring(1,23,"Enter X label? "));
      strcpy(wd[jj].ylabel,getstring(1,24,"Enter Y label? "));
      wd[jj].startx=getfloat(1,23,"Enter Xmin? ");
      wd[jj].endx= getfloat(40,23,"Enter Xmax? ");
      wd[jj].starty=getfloat(1,24, "Enter Ymin? ");
      wd[jj].endy=getfloat(40,24,"Enter Ymax? ");
      env.Xchannels[jj]=getint(1,24,"Channel # for X? ");
      env.Ychannels[jj]=getint(40,24,"Channel # for Y? ");
    }
  }
} while (yes);
}

```

## APPENDIX C

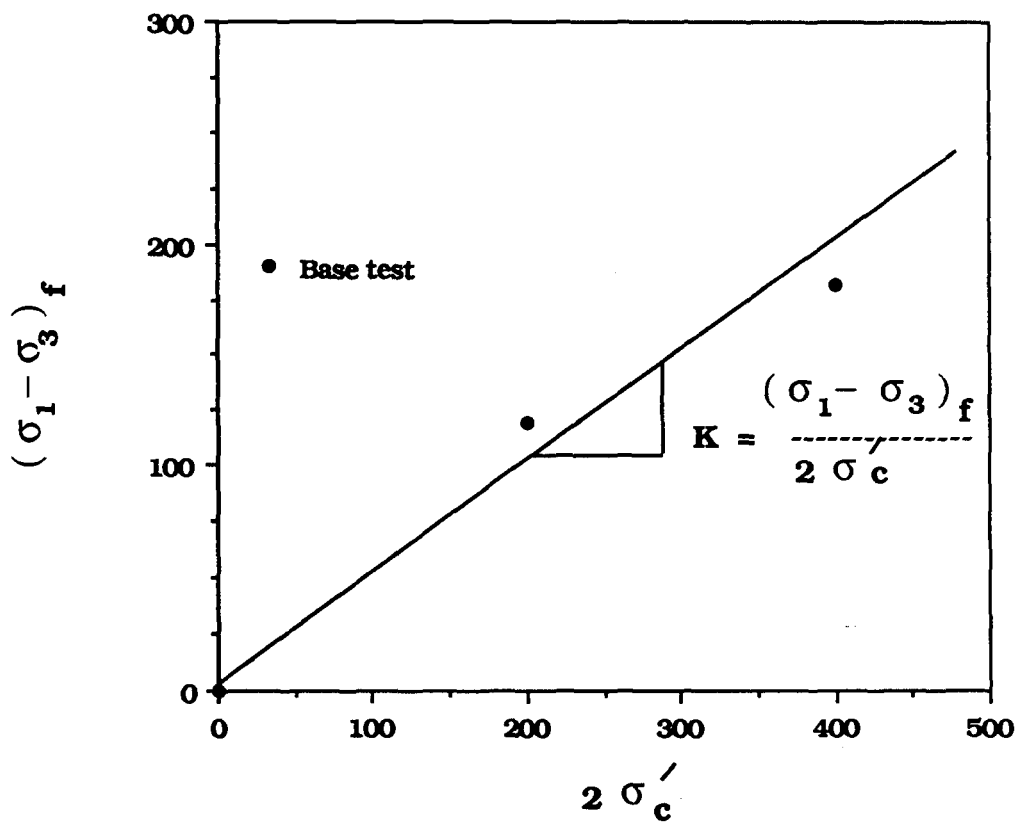
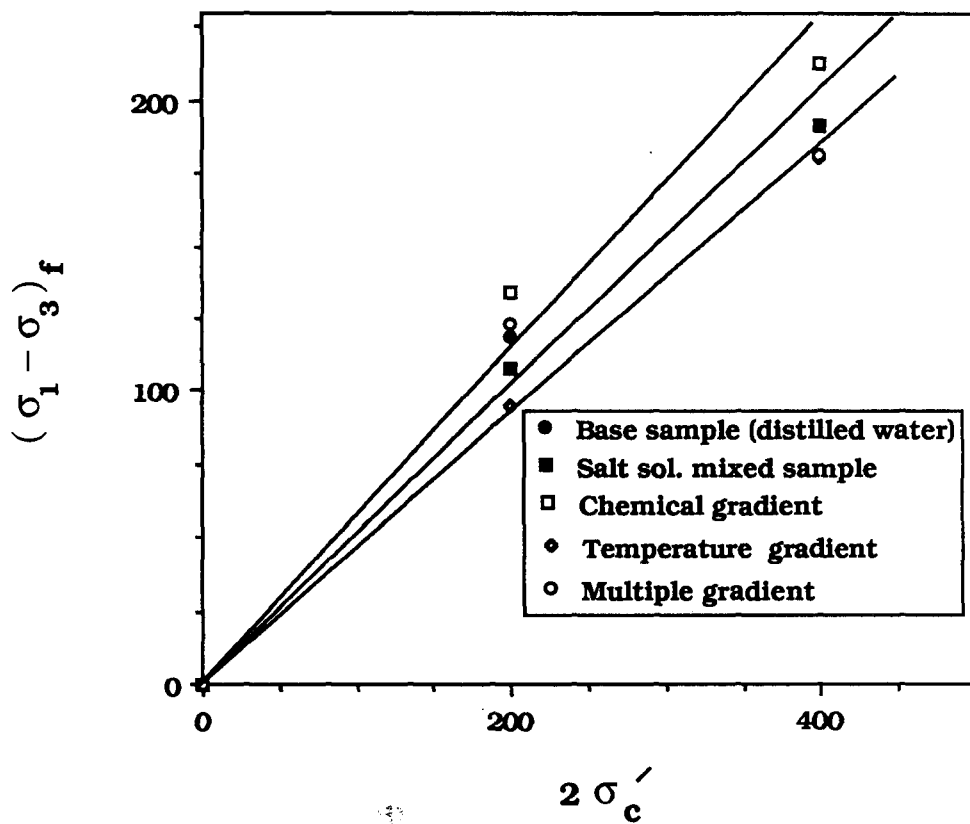


Figure D.1: Determination of K coefficient for normally consolidated kaolinite specimens with distilled water



**Figure C.2 : Variation of K coefficient with the induced gradients.**

## **VITA**

Mustafa Tuncan was born in Eskisehir , Turkey on January 2, 1960, the son of Ismail Tuncan and Guner Tuncan. After graduating from Electronic branch of Technical High School in Eskisehir in 1976, he entered the Anadolu University at Eskisehir, Turkey in September, 1976. He received a Bachelor of Science Degree in Civil Engineering from Anadolu University in June, 1981. He spent 1 year at the English Prep School of Bogazici University in Istanbul to learn English as a foreign language, before entering the graduate school of Bogazici University, Turkey in August, 1982. Upon receiving the Master of Science Degree in Civil Engineering in August, 1984, he was employed as a Research Fellow at the Anadolu University in Eskisehir. In the summer of 1984, he entered Istanbul Technical University to pursue his doctoral studies. He received scholarship from Anadolu University to continue his studies abroad in 1987. He then entered the doctoral program at Lehigh University Civil Engineering Department, in 1987 pursuing his studies in Geotechnical Engineering. He was married in August 1989 and he has two sons. Upon completion of his doctoral studies, he will be employed as an Assistant Professor of Civil Engineering at the Anadolu University , Eskisehir, Turkey.